Summer 8-2011

APPLICATION OF SHREDDED-TIRE BIOFILTER AND MEMBRANE BIOREACTOR FOR GREYWATER RECLAMATION

Meng Hu
University of Nebraska – Lincoln, mhu@huskers.unl.edu

APPLICATION OF SHREDDED-TIRE BIOFILTER AND MEMBRANE BIOREACTOR FOR GREYWATER RECLAMATION

by

Meng Hu

A THESIS

Presented to the Faculty of

The graduate college at the University of Nebraska

In Partial Fulfillment of Requirements

For the Degree of Master of Sciences

Major: Civil Engineering

Under the Supervision of Professor Tian C. Zhang

Lincoln, Nebraska

August, 2011

APPLICATION OF SHREDDED-TIRE BIOFILTER AND MEMBRANE BIOREACTOR FOR GREYWATER RECLAMATION

Meng Hu, M.S.

University of Nebraska, 2011

Advisor: Tian C. Zhang

Water scarcity is a pressing global issue. Greywater (GW) reclamation is a viable option to reduce freshwater demand. The objectives of this work were to: a) evaluate the feasibility of the combination of shredded tire biofilter (STB) technology and membrane bioreactor (MBR) technology in GW reclamation; b) study the effects of various parameters on STB performance; and c) understand the fouling mechanisms to lower the energy consumption in MBRs. Bench-scale STBs and MBRs (flat-sheet membranes) were constructed to address the first two objectives, while an independent membrane (hollow-fiber membranes) fouling experiment was designed for the third objective.

It was found that STBs packed with tire shreds not only could pre-treat GW before MBRs, but also present an alternative to the issue of tire disposal. The investigation on the biofilm in STBs showed that shredded tires could support the growth of microorganisms, which may extend their use in bio-retention basins, constructed wetlands, etc. The effluent from STBs was further treated in MBRs, the effluent of which reached the wastewater reuse guidelines suggested by the U.S. Environmental Protection Agency (EPA). The combination was thus proved to be capable of producing reusable water for non-potable purposes.

With the aid of confocal laser scanning microscopy (CLSM) and the image analysis software (ImageJ and Imaris®), the fundamental membrane fouling mechanisms were studied in terms of internal and external fouling. In an independent MBR experiment, sampling of membranes were such designed to represent the 3-stage fouling map, that changes in foulants contribution were monitored throughout an entire filtration process. Protein and polysaccharides were found to be the major foulants. Internal fouling was responsible for the two trans-membrane pressure (TMP) jumps at the first and third stages, while external fouling dominated the extended second stage. A mathematical model was proposed to link the porosities and TMP from the basic filtration theory point of view. The model verifies the experimental findings.

To

My Late Grandpa, Wu Zhongguo

And

My Late Little Brother.

ACKNOWLEDGEMENTS

I would like to express my sincere appreciation and gratitude to my advisor, Dr. Zhang, for his guidance and support during the course of this work. I'm grateful to the other supervisory committee members, Dr. Shannon L. Bartelt-Hunt and Dr. John S. Stansbury, for their participation in the review and evaluation of my thesis.

My academic program at the University of Nebraska was supported by the U.S. Environmental Protection Agency under the Project No. CR-83419301. During my study in the program, the following people kindly offered their help and assistance: Qi Yuan, Haiyang Huang and Xueyi Wang of the Peter Kiewit Institute, Dr. William Tapprich of the University of Nebraska at Omaha, Drs. Joe Zhou and Han Chen of the Beadle Center at the University of Nebraska-Lincoln, Dr. Yongfeng Lu and Lisha Fan of the University of Nebraska-Lincoln, Dr. Edward J. Garboczi of the National Institute of Standards and Technology, and Dr. Barbara Morely and Steven Ready of the Boys Town National Research Hospital. I am thankful to these people and organizations.

Thanks also go to Dr. Zhang for his care during my illness in 2010 and the valuable advices, and Ms. Cheryl Campbell for providing counseling services.

Finally, I want to thank my family for their support and encouragement. It goes without saying that this achievement, however small it may be, is built upon my previous education and development, for which they spent every possible effort and even sacrificed their own careers.

TABLE OF CONTENTS

LIST OF FIGURES

List of Tables

CHAPTER 1

INTRODUCTION

1.1 Project Background

The study in this thesis is a part of the project entitled *Advanced Decentralized Water/Energy Network Design for Sustainable Infrastructure*, funded by the U.S. Environmental Protection Agency (EPA) under the EPA Project Number CR-83419301.

The issue of aging and deteriorating water infrastructure is of high-priority for the U.S. EPA. A more sustainable water infrastructure into and beyond the 21st century, as the organization claims, must include drinking water distribution systems and wastewater collection systems that account for the diminishing water supply, increasing demands, global climate change, energy cost and availability. Meanwhile, energy consumption by the water wastewater sector has increased noticeably due to the implementation of technologies and approaches to safeguard water quality and comply with more stringent regulations. Energy price has considerably increased as well, making imperative the optimization of energy use, more efficient treatment technologies, etc.. The project was thus formulated to address these water-related issues to fulfill the U.S. EPA's mission to safeguard human health and the environment (USEPA, 2009).

The project objectives are to develop and evaluate advanced decentralized drinking water and wastewater technologies by coupling them with innovative renewable energy and energy saving/recovery technologies, and then incorporate the proven technologies into green building and community design and construction (USEPA, 2009).

The research activities in this work were conducted according to the following tasks in Area 1 of the project:

1. Lab studies on water quality/biofilm;
2. Develop/test systems for gray/rain water collection, storage and reuse; and
3. Develop/test lab-scale gray/rain water treatment technologies (community-level).

1.2 Research Objectives

The aim of the research was to evaluate the feasibility of the application of the combination of biofilters packed with shredded tires (STBs) and membrane bioreactors (MBRs) in greywater reclamation. It was achieved specifically in the following objectives:

1. To assess whether STBs could effectively treat GW (or whether shredded tires can be used as a packing material in biological filters) by investigating the performance of treating GW at various hydraulic retention times (HRTs);
2. To study the impact of tire shred size on the treatment performance of STBs, the treatment performance at different depths along STBs, and properties of biofilms in STBs if they were proved to be effective;
3. To investigate the performance of MBRs in reclaiming GW by comparing the effluent water quality with the water reuse guidelines suggested by the U.S. EPA (USEPA, 2004); and
4. To fundamentally understand the mechanisms behind the membrane fouling phenomenon in MBRs.

1.3 Scope of Work and Thesis Structure

The work presented herein was aimed to evaluate the feasibility of the application of the combination of STBs and MBRs in greywater reclamation. The rest of this chapter lists the organization and structure of the thesis.

Chapter 2 reviews the membrane processes for GW and rainwater (RW) reclamation as well as the application of shredded tires in water quality protection.

Chapter 3 is the core of the thesis, targeting at the goal of the work. It includes comprehensively the performances of STBs and MBRs, and covers the Objectives 1-3.

Chapter 4 deals with Objective 4. It provides not only the findings which facilitates in-depth comprehension of membrane fouling mechanisms, but also a mathematical model linking the porosities of both the cake layer and the membrane for the first time in the area.

Chapter 5 summaries the work, and predicts the potential for the combination of STBs and MBRs.

1.4 References

U.S. Environmental Protection Agency (2004). *Guidelines for Water Reuse*. EPA/625/R-04/108, Office of Water, Washington, D.C.

U.S. Environmental Protection Agency (2009). *Advanced Decentralized Water/Energy Network Design for Sustainable Infrastructure*. EPA/600/F-09/016, Washington, D.C.

CHAPTER 2

LITERATURE REVIEW

2.1 Introduction

For the project, a literature review was conducted for the following topics:

1. Greywater/rainwater reclamation;
2. Membrane processes for greywater/rainwater reclamation; and
3. The application of shredded tires in water quality protection.

2.2 Greywater/rainwater Reclamation

2.2.1 Background for Greywater/Rainwater Reclamation

As water scarcity being more urgent, water reuse has been receiving increased attention. Greywater (GW) is generally considered as municipal wastewater excluding that from kitchen and toilet flushing system (Nolde, 1999). With its low pollution level characteristics and representation of 60–70% of domestic wastewater (Friedler et al., 2005), GW is an ideal source for water reclamation. On the other hand, rainwater (RW) or stormwater also serves as an alternative water source, and is considered as one of the best existing approach to sustainable urban development (Kim et al., 2005). People in Thailand have been using RW as drinking water for centuries, especially in rural areas. Similar practice occurs in Bermuda as the residents harvest RW on rooftops to satisfy their freshwater needs (Levesque et al., 2008). Common pollutants in RW are found to be microorganisms, particles, colloids, heavy metals, organics, etc.. They originate from the

contacts with the air and catchment surfaces, which make RW even less contaminated than GW, and hence an alternative for water recycling.

2.2.2 Quantity and Characteristics of GW and RW

GW. Both the quantity and quality of GW are significantly variable, highly contingent upon lifestyles, living standards, population structures (age, gender), customs and habits, water installations and the degree of water abundance (Morel and Diener, 2006). The ratio of domestic water for toilet flushing to total domestic water usage ranges from 29 to 47% (Friedler et al., 2005; Lazarova, 2001; Surendran and Wheatley, 1998; Edwards and Martin, 1995). Water consumptions in different countries also vary. For example, the average water consumption (in L/captia·d) is 149 in the UK (OFWAT, 2001), 125 in France, and 260 in the United States (AWWARF, 1999). Both the ratio and water consumption make impossible a universal number on GW quantity; estimations of it in different areas seem more reasonable. Morel and Diener (2006) reported the typical volume of GW varied from 90 to 120 L/capita·d, and that in low income countries with water shortage could be 20–30 L/capita·d (except for Malaysia, whose GW production is as high as 225 L/capita·d). 70 L/capita·d has been adopted as the basis for GW production calculation for new buildings or buildings where sanitary equipment have been refurbished (fbr- Information Sheet H201, 2005).

Depending on living habits and the source, GW composition can be highly variable. GW generally contains shampoos, soaps, toothpastes, gels, laundry chemicals, personal care products, hair, skin residues, etc., which contribute to the contamination of GW. Many researchers have characterized GW. Li et al. (2009) studied the four

distinctive categories (bathroom, laundry, kitchen and mixed GW) of GW. They suggested that all types of GW possess good biodegradability regarding the ratios of chemical oxygen demand (COD) to five-day biochemical oxygen demand (BOD_5); the collection of kitchen GW with other streams will be beneficial to maintaining an optimal COD : N : P ratio in order to biologically treat GW. Aside from the conventional water quality parameters like COD, BOD_5, nitrogen, phosphorus, solids, and bacteria, contaminants of emerging concerns (e.g., trace organics, endocrine disrupting compounds (EDCs), heavy metals, brominated flame retardants, and boron) have also been found in GW (Gross et al., 2005; Palmquist and Hanæus, 2005; Eriksson et al., 2003). An overview of GW characterization can be found in Eriksson et al. (2002).

Researchers have been using both real GW and synthetic GW in their studies. Real GW is typically collected from houses (Abegglen et al., 2008), residential complexes (Kim et al., 2009; Jefferson et al., 2001), or public water-consuming facilities (Merz et al., 2007; Liu et al., 2005). The compositions (or recipes) for synthetic GW differs from one another in published literatures (Table 2.1). For instance, Jefferson et al. (2001) developed a synthetic GW recipe from a recipe used in the UK water industry, containing synthetic soap, hair shampoo, sunflower oil, and tertiary effluent, whereas Nghiem et al. (2006) used pure chemicals (humic acid, kaolin, cellulose, $CaCl_2$, NaCl, and $NaHCO_3$) to prepare the synthetic GW.

Table 2.1 Summary of synthetic GW recipes.

1. Synthetic soap (0.64 g), hair shampoo (8.0 mL), sunflower oil (0.1 mL), tertiary effluent (24.0 mL), and tap water (10 L) (Jefferson et al., 2001)
2. Toothpaste, shower gel, soap, oil, shampoo, bubble bath, washing powder, other washing agents and softener, raw wastewater (3%), and tap water (Chang, 2007)
3. Humic acid (20 mg/L), kaolin (50 mg/L), cellulose (50 mg/L), $CaCl_2$ (0.5 mM), NaCl (10 mM), and $NaHCO_3$ (1 mM at pH 8) (Nghiem et al., 2006)
4. Starch (0.3750 g), dextrose (0.1755 g), peptone (0.1800 g), beef extract (0.1275 g), sodium carbonate (0.2250 g), sodium bicarbonate (0.1170 g), trisodium phosphate (0.0810 g), urea (0.2355 g), ammonium sulfate (0.1305 g), solid detergent (0.1500 g), liquid detergent (0.3000 g), and water (1000 g) (Young and Xu, 2008)
5. Toothpaste (6.0 mg/L), shower gel (0.05 mL/L), cleaner (0.1 mL/L), shower oil (0.05 mL/L), shampoo (0.013 mL/L), bubble bath (0.035 mL/L), urea (20.0 mg/L), NH_4Cl (12.5 mg/L), and K_2HPO_4 (2.5 mg/L) (Scheumann and Kraume, 2009)

RW. Compared with GW, collected RW requires less stringent treatment due to the fewer amounts of pollutants it contains (Kim et al., 2007). The level of contamination in RW, however, has become an emerging concern (Dorfler and Scheunert, 1997; Reimann et al., 1997). Ionic and organic pollutants may be harmful to an urban water environment (Lee et al., 2003), whereas bacterial contamination may lead to human infection (Kim et al., 2005). The concentrations of heavy metals have been reported to exceed the recommended levels, rendering human consumption of RW inappropriate (Magyar et al., 2008, 2007; Han and Mun, 2007; Han et al., 2006). Kim et al. (2005) analyzed total viable bacteria in RW collected from roof and roof garden, and stored in storage tanks; the numbers per mL were all over 300. Fecal coliform and total coliform were even as high as 920 and $\geq$ 1,000 MPN/100 mL, respectively, in Kitiphatmontree et al. (2009). The quality of RW usually varies with the collection techniques, sampling locations and air conditions. Table 2.2 lists the typical water parameters and their values extracted from a few studies available on RW quality. Another issue regarding RW utilization is the fluctuating quantity because of its dependence upon precipitation intensity and extreme

spatial and temporal rainfall variability (Helmreich and Horn, 2009). Therefore, it is suggested to combine RW and GW for recycling (Kim et al., 2007).

Quite similar to drinking water distribution systems, the reclaimed water distribution system shares most of its traits. Both an individual reclaimed water system and a dual distribution system may be possible for reclaimed water delivery. Yet the integrated planning, design, and construction of a dual system gains its advantages of water resource management and cost savings over an individual one (Asano et al., 2007). Detailed information about dual distribution systems can be found in AWWA (1994) and Okun (2005). While there is adequate information about the distribution systems of reclaimed water, the literature is lacking of that of collection systems of source water, namely GW and RW. Special attention, however, should be paid to collecting and storing GW and especially RW, as any failure may lead to potential health hazards. In the case studies of Nolde (1999), GW from showers, bathtubs and hand-washing basins from 70 persons was collected and treated in a community-level GW treatment plant; in another case, a two-stage fluidized-bed reactor was placed above the toilet in the bathroom and used to treat GW from shower and bathtub of a two-person household. Rooftops, courtyards and low frequently used streets may serve as catchments for RW collection; open containers are not recommended for reclamation for drinking purposes (Helmreich and Horn, 2009). RW collected from roofs made of tiles, slates and aluminum sheets may be slightly or not polluted (Helmreich and Horn, 2009). Bricks, stabilized soil, rammed earth, plastic sheets, mortar jars, pottery, ferrocement, and polyethylene are common materials for storage tanks (Gould, 1992). RW can be either stored in underground or

above ground tanks (Mwenge Kahinda et al., 2007). RW may also be collected, managed and treated together with or separately from GW (Kim et al., 2007; Hiessl et al. 2001).

2.2.3 Overview of Treatment Technologies and Reuses

Treatment Technologies. Depending on the applications of reclaimed GW and/or RW, treatment technologies generally fall into the following categories:

- Physical (sedimentation, coarse filtration, sand filter, membrane filtration, and adsorption);
- Chemical (coagulation, electro-coagulation, photocatalysis, and membrane chemical reactor);
- Biological (membrane bioreactor, biological aerated filter, and rotating biological contactor); and
- Natural (green roof, reed beds, and constructed wetlands).

Sedimentation is usually preferred as pretreatment (such as screening) to subsequent processes in GW treatment. Sedimentation was also used to treat GW for subsurface irrigation in Western Australia (Mars, 2004). Also assessed was coarse filtration. These simple technologies were applicable due to the regulations that allow the reuse of simply treated GW for such reuse purposes. For stricter regulations, advanced technologies such as above-listed chemical, biological and physical (excluding sedimentation and coarse filtration) technologies were employed. For example, biofilters were used as pretreatment. Kitiphatmontree et al. (2009) used a granular activated carbon (GAC) filtration unit followed by a microfiltration (MF) unit to treat RW, where GAC

removed up to 40% of dissolved organic compound (DOC), over 80% of nitrate and 35% of phosphate, and MF removed all microorganisms.

Table 2.2 RW quality reported in different studies.

Parameter	Study 1[a]	Study 2[a]	Study 3[a]	Study 4[a]
pH	7–9	6.7	7.41	6.9
Conductivity (EC, µS/cm)	150–500	780	187.1	28.5
Total dissolved salts (mg/L)	–	160	–	–
Total suspended solids (mg/L)	–	428	–	5.2
Turbidity (NTU)	1–5	42	4.76	1.0
Hardness (mg/L as $CaCO_3$)	–	59	–	–
Nitrate(mg-N/L)	–	18.6	–	0.8 (TN)b
Chloride (mg/L)	–	1.35	–	–
Sulfate (mg/L)	–	5.8	–	–
Phosphate (mg/L)	–	1.5	–	0.21 (TP)b
Calcium (mg/L)	–	21.2	–	–
Copper (mg/L)	–	0.19	–	0.04
Iron (mg/L)	–	0.875	–	0.02
Manganese (mg/L)	–	0.006	–	–
Lead (mg/L)	–	0.174	–	–
Zinc (mg/L)	–	0.19	–	0.08
Total coliform	880–1100 CFU/100 mL	⩾ 1000MPN/1	–	351 (TVBC/mL)
Fecal coliform	400–450 CFU/100mL	920MPN/10 0 mL	–	–
E. coli	200–250 CFU/100mL	20MPN/100 mL	–	–
Color	–	–	24	8
COD (mg/L)	–	–	12.6	
DO (mg/L)	5–9	–	–	–
DOC	–	3.3	–	–

[a] References for studies 1, 2, 3 and 4 are Amin and Han (2009); Kitiphatmontree et al. (2009); Kim et al. (2007); and Kim et al. (2005) (runoff from roof), respectively. [b] TN = total nitrogen; TP = total phosphate; and TVBC = total viable bacteria count.

Recently, environmentally friendly and inexpensive, natural treatment technologies are gaining more popularity. In a case study in Santa Elena-Monteverde, Costa Rica, reed beds were used to treat GW that would otherwise discharged to the nearest street or stream (Dallas et al. 2004). The treated GW reached the wastewater reuse guidelines in Costa Rica. Shirley-Smith (2005) reported a system of green roof and ultraviolet (UV) disinfection for GW treatment; appropriate non-potable water quality standards were achieved. A comprehensive review of GW treatment could be found in Pidou et al. (2007).

With the proved performance of membrane processes in wastewater and GW treatment, membrane filtration is also widely accepted in RW treatment (Kitiphatmontree et al., 2009 ; Kim et al., 2005, 2007). Han and Mun (2009) studied sedimentation of particles in a RW storage tank to maximize the settling capacity, and thus, water quality improvement. For disinfection of RW, chlorination, slow sand filtration and solar disinfection (SODIS) were proposed by Helmreich and Horn (2009). Amin and Han (2009) applied solar collector disinfection (SOCO-DIS) to treat roof-harvested RW for potable purposes. Compared with SODIS system, disinfection was improved by 20–30% in the SOCO-DIS system.

Reuses and Related Regulations. The past decade has seen many applications of reclaimed GW, especially in arid or semi-arid areas. Typical types of applications include toilet flushing, laundry and car washing, lawn, garden and crop irrigation, and fire protection (Friedler and Hadari, 2006; Eriksson et al., 2003; Nolde, 1999). Combined with GW, RW was reused in office buildings in Korea (Kim et al., 2007). RW can also be

used as drinking water with or without disinfection (Helmreich and Horn, 2009; Kitiphatmontree et al., 2009).

Different regulations and/or guidelines on the quality of recycled GW and RW apply to different reuse purposes. Different countries, meanwhile, develop their own regulations or guidelines. Table 2.3 is a summary of selected water quality standards for water reuse in several countries and areas. It should be noted that the criteria established by the U.S. Environmental Protection Agency (USEPA) are suggested to those states that have not produced their own regulations or guidelines. The regulations and guidelines for GW reuse are still not considered sufficient or specific (Li et al., 2009; Kim et al., 2009). Kim et al. (2009) attributed the over emphasize of health risks over environmental risks to the situation.

2.3 Membrane Processes for GW/RW Reclamation

Membrane bioreactor (MBR) technology is promising in water reclamation as it produces good effluent quality, provides various plant sizes, and increases treatment system reliability while lowers the latent reuse risks (Fane and Fane, 2005). The feature of long solids retention times (SRTs) results in the ease of MBR operation. Recently, considerable research has been conducted on using MBRs to treat GW and RW, together with other treatment technologies; the effluent quality of MBRs has been found to be sufficient to meet current domestic wastewater reuse standards. However, information has not been reviewed and summarized on the performance (e.g., treatment efficiency and membrane fouling) of MBRs in GW and RW treatment under different conditions,

with the influence of different operational parameters, and in combinations with different pretreatment technologies, which is the focus of this chapter.

2.3.1 MBR and Its Performance in GW/RW Reclamation

The MBR effluents generally are sufficient to meet the water reuse criteria (Table 2.3). Table 2.4 summarizes the qualities of MBR effluents from different studies. Details of different studies are described below.

Generally, effluents from MBRs are of high quality, which is attributed mainly to long SRTs of bioreactors. Long SRTs result in elongated contact time of activated sludge and pollutants, and thus, facilitate the removal of slowly biodegradable pollutants (Scott and Smith, 1997). Liu et al. (2005) investigated the feasibility of bath wastewater reclamation with an MBR (polyethylene hollow fiber membrane, pore size of 0.4 μm) in a pilot plant. During an operation of 216 days without sludge discharge and chemical cleaning of membrane modules, the effluent quality satisfied the wastewater reclamation standard of China (see Table 2.3), with COD < 40 mg/l, NH_4^+-N < 0.5 mg/l and anionic surfactant (AS) < 0.2 mg/l, respectively. They also found biological treatment contributed to the removal of 34–85% of COD and 98% of AS; the membrane separation balanced the unstable biological treatment of COD but didn't contribute to AS removal. Merz et al. (2007) used a 3-L lab-scale MBR (hollow fiber UF membrane, pore size of 0.1 μm) to treat shower effluent from a sports club in Rabat, Morocco; they concluded that the permeate characteristics met commonly adopted standards for recycling for toilet flushing or other household uses. Lesjean and Gnirss (2006) studied an MBR pilot plant with unusual and extreme conditions of low SRTs (down to 4 d) and low hydraulic retention

times (HRTs, 2 h); they found that suspended solids (SS) decreased from 90 to less than 1 mg/l, COD from 493 to 24 mg/l, NH_4^+-N from 5.7 to less than 0.2 mg/l, etc.. Young and Xu (2008) used a low sludge discharge MBR (hollow fiber micro-filtration membrane, pore size of 0.2 μm) for GW reclamation; they achieved 95% AS removal with an effluent concentration being < 0.2 mg/l and 90% BOD removal with the effluent concentration being < 7 mg/l, respectively. The effluent ammonia and total Kjeldahl nitrogen (TKN) concentrations were reduced to less than 1 mg/l and 6 mg/l, respectively. The HUBER MBR process was applied for GW recycling in Vietnam recently (Paris and Schlapp, 2010). The wastewater from kitchen sinks and bathrooms of a dormitory was treated in the HUBER GreyUse® plant over a period of three months. The properties of the MBR plant effluent met reuse requirements (fbr- Information Sheet H201, 2005) with BOD_7 of less than 4.2 mg/l, anionic tensides of 0.79 and both total and fecal coliform bacteria of less than 1 /ml, respectively. Huelgas and Funamizu (2010) employed a 10-L lab-scale flat-plate submerged MBR (micro-filtration, pore size of 0.4 μm, polyolefin) for treatment of higher-load GW (a mixture of washing machine wastewater and kitchen sink wastewater); after an operation of 87 days, they observed effluent concentrations of COD, NH_4^+-N and linear alkylbenzene sulfonate (LAS) being reduced to 26, < 1, and < 1 mg/l, respectively.

Table 2.3. Water quality standards (selected parameters) for domestic wastewater reuse around the world.

Country/ Region	Application	Coliform (cfu/100 ml)		BOD_5 (mg/l)	Turbidity (NTU)	pH	TSS (mg/l)
		Total	Fecal				
US EPA[a]	Urban reuse	–	ND[b]	10	2	6–9	–
EU Directive for Bathing Water (2006/7/EC)[c]	Bathing	–	250 (m)[d]	–	–	–	–
Germany[e]	Wastewater recycling	10,000 (g)[d]	1,000 (g)	20 (g)	–	–	–
China[f]	Wastewater recycling	3[g]	–	10	10	6.5–9	10
British Columbia, Canada[h]	Unrestricted urban reuse	–	2.2	10	2	–	5
Queensland, Australia[i]	Garden watering in unsewered area	100	–	20	–	–	30
Canary Islands, Spain[a]	Wastewater recycling	2.2	–	10	2	–	3
Israel[j]	Wastewater recycling	–	< 1	10	–	–	10
Korea[k]	Toilet flush	1,000	–	–	5	5.8–8.5	–
	Toilet flush	ND	–	–	2	–	–
Japan[l]	Landscape	1,000	–	–	2	5.8–8.6	–
	Recreational	ND	–	–	2	5.8–8.6	–

[a] USEPA (2004); [b] ND = Non-detectable; [c] EU Directive for Bathing Water (2006); [d] m = mandatory, g = guideline; [e] Berlin Senate Department of Urban Development (Senatsverwaltung für Stadtentwicklung) (2003); [f] P.R. China Ministry of Construction (1989); [g] cell/L; [h] Canada Mortgage and Housing Corporation (2004); [i] Queensland Government (2003); [j] Halperin and Aloni (2003); [k] Kim et al. (2005); [l] MLIT (2005) and Tajima et al. (2005).

Table 2.4. Performance of MBR in GW treatment.

Parameters		Reference #							
		1	**2**	**3**	**4**	**5**	**6**	**7**	**8**
COD (mg/L)	Inf[a]	133–322	493	109 ± 33	562 ± 120	106.3	230	–	675
	Eff[b]	< 40	24	15 ± 11	38.1 ± 6.8	7.8–17.5	18.9	< 28.2	26.28 ± 5.43
BOD (mg/L)	Inf	99–212	–	59 ± 13	–	6506	–	–	–
	Eff	< 5	–	4 ± 1.2	–	3.0–6.1	–	< 4.2	–
SS (mg/L)	Inf	15–50	90	–	–	75	–	–	–
	Eff	ND[c]	< 1	–	–	3.4–4.0	–	–	–
Turbidity (mg/L)	Inf	146–185	–	29 ± 11	–	–	–	–	–
	Eff	< 1	–	0.5 ± 0.3		–	–	–	–
AS/LAS (mg/L)	Inf	3.5–8.9	–	299 ± 233	–	3.8	–	–	30.8
	Eff	< 0.2	–	10 ± 5	–	0.12–0.16	–	0.79	0.025 ± 0.39
NH_4-N (mg/L)	Inf	0.6–1.0	5.7	11.8 ± 4.2	84.3 ± 12.9	3.7	11.9	–	0.17
	Eff	< 0.5	< 0.2	3.3 ± 2.9	1.04 ± 1.08	0.53–0.92	0.37	–	0.16 ± 0.39
NO_3-N (mg/L)	Inf	–	–	0.0 ± 0.0	–	–	0.42	–	0
	Eff	–	–	2.1 ± 2.5	45 ± 6.7	–	3.66	–	9.85 ± 4.3
Total P (mg/L)	Inf	–	7.4	1.6 ± 0.5	23.9 ± 2.0	2.8	–	–	2.37
	Eff	–	3.5	1.3 ± 0.4	17 ± 2.8	0.4–0.79	–	–	–
Coliforms (CFU/100mL)	Inf	–	–	1.4×10^5 ± 1.1×10^5	–	–	–	–	–
	Eff	ND[c]	–	68 ± 120	–	–	–	< 1	–

[a] Influent; [b] Effluent; [c] Values below determination thresholds; and [d] Refereces: [1] = Liu et al. (2005); [2] = Lesjean and Gnirss, (2006); [3] = Merz et al. (2007); [4] = Abegglen et al. (2008); [5] = Young and Xu (2008); [6] = Scheumann and Kraume (2009); [7]= Paris and Schlapp (2010); [8] = Huelgas and Funamizu (2010).

In a combined system of anaerobic-anoxic-oxic (A^2O), MF membrane and oxidation process (OP), the removal efficiency of the membrane filtration was 98% for color, 99% for turbidity, 99% for COD, 99% for SS, and 30% for *E. coli*, *total coliform*, *Salmonella* and *Staphylococcus*, while the OP further removed each of the above parameter to 0, 3 NTU, 14 mg/l, 5 mg/l, and 0 CFU/100 ml, respectively (Kim et al., 2009). Scheumann and Kraume (2009) integrated a submerged membrane with a

sequencing batch reactor (SBR) to treat synthetic GW at different HRTs. The permeate concentrations over an operation period of 400 days were as follows: 18.9 mg/l of COD, 0.37 mg/l of NH_4^+-N, and 3.66 mg/l of NO_3-N, which were sufficient to meet reuse guidelines of Germany. Abegglen et al. (2008) studied the biological nutrient-removal potential of an on-site MBR located in the basement of a four-person house treating domestic wastewater. With the first reactor being operated as either a primary clarifier or an anaerobic/anoxic reactor by recycling activated sludge, the small-scale MBR achieved nitrogen and phosphorus removals of 50% and 25 %, in the first scenario, and 90% and 70% in the second scenario, respectively. Using the same system and schemes, Abegglen et al. (2009) investigated the fate of selected micro-pollutants, and observed a removal of pharmaceuticals in the small MBR, comparable to centralized wastewater treatment plants but slightly better elimination of slowly degradable substances.

2.3.2 Other Membrane Processes for GW/RW Reclamation

A membrane chemical reactor (MCR) is similar to an MBR except that the biomass is replaced with nano-sized titanium dioxide (TiO_2) particles in the presence of ultraviolet (UV) light, which generates highly reactive hydroxyl radicals with a potential of 2.33 V (Huang et al., 1993) to treat GW or RW. Treated GW or RW then is filtrated through an external MF membrane module. Figure 2.1 is a schematic diagram of a typical MCR. Rivero et al. (2006) studied MCR for GW treatment under different air velocities, TiO_2 concentrations and permeate fluxes; COD, BOD and turbidity were decreased to 56–98 mg/L (reduction of 67–83%), 2–17 mg/L (87–98%), and 0.35–3.57 NTU (77–98%), respectively. Under the optimal combination of experimental conditions, values of such

parameters were 86 mg/L, 9 mg/L, and 0.35 NTU, suggesting that permeate was reusable. Similar results were achieved in other investigations (Pidou et al., 2008a, b), with average effluent residuals of below 10 mg/L for BOD, below 1 NTU for turbidity, below 2 mg/L for suspended solids. These long term trials have demonstrated that MCR might be an effective technology to treat GW to the most stringent water quality standards available, as comparable to MBR (Pidou et al., 2007).

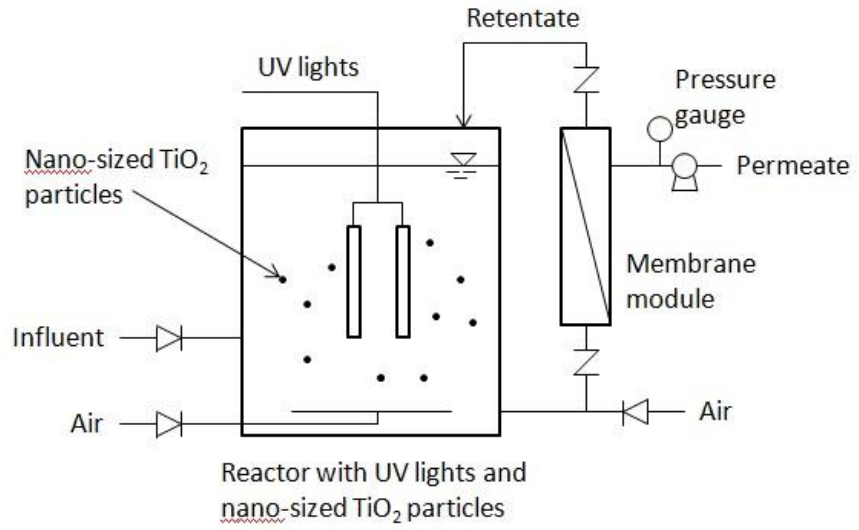

Figure 2.2. A schematic diagram of a membrane chemical reactor.

Metal membranes have recently gained attention in GW and RW reclamation as they can sustain pressures as high as up to 1 MPa, temperature as high as 350 °C, outer shock power, and chemical oxidation (Kim and Somiya, 2002). Kim et al. (2005, 2007) used metal membranes to treat GW and RW, separately and together. With membranes of the smallest pore size (0.5 μm), the effluent water qualities were obtained as follows: 6.81 of pH, 163.8 μS/cm of EC, 3.20 of turbidity, 13 of color, and 6.8 of COD for GW only; 7.08 of pH, 124.2 μS/cm of EC, 1.36 NTU of turbidity, 11 of color, and 5.6 of COD for GW and RW (volume ratio = 1:1); 7.18 of pH, 87.0 μS/cm of EC, 0.55 NTU of

turbidity, 11 of color, and 2.0 of COD for RW only. They concluded that metal membranes were efficient in rejecting particles in GW and RW, but based on the effluent water quality, the process could only be used as pretreatment if reuse is concerned.

2.3.3 Operating and Control Parameters

From Table 2.4, it can be seen that each quality item of the effluents is within the same range despite the differences in feed characteristics, membrane modules (Table 2.5) and operating parameters such as HRT, SRT, etc.. It has been found that removal efficiencies of MBR treating domestic wastewater are quite independent of HRTs in the range of 2–24 h (Stephenson et al., 2000). Higher fluxes, thus increased HRTs are desirable due to economic reasons. HRTs as low as 2 h are found in the literature (Lesjean and Gnirss, 2006), while Hu (2002) reported an optimal HRT of only 1.5 h for GW treatment with MBRs. Lesjean and Gnirss (2006) challenged the MBR unit with an extremely low SRT of 4 d and low HRT of 2 d, and achieved similar results to those under normal conditions. On the other hand, Young and Xu (2008) observed a trend of slightly increasing performance as SRT decreased from 65 to 48 d. SRTs also showed its effect on nitrogen removal. A low food-to-microorganism (F/M) ratio and a long SRT accounted for higher nitrifying rates and enhanced nitrogen removal efficiency (Schmidt et al. 2003; Fan et al. 2000). It is those variations that render conclusions of effects of different parameters on MBR performance hardly possible. A common practice is to design MBRs under critical fluxes with no sludge wasting (Scheumann and Kraume, 2009; Merz et al., 2007; Liu et al., 2005).

Table 2.5. Different membranes used in GW treatment.

Membrane	Description	Manufacturer	Reference
Hollow fiber	Polyethylene Pore size = 0.4 μm	Mitsubishi Rayon Co. Ltd.	Liu et al., 2005
Hollow fiber	Ultrafiltration Pore size = 0.1 μm	Zenon	Merz et al., 2007
Flat-sheet	Pore size = 0.04 μm	-	Abegglen et al., 2008
Hollow fiber	Microfiltration Pore size = 0.2 μm	Motian Polytechnic Group	Young and Xu, 2008
Flat-sheet	Pore size = 0.4 μm	-	Scheumann and Kraume, 2009
Hollow fiber	Polyvinyl difluoride Pore size = 0.4 μm	-	Kim et al., 2009
Flat-sheet	Polyolefin Pore size = 0.4 μm	Kubota	Huelgas and Funamizu, 2010

2.3.4 Membrane Fouling and Fouling Control

Membrane fouling in MBRs is indicated by either a sudden trans-membrane pressure (TMP) rise at constant flux operation or a sudden flux decrease at fixed TMP operation. Membrane fouling is inevitable as foulants (e.g., inorganic scales, microorganisms, particulates and organic matter) accumulate on the membrane surface (Schafer et al., 2004) and within membranes pores. Fouling often brings about productivity losses, premature module replacement and sometimes effluent quality variation (Nghiem and Schafer, 2006). Although considerable research has been done about membrane fouling in MBRs used for drinking water and wastewater treatment, few studies have been carried out specifically on membrane fouling in GW treatment, suggesting that it is not well investigated.

Pidou et al. (2009) studied the relationships among product type, dose, UV irradiation time and fouling rates in an MCR used for GW treatment. In their investigation on fouling rates under different combinations of product types, dosages and illuminations, rapid fouling occurred only with shower gels and conditioners. In another

study of using direct ultrafiltration (UF) to treat GW, it was found that increasing particulate matter concentrations led to a thicker cake layer, whose hydraulic resistance depended on calcium and organic matter (Nghiem et al., 2006). While fouling had a positive linear correlation with organic matter concentration, it might increase tremendously with a small amount of calcium. Based on the research of comparing wastewater and GW in UF following biological treatment, Lodge et al. (2004) found similar fouling behaviors. They further attributed the difference to a higher SS concentration in wastewater treatment. However, Liu et al. (2005) observed a slightly deposited cake layer and a heavily developed gel layer on the membrane's outer surface; while the fouling of the membrane's inner surface was caused by attachment of micro-organisms. The discrepancy could be explained by the different origins of GW used in these two studies. GW in the latter was bath wastewater with a high content of anionic surfactants.

Since membrane fouling is inevitable, fouling control is important to minimize the cost associated with frequent physical and chemical cleaning. In the A^2O-MF-OP system studied by Kim et al. (2009), fouling of the MF membrane hardly occurred because suspended solids were removed effectively by the A^2O process. Less than 5 Pa of pressure development was observed for the MF unit (8 L/m^2-h, LMH) in the combination of a biofilter and a submerged membrane system (Kitiphatmontree et al., 2009), suggesting negligible fouling. The reason might also likely be the retention of solids (DOC in the case) in the GAC unit.

Different fouling phenomena were reported about MCRs in GW treatment. Rivero et al. (2006) observed very little or no fouling when the MCR pilot plant was operated in

a batch mode with fluxes up to 120 LMH. While Pidou et al. (2008a, b) found that a chemical cleaning was necessary after only 10 days of operation at a flux of 5 LMH in a continuous mode. The contradictory might be due to the fact that GW was rapidly treated for the higher fluxes and TiO_2 was dispersed in fairly clean water, which resulted in very little or no fouling (Pidou et al., 2009).

2.4 Application of Shredded Tires in Water Quality Protection

U.S. EPA estimated that approximately 290 million scrap tires were generated in the U.S. at the end of 2003 (USEPA, 2005). The latest data from the Rubber Manufacturers Association (RMA) showed that about 4595.7 thousand tons of tires were generated in the U.S. in 2007. This enormous amount of tires makes their disposal a predicament. The disposal of scrap tires, on the other hand, also causes many other issues, like breeding grounds for mosquitoes, fire threat, public health hazard, etc. (Sullivan, 2006; Jang et al., 1998). Thus, the temptation of scrap tire reuse is great.

Currently, scrap tires find their market in tire-derived fuel (54%), ground rubber application (17%), and civil engineering (road, landfill construction, etc., 12%), and the remaining 17% (at least 128 million) were still in stockpiles at the end of 2007 (RMA, 2009). Other than the application of landfills in civil engineering, shredded tires have also been used to treat wastewater and protect water quality (Tang et al., 2006; Shin et al., 1999; Park et al., 1996).

Park et al. (1996) studied the sorption property of tire chips, and concluded that tire chips had a relatively high organic compound sorption capacity (1.4-5.6% of that for granular activated carbon on a volume basis), which could reduce the amounts in the

leachate liquid. Kershaw and Pamukcu (1997) also found that ground rubber was effective at removing benzene, toluene, ethylbenzene, and xylenes from water, albeit 10 times less effective as activated carbon. Combining shredded-tire particles for absorption and sodium silicate for encapsulation is a promising method for immobilization of volatile organic compounds (VOCs) in soil (Arocha et al., 1996). Oh et al. (2009) investigated the effects of ground tire rubber (GTR) and other adsorptive materials on the biofilter performance of removing toluene; they did not observe significant improvement for the compost/GTR mixture due to the low toluene adsorption capacity and the difficulty in maintaining optimal moisture content. The kinetics of anaerobic digestion of cane molasses distillery slops was investigated by Borja et al. (1996), using a continuous-flow bioreactor which contained waste tire rubber as support. It showed that microorganisms could become immobilized onto the shredded tires. Shin et al. (1999) used scrap tire chips as packing material for sequential anaerobic-aerobic biofilm reactors to remove persistent chlorinated hydrocarbons, and reported that shredded tires might be an economical biofilter medium. Tang and co-workers used crumb rubber filtration to treat ballast water, and studied the effects of media size, filter depth, filtration rate, temperature, turbidity, and running time on its performance (Tang et al., 2006a, 2006b, 2009). They found that a substantial reduction in turbidity, particles, phytoplankton and zooplankton in ballast water was achieved, and media size had the most significant influence on the removal efficiency. They also found that crumb rubber filtration had the potential to be used as a primary treatment technology prior to secondary processes. Mondal et al. (2007) compared the performance of trickling filters packed with tires of two different sizes (1.5 to 6.5 and 12 to 50 mm, respectively) for removal of BOD_5, COD,

ammonia nitrogen and suspended solids from synthesized leachate. It was observed that the trickling filter with smaller tires displayed a more consistent organic removal. Recently, the first field-scale constructed wetland with tire-chip media has been put into practice in Fisherman Bay Sewer District (Lopez Island, Wash.) to remove algae in the effluent from a preceding lagoon (Li and Holmes, 2010). For the last two year's operation, plant effluent has consistently met the state's Class D reclaimed-water standards.

Shredded tires also adsorb metals. Ground rubber was found to be more effective at removing inorganic mercury (95%) than methyl mercury (70%) when mixed with water containing either mercury (Ramamoorthy and Miller, 1979). Most metals in contaminated soil absorbed onto shredded tires more effectively under basic conditions, except for elementary mercury which bound more tightly at acidic to neutral pH than at basic pH (Meng et al., 1998). Netzer et al. (1974) reported greater than 99% removal rates for various metals (Cd, Al, Cu, Zn, etc.) at different pH ranges. These studies indicate that the adsorption of metals to tire chips is a function of pH.

It was concluded that scrap tires did not contaminate the environment by leaching contaminants, since the concentrations of the contaminants were all below the regulatory limits by the USEPA (U.S. House of Representatives, 1990). In the recent leaching tests of crumb rubber by Mays et al. (2011), however, zinc concentrations in many of their experiments exceeded the more stringent stream discharge standard of 0.117 mg/L. Although none of the results were above the EPA maximum contaminant level (MCL) of 5 mg/L, of which the level is considered safe for human consumption but not for aquatic habitats. They suggested mixing the tire crumb rubber with another granular medium which would absorb zinc leached from the tire chips.

2.5 Summary

Reviewed in this chapter are GW/RW reclamation, membrane technology in GW/RW reclamation and shredded tires in the cause of water quality protection. GW/RW is an excellent water source for water reuse in terms of quality and quantity. Membrane processes, especially MBRs, proved their competence in reclaiming GW/RW, and should play an important role in the application. With the enormous amount of scrap tires generated each year, the disposal of them becomes an pressing issue. The review indicates that if handled properly (in the case of metal leaching from tires), tire shreds may be a feasible and economic packing material for the purpose of protecting water quality in constructed wetlands, bio-retention basins, biological filters, etc.

2.6 References

Abegglen, C., Ospelt, M., and Siegrist, H. (2008). "Biological nutrient removal in a small-scale MBR treating household wastewater." *Wat. Res.*, 42(1–2), 338–346.

Abegglen, C., Joss, A., McArdell, C.S., Fink, G., Schlusener, M.P., Ternes, T.A., and Siegrist, H. (2009). "The fate of selected micropollutants in a single-house MBR." *Wat. Res.*, 43(7), 2036–2046.

Arocha, M.A., McCoy, B.J., and Jackman, A.P. (1996). "VOC immobilization in soil by adsorption, absorption and encapsulation." *J. Haz. Materials*, 51, 131–149.

Asano, T., Burton, F.L., Leverenz, H.L., Tsuchihashi, R., and Tchobanoglous, G. (2007). *Water Reuse: Issues, Technologies, and Applications*. 3rd ed., *Metcalf & Eddy*, McGraw-Hill, New York

AWWA (American Water Works Association) (1994). *Dual Distribution Systems*. AWWA Manual M24 (2nd ed.), Denver, CO.

AWWARF (American Water Works Association Research Foundation) (1999). *Residential End Use of Water*. Denver, CO.

Berlin Senate Department of Urban Development (Senatsverwaltung für Stadtentwicklung) (2003). Innovative Wasserkonzepte: Betriebswassernutung in Gebäuden. Berlin, 2003.

Borja, R., Sanchez, E., Martin, A., and Jimenez, A.M. (1996). "Kinetics behaviour of waste tyre rubber as microorganism support in an anaerobic digester treating cane molasses distillery slops." *Bioproc. Eng.*, 16, 17–23.

Canada Mortgage and Housing Corporation (2004). *Water Reuse Standards and Verification Protocol*. Research Report 1611–06, CHMC, Ottawa.

Chang, Y., Wagner, M., and Cornel, P. (2007). "Treatment of grey water for urban water reuse." *Proceedings of the Advanced Sanitation Conference*, 32/1–32/10, Aachen, Germany, 2007.

Dallas, S., Scheffe, B., and Ho, G. (2004). "Reed beds for greywater treatment—case study in Santa Elena-Monteverde, Costa Rica, Cental America." *Ecolog. Eng.*, 23, 55–61.

Dorfler, U., and Scheunert, I. (1997). "S-triazine herbicides in rainwater with special reference to the situation in Germany." *Chemosphere*, 35, 77–85.

Edwards, K., and Martin, L. (1995). "A methodology for surveying domestic water consumption." *J. Chart. Inst. Water. E.*, 9, 477–488.

Eriksson, E., Auffarth, K., Henze, M., and Ledin, A. (2002). "Characteristics of grey wastewater." *Urban Water*, 4, 85–104.

Eriksson, E., Auffarth, K., Eilersen, A.M., Henze, M., and Ledin, A. (2003). "Household chemicals and personal care products as sources for xenobiotic organic compounds in grey wastewater." *Water SA*, 29, 135–146.

EU Directive for Bathing Water (2006). Council Directive of 15 February 2006 concerning the management of bathing water quality and repealing Directive 76/160/EEC. Jo L 64, 4.3.2006.

Fan, S., Urbain, V., and Qian, Y. (2000). "Nitrification in a membrane bioreactor (MBR) for wastewater treatment." *Water Sci. Technol.*, 42, 289–294.

Fane, A.G., and Fane, S.A. (2005). "The role of membrane technology in sustainable decentralized wastewater systems." *Wat. Sci. Tech*., 51, 317–325.

fbr Information Sheet H 201 (2005). *Greywater Recycling: Planning fundamentals and operation information*. Rainwater Harvesting and Water Utilisation Association (fbr), Darmstadt, Germany.

Friedler, E., and Hadari, M. (2006). “Economic feasibility of on-site grey water reuse in multi-storey buildings.” *Desalination*, 190, 221–234.

Friedler, E., Kovalio, R., and Galil, N.I. (2005). “On-site graywater treatment and reuse in multi-storey buildings.” *Wat. Sci. Tech.*, 51, 187–194.

Halperin, R., and Aloni, U. (2003). *Standards for Treated Wastewater Reuse in the City, for Recreation and in Industry*. (in Hebrew) Ministry of Health, Jerusalem, Israel.

Han, M.Y., and Mun, J.S. (2007). “Particle behavior consideration to maximize the settling capacity of rainwater storage tanks.” *Water Sci. Technol.*, 56, 73–79.

Han, M.Y., Park, S.W., Kim, H.R., and Kim, S.R. (2006). “Analysis of rainwater quality in rainwater harvesting system at dormitories in Seoul National University, Seoul, Korea.” *Proceedings of the 2nd International Rainwater Harvesting Workshop*, Beijing, China, pp 243–253.

Helmreich, B., and Horn, H. (2009). “Opportunities in rainwater harvesting.” *Desalination*, 248, 118–124.

Hiessl, H., Walz, R., and Toussaint, D. (2001). “Design and sustainability assessment of scenarios of urban water infrastructure systems.” In: Management UoDFoTa (ed.), *Proceedings of Critical Infrastructures*. Delft, Utrecht: Lemma.

Hu, B. (2002). “The most optimal retention time for GW bio-chemical treatment.” *Huanjing Wuran Zhili Jishu Yu Shebei*, 3, 30–31.

Huang, C.P., Dong, C., and Tang, Z. (1993). “Advanced chemical oxidation: its present role and potential future in hazardous waste treatment.” *Waste Management*, 13, 361–377.

Huelgas, A., and Funamizu, N. (2010). “Flat-plate submerged membrane bioreactor for the treatment of higher-load graywater.” *Desalination*, 250, 162–166.

Jang, J.W., Yoo, T.S., Oh, J.H., and Iwasaki, I. (1998). “Discarded tire recycling practices in the United States Japan and Korea.” *Resources, Conserv. Recycl.*, 22, 1–14.

Jefferson, B., Burgess, J.E., Pichon, A., Harkness, J., Judd, S.J. (2001). “Nutrient addition to enhance biological treatment of GW.” *Wat. Res*., 35, 2702–2710.

Kershaw, D.S. and Pamukcu, S. (1997). “Use of ground tire rubber in reactive permeable barriers to mitigate BTEX compounds.” in Wasemiller, M.A. and Hoddinott, K.B. (eds.). Testing soil mixed with waste or recycled materials, ASTM STP 1275. American Society for Testing and Materials. pp.314–329.

Kim, J., and Somiya, I. (2002). "Innovative fouling control by intermittent back-ozonation in metal membrane micro filtration system." *The 3rd World Water Congress*, Melbourne, Australia.

Kim, R., Lee, S., and Kim, J. (2005). "Application of a metal membrane for rainwater utilization: filtration characteristics and membrane fouling." *Desalination*, 177, 121–132.

Kim, R., Lee, S., Jeong, J., Lee, J., and Kim, Y. (2007). "Reuse of greywater and rainwater using fiber filter media and metal membrane." *Desalination*, 202, 326–332.

Kim, J., Song, I., Oh, H., Jong, J., Park, J., and Choung, Y. (2009). "A laboratory-scale graywater treatment system based on a membrane filtration and oxidation process-characteristics of graywater from a residential complex." *Desalination*, 238, 347–357.

Kitiphatmontree, N.A., Duangduen, J.K., and Vigneswaran, S.P. (2009). "Submerged membrane system with biofilter as a treatment to rainwater." *Water Air Soil Pollut: Focus*, 9, 431–438.

Lazarova, V. (2001). "Role of water reuse in enhancing integrated water management in Europe." *Final Report of the EU project CatchWater*, V. Lazarova (Ed.), ONDEO, Paris, France, pp. 708.

Lee, B., Kim, H., and Lee, J. (2003). "Effects of acid rain on coatings for exterior wooden panels." *J. Indust. Eng. Chemi.*, 9, 500–507.

Lesjean, B., and Gnirss, R. (2006). "Grey water treatment with a membrane bioreactor operated at low SRT and low HRT." *Desalination*, 199, 432–434.

Lévesque, B., Pereg, D., Watkinson, E., Maguire, J.S., Bissonnette, L., Gingras, S., Rouja, P., Bergeron, M.G., and Dewailly, É. (2008). "Assessment of microbiological quality of drinking water from household tanks in Bermuda." *Can. J. Microbiol.*, 54, 495–500.

Li, F., Wichmann, K., and Otterpohl, R. (2009). "Evaluation of appropriate technologies for grey water treatments and reuses." *Wat. Sci. Technol.*, 59, 249–260.

Li, W., and Holmes, G. (2010). "A new life for old tires: Constructed wetland with shredded-tire chips produces consistently high quality lagoon effluent." *Water Environment & Technology Magazine*, 22, 48–53.

Liu, R., Huang, X., Chen, L., Wen, X., and Qian, Y. (2005). Operational performance of a submerged membrane bioreactor for reclamation of bath wastewater. *Process Biochem.*, 40, 125–130.

Lodge, B., Judd, S.J., and Smith, A.J. (2004). "Characterisation of dead-end ultrafiltration of biotreated domestic wastewater." *J. Membr. Sci*., 231, 91–98.

Magyar, M.I., Mitchell, V.G., Ladson, A.R., and Diaper, C. (2007). "An investigation of rainwater tanks quality and sediment dynamics." *Water Sci. Technol.*, 56, 21–28.

Magyar, M.I., Mitchell, V.G., Ladson, A.R., and Diaper, C. (2008). "Lead and other heavy metals common contaminants of rainwater tanks in Melbourne." *Proceedings of Water Dome*, 2008, 409–417.

Mars, R., (2004). "Case studies of graywater recycling in Western Australia." *Proceedings of the 1st International Conference on Onsite Wastewater Treatment and Recycling*, Fremantle, CD-rom.

Mays, D., Ren, Z.J., and Phodes, E.P. (2011). "Colorado Department of Public Health and Environment Advanced Technology Fund Research Grant Final Evaluation Report." Denver, CO. Available at http://www.cdphe.state.co.us/oeis/p2_program/presentations/ucd-atg.pdf (accessed June, 2011).

Meng, X., Hua, Z., Dermatas, D., Wang, W., and Kuo, H.Y. (1998). "Immobilization of mercury (II) in contaminated soil with used tire rubber." *J. Haz. Materials*, 57, 231–241.

Merz, C., Scheumann, R., Hamouri, B. E., and Kraume, M. (2007). "Membrane bioreactor technology for the treatment of graywater from a sports and leisure club." *Desalination*, 215, 37–43.

MLIT (Ministry of Land, Infrastructure and Transport, Japan) (2005). *Gesui-syorisui-no Sairiyou Suishitsukijun-tou manyuaru (in Japanese) (Guidelines for the Reuse of Treated Wastewater)*, MLIT, Japan.

Mondal, B., Warith, M.A., and Burns, S.D. (2007). "Comparison of Shredded Tire Chips and Tire Crumbs as Packing Media in Trickling Filters." *Water Qual. Res. J. Canada*, 42 (4), 319–326.

Morel, A., and Diener, S. (2006). "Grey water management in low and middle-income countries." *Water and Sanitation in Developing Countries (Sandec)*, Eawag, Swiss Federal Institue of Aquatic Science and Technology.

Mwenge Kahinda, J., Taigbenu, A.E., and Boroto, J.R. (2007). "Domestic rainwater harvesting to improve water supply in rural South Africa." *Phys. Chem. Earth*, 32, 1050–1057.

Netzer, A., Wilkinson, P., and Beszedits, S. (1974). "Removal of trace metals from wastewater by treatment with lime and discarded automotive tires." *Wat. Res.*, 8, 813–817.

Nghiem, L.D., Oschmann, N., and Schafer, A.I. (2006). "Fouling in graywater recycling by direct ultrafiltration." *Desalination*, 187 (1–3) 283–290.

Nghiem, L.D., and Schafer, A.I. (2006). "Fouling autopsy of hollow-fibre MF membranes in wastewater reclamation." *Desalination*, 188, 113–121.

Nolde, E. (1999). "GW reuse systems for toilet flushing in multi-storey buildings-over ten years experience in Berlin." *Urban Water*, 1 (4), 275–284.

Oh, D.I., Song, J., Hwang, S.J., and Kim, J.Y. (2009). "Effects of adsorptive properties of biofilter packing materials on toluene removal." *J. Haz. Materials*, 170, 144–150.

Okun, D.A. (2005). "Dual systems to conserve water while improving drinking water quality." 20th Annual WaterReuse Symposium, Denver, CO.

Palmquist, H., and Hanæus, J. (2005). "Hazardous substances in separately collected grey and blackwater from ordinary Swedish households." *Sci. Total Environ.*, 384, 151–163.

Paris, S., and Schlapp, C. (2010). "Graywater recycling in Vietnam-Application of the HUBER MBR process." *Desalination*, 250, 1027–1030.

Park, J.K., Kim, J.Y., and Edil, T.B. (1996). "Mitigation of organic compound movement in landfills by a layer of shredded tires." *Water Environ. Res.*, 68(1), 4–10.

Pidou, M., Memon, F.A., Frazer-Williams, R., Jeffrey, P., Stephenson, T., and Jefferson, B. (2008a). "Technologies for urban water recycling." *Water Pract. Technol.*, doi:10.2166/wpt.2008.046.

Pidou, M., Autin, O., Battrick, C., Macadam, J., Jefferson, B., and Parsons, S.A. (2008b). "Membrane chmical reactor for the treatment of industrial effluents." *Proceedings of MWDI 2008 Conf. on Membranes for Drinking Water Production and Wastewater Treatment*, Oct. 20–22, 2008, Toulouse, France, PP.4.

Pidou, M., Memon, F.A., Jeffrey, P., Stephenson, T., and Jefferson, B. (2007). "Greywater recycling: treatment options and applications." *Proceedings of the Institute of Civil Engineers: Engineering Sustainability*, 160, 119–131.

Pidou, M., Parsons, S.A., Raymond, G., Jeffrey, P., Stephenson, T., and Jefferson, B. (2009). "Fouling control of a membrane coupled photocatalytic process treating greywater." *Wat. Res.*, 43, 3932–3939.

P.R. China Ministry of Construction (1989). *Water quality standards for water reclamation*. CJ 25.1-89. Beijing, China.

Queensland Government (2003). *Guidelines for the Use and Disposal of GW in Unsewered Areas.* Queensland Government Local Government and Planning, Brisbane, Australia.

Ramamoorthy, S. and Miller, D.R. (1979). "Removal of mercury and methylmercury from waste waters by sorption." *Bulletin of Environ. Contam. Toxi.*, 22, 196–201.

Reimann, C., Caritat, P.D., and Halleraker, J.H. (1997). "Rainwater compostion in eight arctic catchment in northern Europe (Finland, Norway, and Russia)." *Atmos. Environ.*, 31, 159–170.

Rivero, M.J., Parsons, S.A., Jeffrey, P., Pidou, M., and Jefferson, B. (2006). "Membrane chemical reactor (MCR) combining photocatalysis and microfiltration for grey water treatment." *Water Sci. Technol.*, 53, 173–180.

RMA (2004). "State legislation – scrap tire disposal Nov. 2004." Rubber Manufacturers Association, Washington, D.C.

RMA (2009). "Scrap Tire Markets in the United States: 9th Biennial Report." Rubber Manufacturers Association, Washington, D.C.

Schafer, A., Andritsos, N., Karabelas, A.J., Hoek, E.M.V., Scheider, R., and Nystrom, M. (2004). "Fouling in nanofiltration." In: *Nanofiltration–Principles and Applications*, Schafer, A., Waite, D., and Fane, A. (eds.), Elsevier, 169–239.

Scheumann, R., and Kraume, M. (2009). "Influence of hydraulic retention time on the operation of a submerged membrane sequencing batch reactor (SM-SBR) for the treatment of GW." *Desalination*, 246, 444–451.

Schmidt, I., Sliekers, O., Schmid, M., Bock, E., Fuerst, J., Kuenen, J.G., Jetten, M.S., and Strous, M. (2003). "New concepts of microbial treatment processes for the nitrogen removal in wastewater." *FEMS Microbiol. Rev.*, 27, 481–492.

Scott, J.A., and Smith, K.L. (1997). "A bioreactor coupled to a membrane to provide aeration and filtration in ice-cream factory wastewater remediation." *Wat. Res.*, 31 (1), 69–74.

Shin, H., Yoo, K., and Park, J. (1999). "Removal of polychlorinated phenols in sequential anaerobic-aerobic biofilm reactors packed with tire chips." *Water Environ. Res.*, 71, 363–367.

Shirley-Smith, C. (2005). "The sustainability value of the green roof water recycling system in urban communities." *WATERSAVE Network Event*, Available at http://www.watersave.uk.net/Presentations/Chris_Shirley-Smith.pdf (accessed Nov., 2010).

Stephenson, T., Judd, S., Jefferson, B., and Brindle, K. (2000). *Membrane Bioreactors for Wastewater Treatment.* IWA publishing (2nd ed.), London.

Sullivan, J.P. (2006). "An assessment of environmental toxicity and potential contamination from artificial turf using shredded or crumb rubber." Turfgrass Producers International, East Dundee, IL. Available at http://www.ardeacon.com/pdf/Assessment_Environmental_Toxicity_Report.pdf (accessed June, 2011).

Surendran, S., and Wheatley, A.D. (1998). "Greywater reclamation for non-potable reuse." *J. CIWEM*, 12, 406–413.

Tajima, A., Yoshizawa, M., Sakurai, K., and Minamiyama, M. (2007). "Establishment of guidelines for the reuse of treatment wastewater." Available at http://www.niph.go.jp/soshiki/suido/pdf/h19JPUS/Abstract/r12.pdf (accessed June, 2011).

Tang, Z., Butkus, M.A., and Xie, Y.F. (2006a). "Crumb rubber filtration: A potential technology for ballast water treatment." *Marine Environ. Res.*, 61, 410–423.

Tang, Z., Butkus, M.A., and Xie, Y.F. (2006b). "The Effects of Various Factors on Ballast Water Treatment Using Crumb Rubber Filtration: Statistic Analysis." *J. Environ. Eng. Sci.*, 23 (3), 561–569.

Tang, Z., Butkus, M.A., and Xie, Y.F. (2009). "Enhanced performance of crumb rubber filtration for ballast water treatment." *Chemosphere*, 74, 1396–1399.

U.S. Environmental Protection Agency (2005). *EPA Office of Compliance Sector Notebook Project: Profile of the Rubber and Plastic Industry, 2nd Edition*. USEPA, Report EPA/310-R-05-003, Washington, DC.

U.S. Environmental Protection Agency (2004). *Guidelines for Water Reuse*. USEPA, Report EPA/625/R-04/108, Washington, DC.

U.S. Environmental Protection Agency (1991). *Markets for Scrap Tires*. USEPA, Report EPA-530/SW-90-074A, Office of Solid Waste, Washington, D.C.

U.S. House of Representatives (1990). "Scrap tire management and recycling opportunities." Committee Small Business, Washington, D.C.

Young, S., and Xu, A. (2008). "Development and testing of a low sludge discharge membrane bioreactor for GW reclamation." *J. Environ. Eng. Sci*., 7, 423–431.

CHAPTER 3

THE COMBINATION OF SHREDDED TIRE BIOFILTERS AND MEMBRANE BIOREACTORS FOR GREYWATER RECLAMATION

3.1 Introduction

Water crisis has been more severe around the world. Water saving technologies and water reuse have been receiving more attention. With its low pollution level and representation of 60–70% of domestic wastewater, greywater (GW) serves an ideal source for water reclamation (Friedler et al., 2005). Membrane bioreactor (MBR) technology is promising in GW reclamation because 1) it can produce treated water that satisfies the criteria set by the U.S. Environmental Protection Agency (USEPA) for water reuse; 2) it fits any plant sizes ranging from a single house to a whole community; and 3) its nature of physical filtration adds to the stability of treatment systems (Fane and Fane, 2005). Membrane fouling, however, still remains the hindrance of wide application of the technique.

On the other hand, millions of scrap tires are discarded and stockpiled each year (USEPA, 1991). It not only causes a disposal problem, but also imposes a health hazard to the public. Shredded tires have been proposed to be used as a substitute medium for a leachate collection system (Park et al., 1996), and a drainage material in cover systems for abandoned landfills (Reddy et al., 2010). Tang et al. (2006) applied crumb rubber filtration for ballast water treatment. Scrap tires are not found to contaminate the environment by leaching contaminants, as the concentrations of the contaminants were all below the regulatory limits of the USEPA (U.S. House of Representatives, 1990). Shin et al. (1999) proposed that shredded tires could be used as an economical biofilter medium.

The objectives of this study are to: 1) evaluate the feasibility of using a biofilter filled with shredded tires (STB) as the medium and an MBR for GW treatment; 2) study the biofilm properties in STBs; and 3) investigate fouling mechanisms in MBRs.

3.2 Materials and Methods

3.2.1 Laboratory-scale STBs

This experiment was carried out in two phases at room temperature (24 ± 1°C). Phase 1 was designed to investigate the effect of hydraulic retention time (HRT) on the performance of STBs in treating GW. In Phase 2, the effect of the size of shredded tires (also called tire chips) was studied along with the performance of STBs and biofilm properties along the height of the filter column.

Three parallel STBs were designed to pre-treat synthesized GW without aeration prior to MBRs in Phase 1. Each STB consists of a filtration column, and feeding and effluent systems (Fig. 3.1). The filtration column is constructed from a transparent, 2.5-in. diameter acrylic pipe and has a total height of 15.5 in (excluding the height of the bottom chamber, which was 2 in). Sampling ports were arranged with an interval of 3 in, and the top port was 3.5 in below the cover. The columns were filled with shredded tires (3–4 mesh, measured filtration porosity of 0.53, Bruckman Rubber Co., Hastings, NE, USA; designated as Type B) to a height of 14.5 in. A summary of the shredded tires used in the investigation can be found in Table 3.1. The details of STB operating conditions are summarized in Table 3.2. The biofilters were inoculated with activated sludge for biofilm accumulation for 7 days, and then were fed continuously with artificial GW for the evaluation of their performance. The artificial GW was prepared according to Jefferson et

al. (2001) listed in Table 3.3. The flow pattern of the STBs was gravity flow. The outlets of the STBs were kept at 15 in. above the bottom of the column so that the STBs were full with GW throughout the study. Aluminum foil was used to wrap the column to prevent light penetration. The effluent of STBs was combined and used as the feed of the MBRs. Influent was prepared as per Table 3.2 in 10 L's, and only influent and effluent samples were taken weekly in this phase for the measurements of pH, turbidity and 5-Day biochemical oxygen demand (BOD_5). Phase 1 lasted for 172 days.

Table 3.1. Summary of the properties of shredded tires used in the study.

	Shredded tires in Phase 1	**Additional shredded tires in Phase 2**
Provider	Bruckman Rubber Co., Hastings, NE	BAS Recycling, Inc., San Bernardino, CA
Size (mesh)	3-4	30
Diameter (mm)	4.8-6.7	0.6
Designation	B	S
Porosity	0.53	0.49

Table 3.2. Operating conditions of STBs in Phase 1.

Reactor #	**Flowrate (mL/min)**	**HRT (h)**
STB-2	2.0	10.0
STB-4	4.0	5.0
STB-8	8.0	2.5

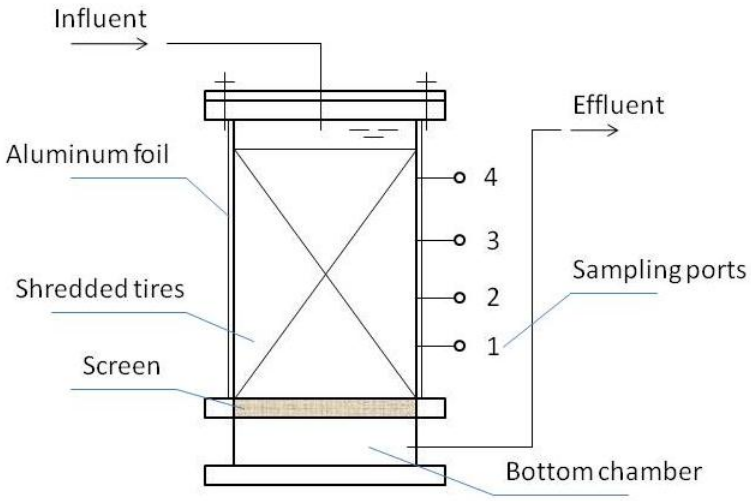

Figure 3.1. A schematic diagram of an STB.

In Phase 2, STB-4 (HRT = 5 h) was stopped, and a 4th STB was added with the same configuration. These two STBs were filled with shredded tires of a smaller size (30 mesh, measured filtration porosity of 0.49, BAS Recycling, Inc., San Bernardino, CA, USA; designated as Type S). Subsequently, the two biofilters were inoculated with activated sludge for biofilm accumulation for 7 days, and then were fed continuously with artificial GW. During the inoculation and thereafter, the other two STBs were kept under the same operating conditions, i.e., HRTs = 2.5 h and 10 h, respectively. The recently inoculated STBs with smaller shredded tires were also operated at HRTs for STBs with 3-4 mesh shredded tires. The operating conditions of the four STBs in this phase are listed in Table 3.4. For the sake of convenience, synthetic GW was prepared in 50 L bottles in this period, and the prepared GW was settled for 1-2 days before use. The amounts of synthetic soap and hair shampoo were increased by more than four times compared to that in the original recipe upon personal communication with Dr. Bruce

Jefferson. Besides the influent and effluent samples (influent samples were taken randomly), water samples from the four sampling ports were also taken to assess the performance of STBs along the height of the column. Samples for each sampling site were taken three times in the first two weeks, and less frequently thereafter until termination of the experiment. pH, turbidity and BOD_5 were measured. Dissolved oxygen (DO) was measured in the sampling ports. This phase was maintained for 136 days.

Table 3.3. Synthetic greywater recipe (Jefferson et al., 2001).

Item	**Quantity (made up with 10 L tap water)**
Synthetic soap	0.64 g
Hair shampoo	8.0 mL
Sunflower oil	0.1 mL
Secondary effluent	24.0 mL

Table 3.4. Operating conditions of STBs in Phase 2.

Reactor #	**Shredded Tire Size (mesh)**	**Flowrate (mL/min)**	**HRT (hr)**
STB-2-B	3-4	2	10
STB-8-B	3-4	8	2.5
STB-2-S	30	2	10
STB-8-S	30	8	2.5

3.2.2 Biofilm Sampling and Evaluation

The shredded tires in STBs were separated into four layers: those between the screen and Sampling Port 1 as Layer 1, those between Sampling Ports 1&2 as Layer 2, those between Sampling Ports 2&3 as Layer 3, and those from Sampling Port 3 to the top as

Layer 4 (see Fig. 3.1). For each biofilm analysis, ten shredded tire chips coated with biofilms were randomly collected from each of the four layers in each STB. It was achieved by first pouring out tire chips in the different layers consecutively, and then randomly selecting from those whose coatings were not compromised (i.e., tire chips with biofilm not touching the bench). The sampled tire chips were analyzed by the following steps: a) drained on an aluminum rack for 20 min; b) weighed both in air and water to determine the volume of the shredded tires before the removal of biofilms (Archimedes' method, assuming 1 g/mL for the density of water) (Taylor et al., 2006); c) vortexed in 20 mL deionized (DI) water for 1 min for three times, and removed from DI water; d) washed with 5 mL DI water; The suspensions in step c) were collected together with the wash water and were used to measure total solids (TS) and total volatile solids (TVS) as per the *Standard Methods* (APHA et al., 2005); e) after biofilm removal, the tire chips were drained on the aluminum rack for 20 min and weighed in both air and water to determine the total volume (V_T) of the 10 STB tire chips after biofilm removal; and f) the total volume of biofilms (V_B) attached on the 10 tire chips was calculated with the difference between the volumes determined before (Step b) and after biofilm removal (Step e). The same analytic scale was used for weighing.

Biofilm dry density can be calculated in the following equation (Tchobanoglous and Burton, 1991):

$$\frac{M_s}{D_d} = \frac{M_f}{D_f} + \frac{M_v}{D_v} \quad (1)$$

where D_d is dry density of biofilm (mg/cm^3 dry biomass); M_s is dry mass of solids in biofilm (mg); D_f is density of fixed mineral solids in biofilm (assuming 2.5 mg/cm^3); M_f is dry mass of fixed mineral solids in biofilm (mg); D_v is density of volatile solids in

biofilm (assuming 1.0 mg/cm^3); and M_v is dry mass of volatile solids in biofilm (mg). Wet density is obtained from equation (2) (Tchobanoglous and Burton, 1991):

$$\frac{1}{D_w} = \frac{W_{ds}}{D_d} + \frac{W_{tw}}{\rho_w} \quad (2)$$

where D_w is wet density of biofilm (g/cm^3 total biofilm); W_{ds} is dry solids content of biofilm (%); W_{tw} is water content of biofilm (including water both inside and outside of cells, %); and ρ_w is density of water (1 mg/cm^3). The equation for porosity calculation is modified from Zhang and Bishop (1994):

$$\varepsilon = \left(1 - \frac{V_w}{V_b}\right) \cdot 100 = \left(1 - \frac{M_s}{D_d} \cdot \frac{1}{(1 - W_{wi}) \cdot V_b}\right) \cdot 100 \quad (3)$$

where ε is porosity of biofilm (%); V_w is the volume of biofilm including water inside cells but excluding water outside of cells (cm^3); V_b is measured total biofilm volume (cm^3) (= volume of biofilm with water inside cells + volume of water outsdie of cells); and W_{wi} is water content inside cells (assuming 80%).

Biofilm thickness was calculated via dividing total biofilm volume (V_T) by the surface area (SA) biofilms possessed. SA was the product of the volume of sampled shredded tires and specific surface area (SSA) calculated from CT analysis (2.282 mm^2/mm^3 for 30 mesh shredded tires, and 1.449 mm^2/mm^3 for 3-4 mesh shredded tires, respectively).

3.2.3 MBRs

Four MBRs were constructed to further treat synthetic GW. In each MBR, a flat sheet membrane (type H-203, KUBOTA Membrane USA Co., Redmond, WA, USA) with a membrane area of 120 cm^2 was submerged in a 1.8-L container that was inoculated with activated sludge sampled from a local wastewater treatment plant. Air was supplied by an

air pump (30–80 GAL, Top Fin Air Pumps, PetSmart, Inc., Phoenix, AZ, USA) through an air stone. Both the feed solution (effluent of STBs in Phase 1) and permeate were pumped into and out of the MBR reactor by a peristaltic pump (Masterflex HV-07575-10; Cole Parmer, Vernon Hills, IL, USA). The trans-membrane pressure was monitored with a digital manometer (Cat. No.: 06-664-19, Thermo Fisher Scientific Inc., Pittsburgh, PA, USA). A schematic diagram of MBR is shown in Fig. 3.2. The solids retention time (SRT) of each MBR was controlled by wasting a corresponding volume of the activated sludge (AS) of the MBR (e.g., to achieve an SRT of 10 d, 10% AS was wasted daily). Descriptions of MBRs are detailed in Table 3.5. The four MBRs were operated for a total of 163 days (03/01/2010-05/12/2010, 07/12/2010-10/18/2010). Effluent was sampled weekly for the measurements of pH, turbidity and BOD_5. Fecal coliforms were measured randomly and immediately after sampling. The sludge was sampled periodically for the measurements of mixed liquor suspended solids (MLSS) and mixed liquor volatile suspended solids (MLVSS).

Table 3.5. Parameters and experimental conditions of MBRs.

Parameters	Descriptions
Membrane area	120 cm^2
Membrane pore size	0.4 µm
Flux	8 LMH (liter per square meter of membrane per hour)
Operating mode	30 min on and 30 min off
HRT	9.4 h
SRT	10, 20, 30, and 100 d

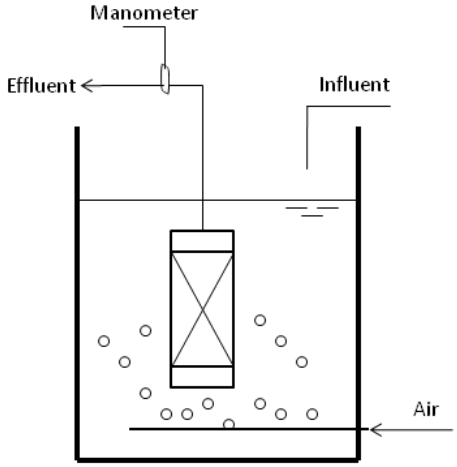

Figure 3.2. A schematic diagram of an MBR.

3.2.4 Analytical Methods

Analyses of liquid and sludge samples were performed in accordance with the *Standard Methods* (APHA et al., 2005). Turbidity was measured by a Hach Turbidimeter (2100N, Hach Co., Loveland, CO, USA). A pH meter (PC 510, OAKTON Instruments, Vernon Hills, IL, USA) was used for the measurement of pH. BOD_5 was measured as per Section 5210B using a DO probe (YSI 5010, YSI Inc., Yellow Springs, OH, USA) connected to a

DO meter (YSI 5100, YSI Inc., Yellow Springs, OH, USA). Fecal coliforms were detected according to Section 9222D. Sections 2540D and E were adopted to measure MLSS and MLVSS, respectively.

3.3 Results and Discussions

3.3.1 STBs

Despite various HRTs and tire sizes, STBs removed a certain amount of BOD_5 and turbidity. It indicates that STBs may be a feasible pretreatment for MBRs to decrease the air supply demand, and thus the cost of MBR operation.

Effect of HRT. The effect of HRTs on the performance of STBs treating GW was addressed in Phase 1. Fig. 3.3 shows the water quality profiles of raw GW and effluents from the three STBs under different HRTs. It can be seen that the increase of HRTs had a positive impact on the treatment of BOD_5 in STBs. As HRT increased from 2.5, 5 to 10 hrs, the removal efficiencies of BOD_5 increased from approximately 33.2, 54.9 to 71.0%, respectively (see Table 3.6).

Effluent turbidity also decreased as the HRT increased. The rise in turbidity of STB-8 (HRT = 2.5 hr) and STB-4 (HRT = 5 hr) might be due to the release of anionic surfactant since white suspended solids were observed in those samples. This might not necessarily imply biofilm sloughing from STBs as the corresponding BOD_5 level kept relatively constant.

Table 3.6. Summary of STB performance at different HRTs in Phase 1 (n = 29).

Paramter	Raw GW	HRT = 10 hr		HRT = 5 hr		HRT = 2.5 hr	
		Effluent	Removal efficiency, %	Effluent	Removal efficiency, %	Effluent	Removal efficiency, %
BOD_5, mg/L	114.5 ± 26.0	33.2 ± 20.8	71	51.7 ± 14.9	54.9	76.5 ± 15.4	33.2
Turbidity, NTU	85.4 ± 39.8	32.5 ± 29.4	62	54.0 ± 49.9	36.8	72.5 ± 48.3	15.1
pH	6.85 ± 0.35	7.15 ± 0.33	-	7.04 ± 0.34	-	6.95 ± 0.25	-

It should also be noted that the performance of STB-2 (HRT = 10 hr) was less dependent on the quality of raw GW. BOD_5 of effluents from the other two STBs fluctuated with that of raw GW (particularly apparent at the 70^{th} day). This may imply that as HRT was longer, the role of biofilms in treating GW became more significant.

Effect of tire size. The effect of tire size on the performance of STBs treating GW was investigated in Phase 2. The effluent profiles of BOD_5, turbidity and pH are shown in Fig. 3.4. Water qualities of raw GW were not monitered but randomly (once or twice a month) measured in this phase. BOD_5 of raw GW ranged from 164.1 to 381 mg/L depending on the time of the settlement of GW, and was generally higher than that in Phase 1 due to the change of the compositions of the GW. Compared with the performance in Phase 1, the effluent BOD_5 of the same two STBs (3-4 mesh shredded tires at HRTs of 2.5h and 10 h, i.e., STB-8-B and STB-2-B) was higher, likely because of the higher BOD_5 in raw GW. It indicates that STBs with 3-4 mesh shredded tires may be subject to the fluctuations of influent GW.

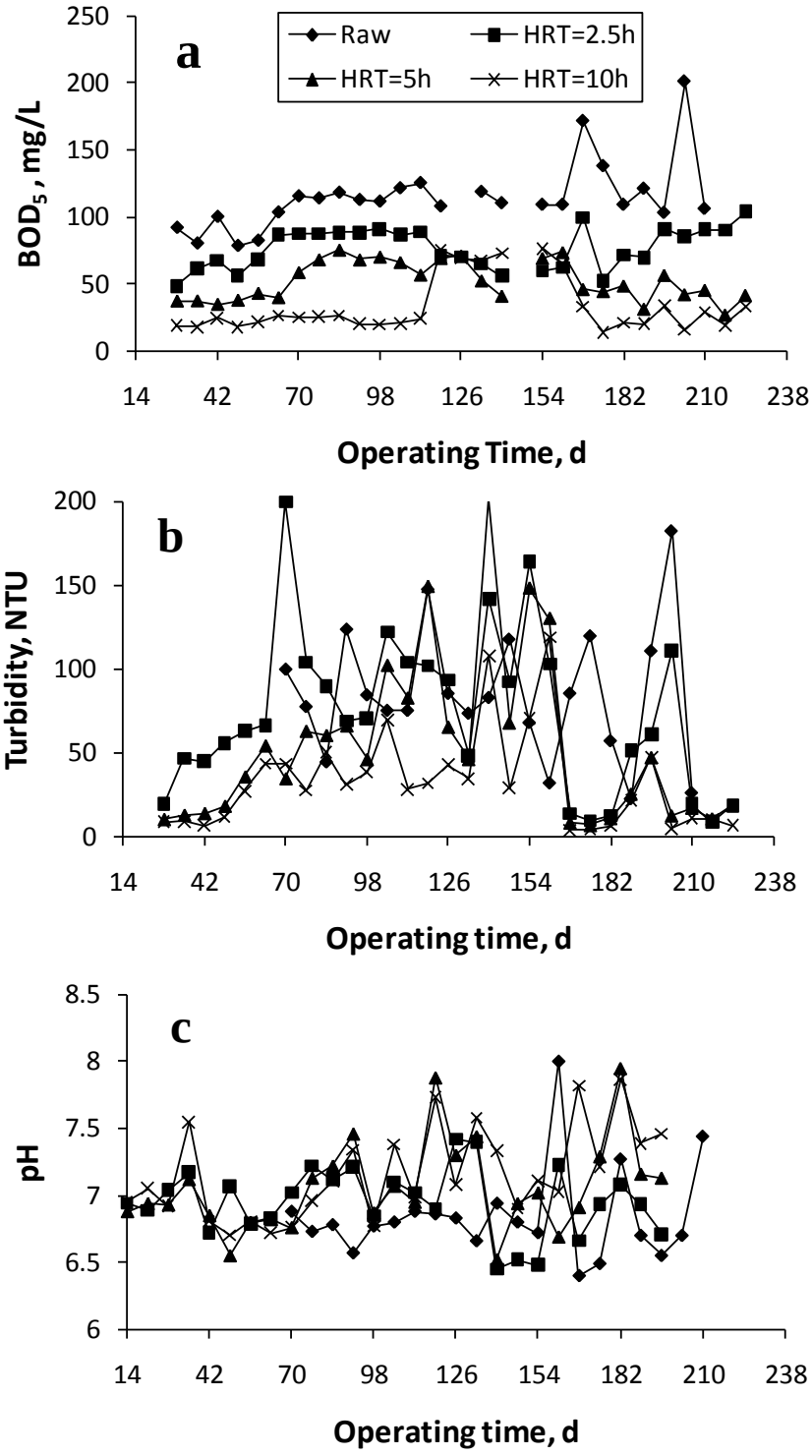

Figure 3.3. Water quality profiles of raw GW and STB effluents in Phase 1: a) BOD_5, b) turbidity, and c) pH.

From Day 65 to 95 in Phase 2, it can be inferred that the decrease in the size of shredded tires enhanced the performance of STBs in treating BOD_5. Mondal et al. (2007) also observed that the trickling filter with smaller tires displayed a more consistent organic removal when comparing the performance of trickling filters packed with tires of two different sizes (1.5 to 6.5 and 12 to 50 mm, respectively) for removal of BOD_5, COD, ammonia nitrogen and suspended solids from synthesized leachate. Sloughing might caused the increased BOD_5 from Day 95 to 105. The phenomenon of sloughing is primarily a function of the organic and hydraulic loading (Tchobanoglous et al., 2003). The increase of influent BOD_5 might be the reason for sloughing as it was measured to be 381 mg/L, which increased the organic loading by about 1.3 times.

The profiles of turbidity and pH for the effluents seemed interwining with one another, and one cannot conclude any statement on the effect of the size of shredded tires on the performance based on them.

Performance of STBs along the depth of the column. To investigate the effect of packing height of shredded tires on the performance of STBs, treated water sampls were also taken at the four sampling ports along the height of the STBs (see Fig. 3.1), and their water quality parameters measured. Fig. 3.5 shows their typical profiles of BOD_5, turbidity and DO. BOD_5 and turbidity of the treated water and the effluent stayed relatively constant for the STBs, except for HRT=2.5h-S (STB packed with 30-mesh shredded tires at HRT of 2.5 hrs), of which BOD_5 first increased instead. It implies that the degradation of BOD_5 mainly occurred in the top layer of tires. The increase of BOD_5 for HRT=2.5h-S might be due to the continuous, small-scale sloughing in plastic filters

(Tchobanoglous et al., 2003). The random increase of turbidity along the depth also showed this effect. As expected, DO decreased as GW moved through the filters. Although no air was supplied in the filters, the oxygen dissolved in the raw GW participated in the degradation of BOD_5.

Clogging of STBs. As a precaution for clogging due to algae, all STBs were wrapped with aluminum foil to prevent light penetration. In practical trickling filters where sunlight is available only in the upper reaches of the filter, algae can cause clogging of the filter surface, which may cause odors (Tchobanoglous et al., 2003). It is also anticipated that hair, cloth fibers and others in the real GW may clog the top layer of the filters. We proposed to use cloth filters to pre-screen those clogging material on the top of the filters. The experiment is under investigation.

3.3.2 Properties of Biofilm in STBs

The study of biofilm properties (densities, porosity, etc.) in STBs is essential for the identification of the significant components of biofilm structure, the proper interpretation of experimental results, the comprehension of the processes taking place within the biofilm, and the control of the performance of biofilm systems (Fruhen et al., 1989; Lawrence et al., 1991; Zhang and Bishop, 1994). As the effort herein was to assess whether shredded tires could be used as a packing material in filters, the purpose was to provide direct proof of the biofilm growth on the tires. Therefore, biofilm densities, porosity, and thickness were adopted as the criteria to evaluate the feasibility.

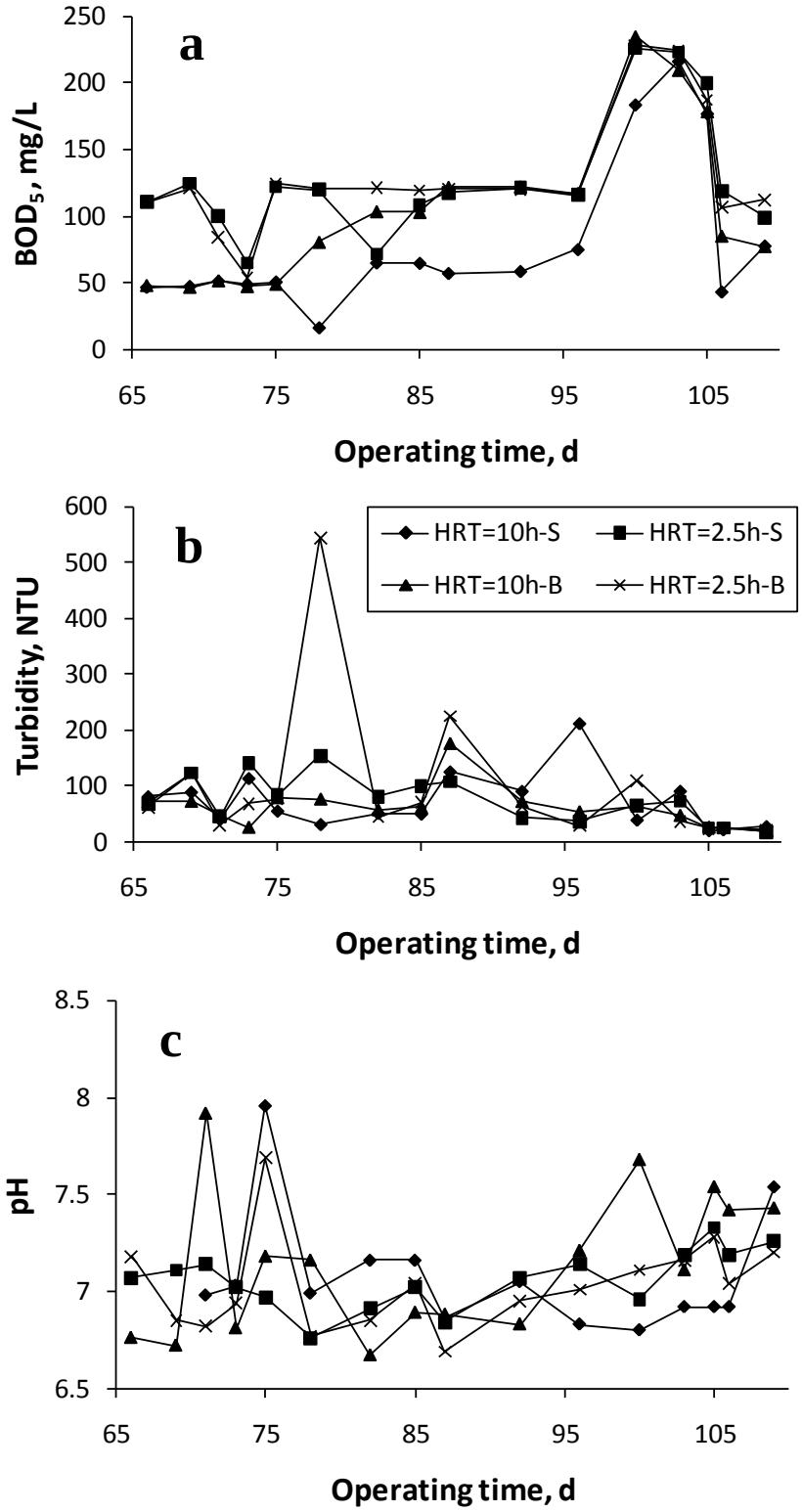

Figure 3.4. Water quality profiles of STB effluents in Phase 2: a) BOD5, b) turbidity, and c) pH.

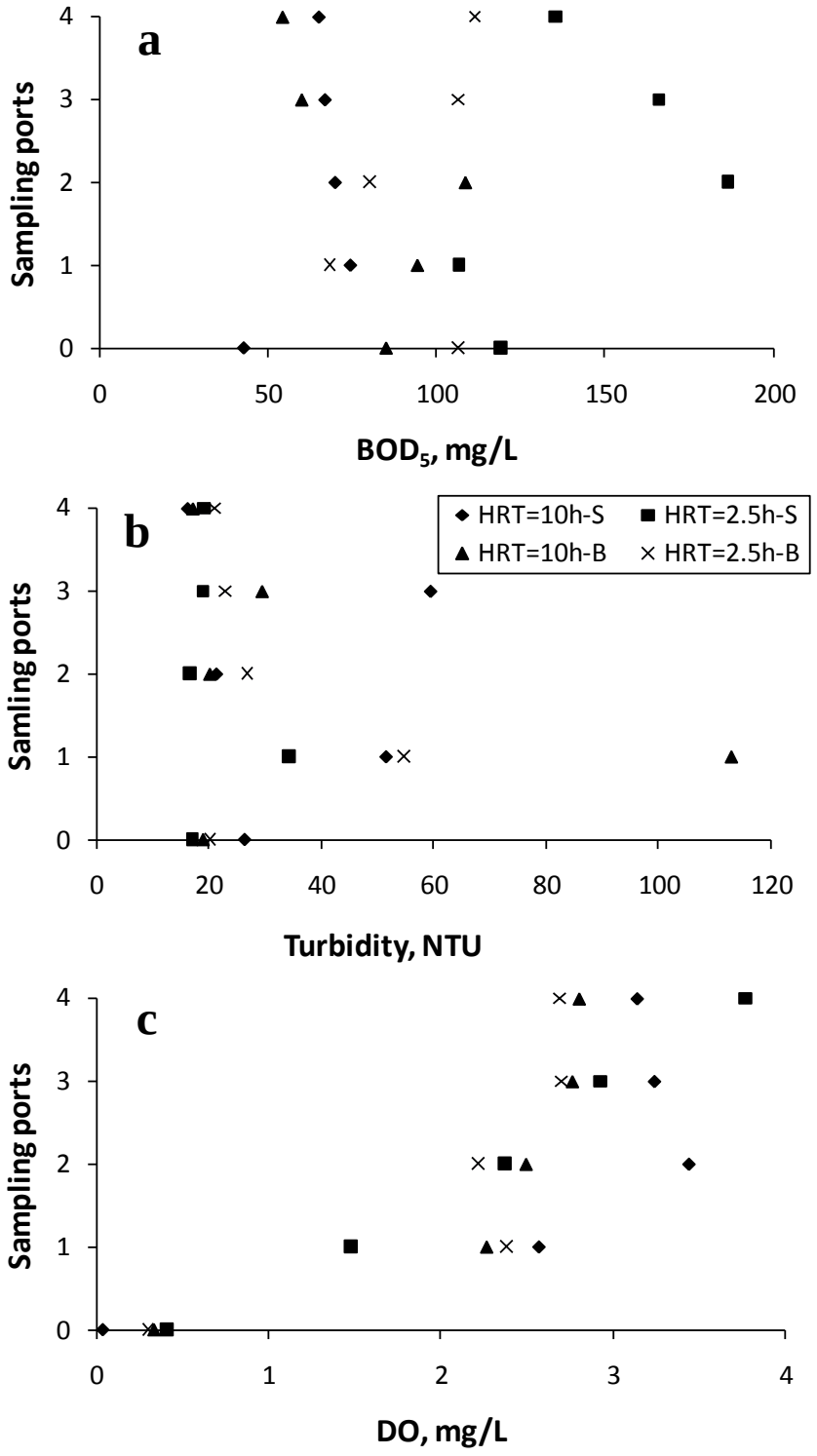

Figure 3.5. Water quality profiles of effluent (sampling port 0) and treated GW at different sampling ports (1-4, see Fig. 3.1): a) BOD_5, b) turbidity, and c) DO.

Fig. 3.6 shows typical profiles of the biofilm properties at different layers in the STBs in Phase 2. Generally, biofilm densities (wet and dry) decreased in the direction of the flow of GW in the STBs, and porosity increased. These were reasonable as the degradation of organic contents occurred most readily in the top layer (discussed earlier) and decreased towards the bottom layer, more bacterial activities happened in upper layers and more bacteria grew accordingly. This was also reflected in the biofilm thickness profile, which decreased from the top layer to the bottom layer.

Although these data did not carry any information on the proper interpretation of experimental results, the comprehension of the processes taking place within the biofilm, or the control of the performance of biofilm systems, they demonstrated that bacteria could attach on the shredded tires and grow, which indicates that shredded tires can be used as a packing material in biological filters.

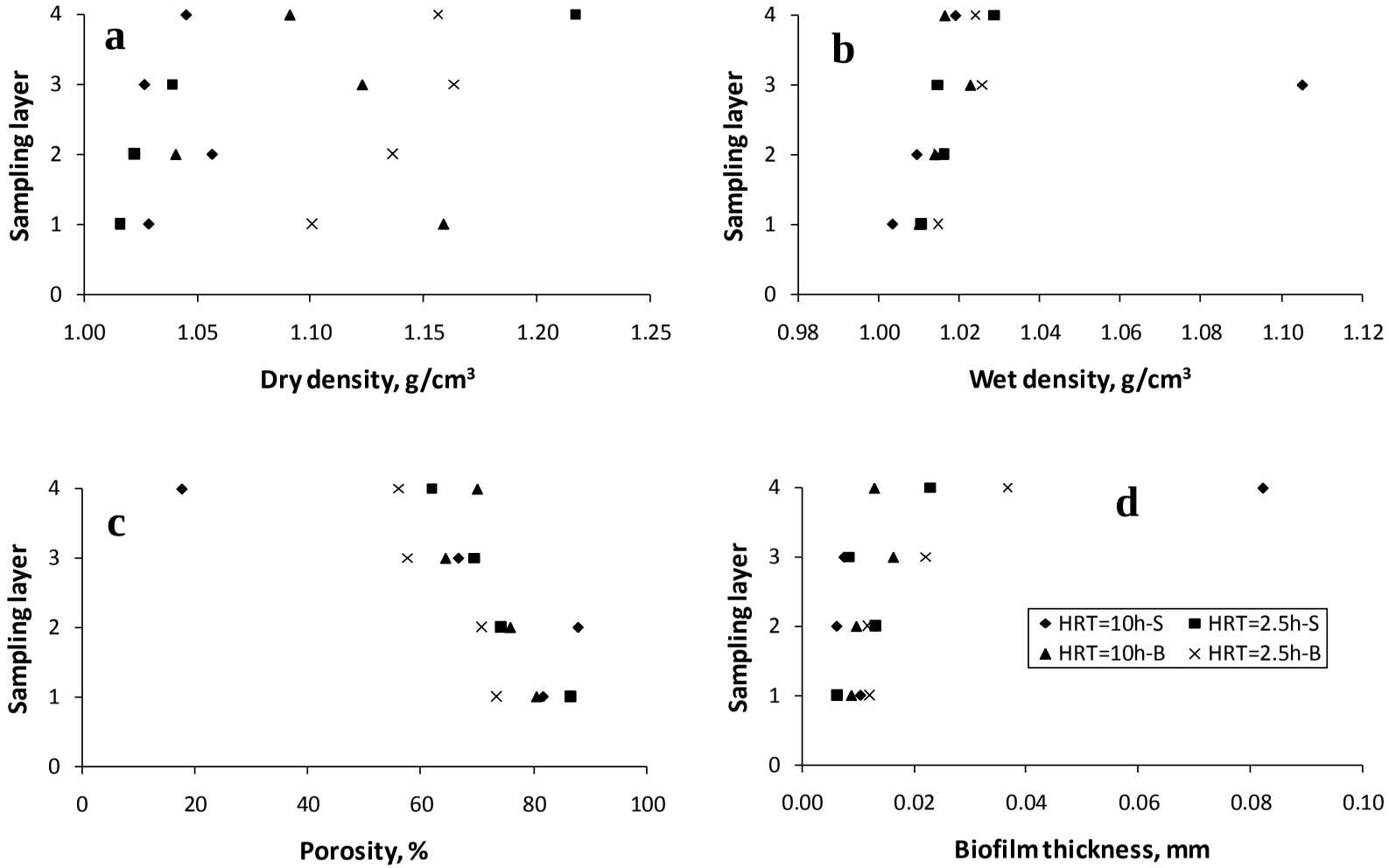

Figure 3.6. Biofilm properties at different layers in the STBs in Phase 2: a) dry density, b) wet density, c) porosity, and d) thickness.

3.3.3 MBRs

MBR operation and maintenance. All MBRs were operated under constant flux, continuous aeration, and intermittent filtration and feeding mode. Compared with constant pressure operation, membrane fouling is generally observed to be slower in constant flux operation (see the review by Le-Clech et al., 2006). Continuous aeration provided shear stress on the deposits on the membrane surface. The intermittent filtration mode was achieved by a timer setting an interval of 30 min (idle) between two filtration cycles, of which the duration was the same. Combined together, continuous aeration and intermittent filtration may decrease the propensity of, and/or remove some foulant cakes in membrane areas where coagulation or aggregation has not occurred (Bacchin et al. 1995).

In the investigation, three MBRs needed the maintenance of sludge waste to achieve different SRTs (10, 20, and 30 days), while the fourth MBR did not. The engineering practice is that MBRs are designed with an SRT infinitely long, which eliminates sludge treatment or disposal; and it is an important advantage of MBRs over traditional wastewater treatment technologies. Once an MBR was terminated either due to a high TMP or a low flux (see the disscusion about membrane fouling below), the sludge layer (slime- or gel-like) on the membrane was removed with a regular lab rubber policeman. It was removed such that the membrane itself was not scratched or compromised. The unit was then rinsed with tap water for three times, each lasting one minute, to further remove the sludge. A chemical cleaning process was finally performed on the physically washed MBR following the protocol provided by the manufacturer. The process includes two cycles, in which the unit was first submerged in a diluted solution of

bleach (sodium hypochlorite with effective chlorine concentration of 1%) for two hours and thereafter in a 1% oxalic acid solution for one hour. Before the cleaned MBRs were put into operation, they were rinsed with tap water for five minutes to flush off the cleaning chemicals.

Effluent quality. Fig. 3.7 shows the time courses of BOD_5, turbidity and pH of the combined effluents of the four MBRs. Preliminary results showed that the MBRs operated under different SRTs achieved quite similar effluent quality (thanks to the role of physical separation by membranes), so the combined effluent water qualities are reported. Generally, the experiment generated similar results to what others found (Merz et al., 2007; Liu et al., 2005). The effluent BOD_5 level was less than 8 mg/L, turbidity less than 2 NTU, and pH between 6 and 9. Values of these parameters were all in the ranges of domestic wastewater reuse guidelines suggested by the USEPA (Table 3.7). The jumps in BOD_5 and turbidity were the result of the broken sealing in the MBR with SRT of 30 days. After the replacement of a new membrane unit, the effluent water quality was again within the guidelines. Fecal coliforms were periodically measured (data not shown). No fecal coliforms were detected throughout the study. This is reasonable as the nominal membrane pore size is approximately 0.4 μm, which should theoretically prevent the larger-sized fecal coliforms (or other bacteria, 0.5-5.0 μm in length) from passing through the membrane. However, Merz et al. (2007) reported fecal coliforms appearance in MBR effluent, which might be due to protein migration through the membrane and the subsequent regrowth of fecal coliforms (Jefferson et al., 2000). Yet another two more plausible explanations may relate to the membrane pore size

distribution and the shape characteristics of fecal coliforms (Crittenden et al., 2005). Pore sizes larger than the nominal size may result in the passage of fecal coliforms. The rod-shaped characteristic may also favor the passage. Thus, to maintain a non-detectable fecal coliform level, a subsequent disinfection process (e.g., ultraviolet irradiation) after the MBR is suggested for water reclamation purpose.

It should be noted that the effluent water quality of STBs was dependent on the influent water quality, yet it has been reported that MBRs are capable of producing high quality effluent despite the fluctuations in the influent (Visvanathan et al., 2000). The merit of STBs lies in the energy saving. Overall, the combination of STB and MBR may be a promising technology for GW reclamation.

Table 3.7. MBR effluent quality (n = 22) and water reuse guidelines suggested by the USEPA.

	pH	Turbidity (NTU)	BOD_5 (mg/L)	Fecal coliforms	Color
MBR effluent	7.65 ± 0.36[a]	0.92 ± 0.92	3.56 ± 3.83	Not detectable	-[b]
Reuse guidelines[c]	6–9	≤ 2	≤10	Not detectable	No color

[a] ± standard deviation; [b] did not measure; [c] Source = USEPA (2004).

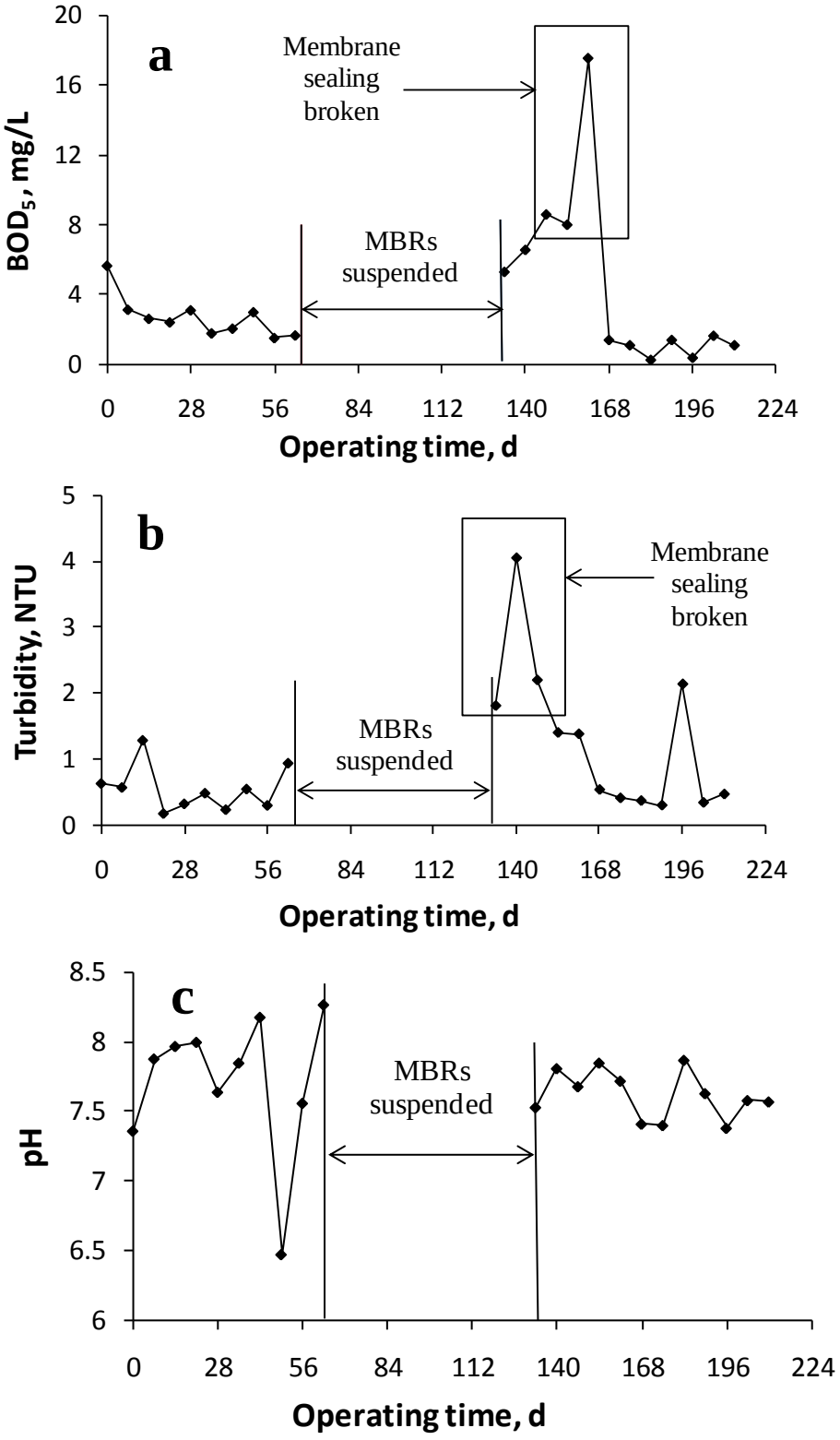

Figure 3.7. Water quality profiles of MBR effluent: a) BOD_5, b) turbidity, and c) pH.

Membrane fouling. TMP was adopted as the indicator of membrane fouling since the filtration flux was fixed (8 LMH) at the start of the experiment. TMPs of the four MBRs were recorded daily (Fig. 3.8). The TMP of each reactor increased sharply at the beginning of the filtration cycle, and then stayed relatively constant at a certain level before it experienced another pressure jump or the flux dropped significantly. The reactors were stopped when the fluxes were observed to decrease abruptly.

The operation cycle lasted longer as the SRT increased. The TMP of the reactor with no sludge wasting (i.e., SRT = 100 d) remained around 600 mbar between the two TMP jumps, and reached 893 mbar when the flux decreased sharply at Day 28. The reactor with an SRT of 30 d experienced only the first TMP jump. It is interesting to note that the TMP decreased slightly from 700 mbar to 600 mbar at Day 25 when it was stopped due to the low filtration flux. The operations of the MBRs with SRTs of 20 and 10 days lasted only two weeks because of the quick flux losses.

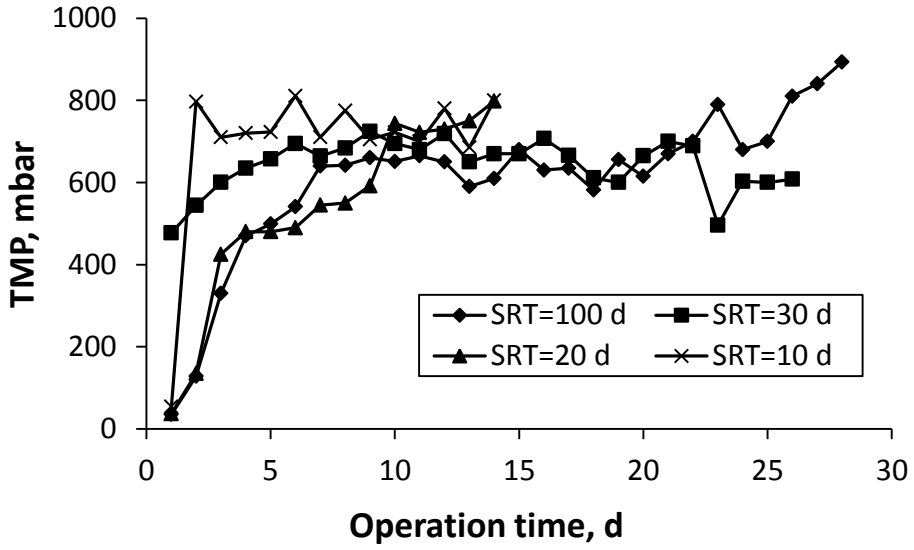

Figure 3.8. TMP profiles of MBRs at different SRTs.

It also can be seen from Fig. 3.8 that the operating TMP was lower for reactors with longer SRTs. Apart from the reactor with an SRT of 20 d, of which the TMP had an increasing trend till it reached 800 mbar, the TMP evolution of the other three reactors shows a decreasing trend as SRT increases. Controversial results about the effect of SRT on membrane fouling has been reported. Increased fouling propensity due to a long SRT has been reported by Yamammoto et al. (1989) and Han et al. (2005), while Fan et al. (2000) observed a reduced fouling rate at a longer SRT. It is thus suggested that an optimal SRT is likely to exist between the high fouling tendency of very short SRT operation and the high viscosity suspension prevalent for very long SRT (Le-Clech et al., 2006). Ng et al. (2006) studied the impact of SRTs on membrane fouling; they attributed the rapid membrane fouling in the MBRs with shorter SRTs to higher concentrations of extracellular polymeric substances (EPS).

Fig. 3.9 shows the time courses of MLSS in the MBRs. It can be seen that as SRT decreased, sludge concentration also decreased. This was expected that since the control of SRTs was achieved by wasting the sludge, and with less amount of sludge wasted in longer SRTs, MLSS concentration should be higher. So MLSS was a result of SRT. It is argued that the MLSS concentration alone is a poor indicator of biomass fouling potential due to the lack of clear correlation between MLSS concentration and other foulant characteristics (Jefferson et al., 2004). Yet the decreases of MLSS concntrations in different SRTs corresponds to the increases of membrane fouling propensity in this study, likely due to the higher concentrations of EPS (Ng et al., 2006).

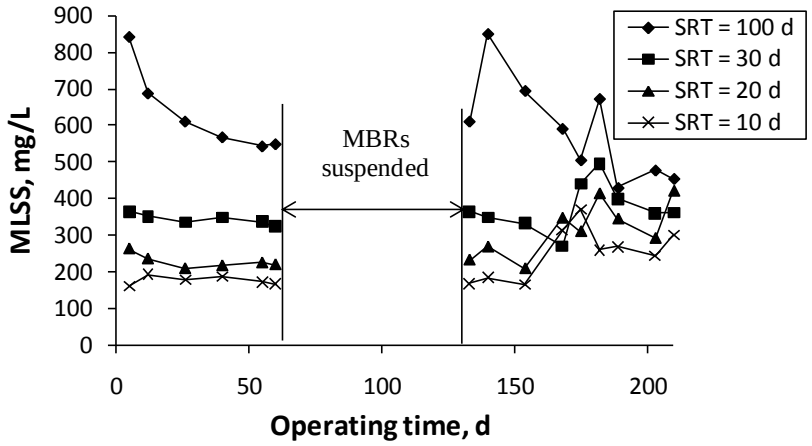

Figure 3.9. MLSS profiles of MBRs at different SRTs.

The effects of SRT and MLSS on membrane fouling are briefly discussed here at this point. Another independent study on membrane fouling mechanisms was conducted, and is fully illustrated in the next chapter.

3.4 Preliminary Estimation of Cost and Feasibility

Although MBRs guarantee the delivery of reusable water, the high-rate energy consumption (in the forms of aeration and pumping) is a drawback. STBs were thus proposed to pre-treat GW before MBRs. The study in this chapter showed that STBs could degrade a portion of BOD in GW without aeration, and could save the energy due to aeration, which would be otherwise needed to remove the same amount of BOD in MBRs. For instance, the combination removed BOD from 114.5 mg/L to 3.56 mg/L in Phase 1, achieving a removal rate of 96.9%. But an STB at HRT of 10 h reduced BOD to 33.2 mg/L. In other words, 71% of BOD was degraded in the STB without any aeration,

so the STB could save 71% of the energy that would be otherwise required for MBRs in the form of aeration.

Based on the combination, Gardels (2011) conducted life cycle assessments (LCA) on an indoor GW reuse (toilet flushing and laundry) system consisting of the combination. The LCA included manufacturing of materials phase, use phase and disposal of materials phase. He concluded that the combination was not economically feasible for an average household (approx. 2.8 people) or under with a benefit to cost ratio of 0.42 (1 is the starting point of what is considered feasible; the higher the ratio, the more economically feasible the process). Nor was the combination environmentally sustainable with a net greenhouse gas emission of over 3000 million tons of CO_2 over a 50-year design life. Yet, for a household with more than the average number of residents, he concluded the combination would be both economically feasible and environmentally sustainable. Also the price of water was a variable in his analysis. With a higher water rate, which is likely, the combination may be feasible for an average household. He finally suggested that improvements be required in order for the combination to be feasible and sustainable.

The combination can be improved in two ways. One is to eliminate the pumping needs for STBs. Since basements are the best location in houses to install the combination, one can take advantage of the gravity flow of GW from hand-basins, baths, etc., and let STB effluents flow into MBRs without any pumps. The other is to study membrane fouling mechanisms in MBRs to decrease aeration and pumping requirements. The investigation on fouling mechanisms is addressed in the next chapter.

3.5 Conclusions

In this investigation, GW was pre-treated in STBs, and the following conclusions on STBs can be reached:

1. STBs degraded certain organic contents and decreased turbidity in GW, and can be used as a pre-treatment process for GW reclamation;
2. The degradation of BOD mainly occurred in the top (first) layers in STBs, and its performance was subject to the fluctuations of influent;
3. As HRT increased, STBs showed better treatment performance;
4. Decrease in shredded tire size enhanced the performance; and
5. The biofilm properties imply that bacteria could attach on shredded tires and grow, and proved that shredded tires can be used as a packing material in biological filters.

MBRs were used to further treat GW that had been treated in STBs, and the following conclusions are drawn:

1. Water quality of MBR effluent met the water reuse guidelines suggested by USEPA; and
2. Although controversial reports on the effects of SRT and MLSS on membrane fouling exist, this study indicated that longer SRT and higher MLSS concentration reduced fouling propensity.

In summary, the combination of STBs and MBRs can be used in GW reclamation. STBs saved a portion of energy that would be required when GW is treated in MBRs alone. This combination was not economically feasible or environmentally sustainable for an average household (approx. 2.8 people) or under, but it could be for larger

households. Improvements are needed to make the combination feasible and sustainable. With a higher water price, the combination may also be both economically feasible and environmentally sustainable.

3.6 References

American Public Health Association (APHA), American Water Works Association, and Water Environment Federation (2005). *Standard Methods for the Examination of Water and Wastewater*, 21st ed. American Public Health Association, Washington, DC.

Bacchin, P., Aimar, P., and Sanchez, V. (1995). "Model for colloidal fouling of membranes." *AIChE J.*, 41, 368–376.

Crittenden, J.C., Trussell, R.R., Hand, D.W., Howe, K.J., and Tchobanoglous, G. (2005). *Water Treatment: Principles and Design*, 2nd ed. John Wiley & Sons, Inc., Hoboken, New Jersey.

Eckenfelder, W.M. (1966). *Industrial Water Pollution Control*, McGraw-Hill, New York.

Fan, X., Urbain, V., Qian, Y., and Manem, J. (2000). "Ultrafiltration of activated sludge with ceramic membranes in a cross-flow process." *Water Sci. Technol.*, 41, 243–250.

Fruhen, M., Christan, E., Gujer, W., and Wanner, O. (1989). "Significance of spatial distribution of microbial species in mixed culture biofilms." *Wat. Sci. Tech.*, 23, 1365–1374.

Gardels, D.J. (2011). "Economic input-output life cycle assessment of water reuse strategies in residential buildings and communities." *M.S. Thesis*, University of Nebraska, Lincoln, NE.

Han, S.S., Bae, T.H., Jang, G.G., and Tak, T.M. (2005). "Influence of sludge retention time on membrane fouling and bioactivities in membrane bioreactor system." *Process Biochem.*, 40, 2393–2400.

Jefferson, B., Brooks, A., Le-Clech, P., and Judd, S. (2004). "Methods for understanding organic fouling in MBRs." *Wat. Sci. Technol.*, 49, 237–244.

Jefferson, B., Burgess, J.E., Pichon, A., Harkness, J., and Judd, S.J. (2001). "Nutrient addition to enhance biological treatment of greywater." *Wat. Res.*, 35, 2702–2710.

Jefferson, B., Laine, A., Parsons, S., Stephenson, T., and Judd, S., (2000). "Technologies for domestic wastewater recycling." *Urban Water*, 1, 285–292.

Lawrence, J.R., Korber, D.R., Hoyle, B.D., Costerton, J.W., and Caldwell, D.E. (1991). "Optical sectioning of microbial biofilms." *J. Bacteriol.*, 173, 6558–6567.

Le-Clech, P., Chen, V., and Fane, T.A.G. (2005). "Fouling in membrane bioreactors used in wastewater treatment." *J. Membr. Sci.*, 284, 17–53.

Merz, C., Scheumann, R., Hamouri, B. E., and Kraume, M., (2007). "Membrane bioreactor technology for the treatment of greywater from a sports and leisure club." *Desalination*, 215, 37–43.

Mondal, B., Warith, M.A., and Burns, S.D. (2007). "Comparison of Shredded Tire Chips and Tire Crumbs as Packing Media in Trickling Filters." *Water Qual. Res. J. Canada*, 42 (4), 319–326.

Ng, H., Tan T., and Ong, S. (2006). "Membrane fouling of submerged membrane bioreactors: impact of mean cell residence time and the contributing factors." *Environ. Sci. Technol.*, 40, 2706–2713.

Park, J.K., Kim, J.Y., and Edil, T.B. (1996). "Mitigation of organic compound movement in landfills by a layer of shredded tires." *Water Environ. Res.*, 68, 4–10.

Reddy, K.R., Stark, T.D., and Marella, A. (2010). "Beneficial use of shredded tires as drainage material in cover systems for abandoned landfills." *J. of Hazardous, Toxic, and Radioactive Waste Management*, 14, 47–60.

Shin, H.S., Yoo, K.S., and Park, J.K. (1999). "Removal of polychlorinated phenols in sequential anaerobic-aerobic biofilm reactors packed with tire chips." *Water Environ. Res.*, 71, 363–367.

Tang, Z., Butkus, M.A., and Xie, Y.F. (2006). "Crumb rubber filtration: A potential technology for ballast water treatment." *Marine Environ. Res.*, 61, 410–423.

U.S. Environmental Protection Agency (1991). *Markets for Scrap Tires*. EPA-530/SW-90-074A, Office of Solid Waste, Washington, D.C.

U.S. Environmental Protection Agency (2004). *Guidelines for Water Reuse*. EPA/625/R-04/108, Office of Water, Washington, D.C.

U.S. House of Representatives (1990). "Scrap tire management and recycling opportunities." Committee Small Business, Washington, D.C.

Visvanathan, C., Ben Aim, R., Parameshwaran, K. (2000). "Membrane separation bioreactors for wastewater treatment." *Critical Reviews in Environmental Science and Technology*, 30, 1–48.

Yamammoto, K., Hiasa, H., Mahmood, T., and Matsuo, T. (1989). "Direct solid liquid separation using hollow fiber membrane in an activated sludge aeration tank." *Water Sci. Technol.*, 21, 43–54.

Zhang, T.C. and Bishop, P.L. (1994). “Density, porosity, and pore structure of biofilms.” *Wat. Res.*, 28, 2267–2277.

CHAPTER 4

INTERNAL and EXTERNAL FOULING IN HOLLOW-FIBER MEMBRANES: IMAGE ANALYSES and MODELING

4.1 Introduction

A membrane bioreactor (MBR) is a combination of biological treatment and physical separation provided by the membrane. MBRs are gaining popularity in wastewater treatment and water reuse due to a) their ability to produce high quality effluent despite the fluctuations in the influent (Visvanathan et al., 2000), b) the flexibility in plant size to fit in various occasions (Fane and Fane, 2005), c) the minimization of excess sludge and d) lower capital investments brought by innovative membrane materials (see the reviews by Meng et al., 2009 and Le-Clech et al., 2006). However, membrane fouling remains a major obstacle for the scale-up of MBRs in spite of decades' of investigations.

Early research efforts on membrane fouling focused on elucidation of the effects of operational parameters (e.g., aeration rate, solid retention time, sludge concentration, etc.). For example, Ueda et al. (1997) first observed an optimum aeration rate in MBRs, above which no significant fouling mitigation would occur. Controversial conclusions have been drawn on the effect of solids retention time (SRT, or mean cell residence time, MCRT). Increased fouling propensity due to a long SRT has been reported by Yamammoto et al. (1989) and Han et al. (2005), while Fan et al. (2000) observed a reduced fouling rate at a longer SRT. Thus, researchers have shifted their focus to the effects of extracellular polymeric substances (EPS) and soluble microbial products (SMP) since late 1990s. Although mixed conclusions on the effect of EPS exist (Rosenberger and Kraume, 2003; Cho et al., 2005), an agreement has been reached that one cannot

attribute membrane fouling solely to EPS; SMP has to be considered as well (Meng et al., 2009). Recently, however, the conventional methods for the physical-chemical analyses of EPS and SMP were deemed not appropriate (Kimura et al., 2009), or insufficient (Ng and Ng, 2010) for the investigation of membrane fouling in MBRs. Research has thus been directed towards the micro-characterization of the foulants on the membrane surfaces; techniques for membrane surface characterization (e.g., chemical structure and morphology) have been combined with image analysis software (e.g., ImageJ, Imaris®, etc.) (Kallioinen and Nyström, 2008; Ferrando et al., 2005). In a recent study with the aid of confocal scanning laser microscopy (CLSM) and the Image Structural Analysis (ISA-2) software, Ng and Ng (2010) found that membrane fouling mechanisms shifted from a biofilm-dominated process towards a non-biofilm, organic fouling process as the flux increased; proteins on the membrane surfaces had the greatest impact on the TMP increase in the initial stage of MBR operations.

However, few, if any, micro-characterizations have been conducted to unveil membrane fouling mechanisms in MBRs, especially with respect to the membrane foulants inside (the support layer) and outside (the cake layer) the membrane, respectively. Additionally, modeling of membrane fouling is far behind the comprehension of fouling mechanisms. The aim of this investigation was hence to characterize the foulants at the micro-scale at critical points of the three stages according to the widely adopted 3-stage fouling map (Cho and Fane, 2002), and to understand the impact of the foulants inside and outside the membrane, respectively, on the increase of TMP.

4.2 Materials and Methods

4.2.1 Experimental Set-up

A bench-scale submerged MBR consisted of a 500 mL plastic container and a 2×10^{-4} m^2 membrane module made of polyvinylidne fluoride (PVDF) hollow fiber membrane (HFM) (inside/outside diameter = 0.6/1.3 mm, nominal pore size = 0.1 μm, UNA 620A, Asahi Kasei Chemicals Corp., Tokyo, Japan). The filtration flux was kept at 50 liters per m^2 of membrane area per hour (LMH) via a peristaltic pump (Masterflex HV-07575-10; Cole Parmer, Vernon Hills, IL, USA), operated at the mode of 8 min on and 2 min off. Activated sludge sampled from a local wastewater treatment plant was inoculated according to Eckenfelder (1966) for two weeks. During both inoculation and MBR operation, the reactor was fed with synthetic wastewater containing dextrose as the sole carbon source (COD of 480 mg/L) and the following constituents (in g/L): K_2HPO_4, 1.28; KH_2PO_4, 0.64; NH_4Cl, 0.48; $MgSO_4 \cdot 7H_2O$, 0.6; $FeSO_4 \cdot 7H_2O$, 0.02; $ZnSO_4 \cdot 7H_2O$, 0.02; $MnSO_4 \cdot 7H_2O$, 0.02; and $CaCl_2$, 0.08 (Eckenfelder, 1966). Air was supplied by an air pump (30–80GAL, Top Fin Air Pumps, PetSmart, Inc., Phoenix, AZ, USA) through an air stone. No sludge was wasted throughout the study. All the experiments were conducted at room temperature (24 ± 1 ^oC).

4.2.2 Sampling and Analytical Methods

Trans-membrane pressure (TMP) was measured with a traceable manometer (06-664-19, Thermo Fisher Scientific Inc., Waltham, MA, USA). On the basis of the preliminary study, clogging of our MBR membrane had three stages: the 1st (initial) stage was 0–60 min with a rapid TMP increase; the 2nd (sub-critical flux) stage 1 h–36 d with a relative

stable TMP, and the 3rd stage after 36 d with a rapid TMP increase due to almost full clogging (data not shown). Therefore, membrane sampling was carried out at the 8th min, 18th min, 28th min (for the 1st stage), 6th h (for the 2nd stage), and 36th d (for the 3rd stage), respectively. Sampled membranes were cut into pieces with a length of approximately 2 cm, and then were randomly selected into two sets for CLSM and SEM imaging, respectively. After a membrane module was sampled, a new one was placed into the reactor, and the MBR with a new membrane module started a new filtration process (timed from 0) until the next sampling times.

Immediately after membrane sampling and cutting, one set of the HFM samples was fixed with 3.7% formaldehyde at room temperature for 1 h, and stored at 4 °C before being transported to the Beadle Center (Lincoln, NE) for staining and CLSM imaging. Membrane samples were stained as described in Juang et al. (2010). All dyes were purchased from Invitrogen Corp. (Carlsbad, CA, USA). Sypro Orange was used to stain proteins; Concanavalin A, Alexa Flour 633 conjugate to stain polysaccharides; and Sytox Green to stain nucleic acid. Stained membranes were observed immediately with a CLSM (Olympus FV500, Japan) under a 10× magnification objective with a step-size of 3 μm. There were 120 images in each CLSM series, with a size of 512 × 512 pixels for each image.

The other set of the HFM samples was fixed with 3.0% (v/v) glutaraldehyde in 0.1 M phosphate buffer at room temperature for 1 h after sampling, and stored at 4 °C before SEM observation. To prepare them for SEM observation, the fixed samples were washed twice with 0.1 M phosphate buffer for 10 min, and then were dehydrated in an ethanol series in a sequence of 30, 50, 70, 95, 100, 100, and 100% for 10 min each. After

dehydration, the samples were air dried overnight and coated with silver. Coated samples were thereafter examined under an SEM (model S-3000, Hitachi, Japan) at 3.5 kV.

4.2.3 Image Analysis

Detailed descriptions on image analyses are presented in Appdendix B. some important procedures are shown below. For 3-D reconstruction and quantification of the volume of different foulant components both inside and outside the membranes, each series of CLSM images were imported to Imaris (v7.1.1, Bitplane AG). The procedures were: i) the *Green* Channel was used to create a surface for masking. The threshold value was adjusted so that all the green color was selected, and the volume data were exported as the volume of the membranes (because the auto-fluorescence of membranes was green); ii) the *Red* Channel was masked with voxels inside surface set to 0, and a new masked channel was created; iii) another new channel was created on the masked channel, and the threshold value was adjusted so that the red color outside the membrane was selected; iv) the volume data were exported from the statistics as the volume of protein outside the membranes; v) Steps ii) and iv) were repeated with voxels outside surface set to 0, and the volume data were exported as the volume of protein inside the membranes; vi) Steps ii) to v) were repeated for the *Blue* Channel, and data were exported as the volumes of polysaccharides both inside and outside the membrane; and vii) another surface was created using the *Red* Channel, and Steps ii) to v) were repeated for *Green* (threshold adjusting was different from others in that no smooth green surface, i.e., membranes, was selected). In order to abate the bias from observation, at least 8 series of the CLSM

images were analyzed for each sample. The volume data were used to calculate the membrane porosities at different sampling events described below.

The CLSM images were also imported to ImageJ 1.43u (National Institute of Health, MD) to analyze the area fraction of each foulant constituent on the membrane surfaces. The analysis included identifying the features of interest, stacking and extracting the measurements of interest, as described in Ferrando et al. (2005). The porosity of the cake layer was the sum of the area fractions of the three foulants components, neglecting the porosity within the foulants.

4.2.4 Model Development

The resistance-in-series model (Crittenden et al., 2005) was adopted in the following form:

$$J = \frac{TMP}{\mu\,(R_m + R_c + R_a)} \tag{1}$$

where, *TMP* = trans-membrane pressure, Pa; *J* = water flux through membrane, L/m^2·h; μ = dynamic viscosity of water, kg/m·s; R_m = intrinsic membrane resistance coefficient, m^{-1}; R_c = cake layer resistance coefficient, m^{-1}; R_a = adsorptive fouling resistance coefficient, m^{-1}. Combining R_m and R_a, Eq. (1) becomes

$$J = \frac{TMP}{\mu(R_{in} + R_c)} \tag{2}$$

where R_{in} = R_m + R_a, the internal fouling resistance coefficient, m^{-1}. Assuming that the TMP can be added together, Eq. (2) can be re-written in the form of

$$TMP = TMP_{in} + TMP_{ex} \tag{3}$$

where TMP_{in} = TMP caused by internal fouling, Pa, and TMP_{ex} = TMP by external fouling, Pa. TMP_{ex} is modeled by the Carmen-Kozeny equation (Carmen, 1938)

$$TMP_{ex} = \frac{180\mu J L_c (1-\varepsilon_c)^2}{d_p^2 \varepsilon_c^3} \tag{4}$$

where L_c = the cake layer thickness, m; ε_c = the cake layer porosity, %; and d_p = the diameter of the particles forming the cake layer, m. Note that d_p evolving during the filtration process (see discussion below). Assuming clogging occurring uniformly with the cake layer (and the support layer), L_c can be obtained with the data from Imaris, that is,

$$L_c = \frac{V_{fo}}{A_m(1-\varepsilon_c)} \tag{5}$$

where V_{fo} = the volume of foulants deposited onto the HFM material (i.e., the cake layer for the case of external resistance) at different sampling events from Imaris, μm^3; and A_m = the membrane area from Imaris that the foulants covered, μm^2. Combining Eqs. (4) & (5), the equation for external TMP is

$$TMP_{ex} = \frac{180\mu J}{d_p^2} \cdot \frac{V_{fo}}{A_m} \cdot \frac{1-\varepsilon}{\varepsilon^3} \tag{6}$$

The internal TMP is derived in the following context. TMP_{in} adopts the form (Svarovsky, 1977)

$$TMP_{in} = \mu J R_{in} \tag{7}$$

In Darcy's basic filtration equation, R_{in} is equal to the medium thickness divided by the permeability of the bed (Svarovsky, 1977). In this case, the bed was the membrane, and

$$R_{in} = \frac{L}{k} \tag{8}$$

where L = the thickness of the membrane, m; and k = the permeability of the membrane, m^{-2}. k can be obtained from the Carmen-Kozeny equation (Carmen, 1938)

$$\frac{k}{k_S} = \frac{3\varepsilon^3}{25\,(1-\varepsilon)} \tag{9}$$

where ε = the membrane porosity, %; and k_S = the Stokes permeability for particles of irregular shape, m^{-2}, which is (Hermanowicz, 2004)

$$k_S = \frac{2(1-\varepsilon)}{s^2} \tag{10}$$

where s = the ratio of pore surface area to the volume of porous material, $\mu m^2/\mu m^3$. Assuming all the pores in the HFM supportive layer are of a circular shape, s is given by definition considering the connections between pores in a channel,

$$s = \frac{C_0 L_e N}{AL(1-\varepsilon)} = \frac{4\varepsilon}{1-\varepsilon} \cdot \frac{1}{d} \cdot \frac{L_e}{L} \tag{11}$$

where C_0 = the circumference of a pore, m, L_e = the equivalent length of the pore channels, m, N = number of pores, unitless, A = the area of the membrane, and d = the diameter of the pore (note that this is not the initial pore size of the membrane, it changes with foulants absorbed onto the pore passages), m. According to Carmen (1937),

$$k_0 \cdot (\frac{L_e}{L})^2 \approx 5.0 \tag{12}$$

where k_0 = a coefficient depending on the shape of the cross-section of pore channels (= 2.0 for the shape of circle). Substituting Eqs. (8)–(12) and k_0 = 2.0 in Eq. (8), TMP_{in} becomes

$$TMP_{in} = \frac{200\mu JL}{3d^2} \cdot \frac{1}{\varepsilon(1-\varepsilon)^2} \tag{13}$$

To consider the volume loss of pores due to random intersections of multiple pores in a HFM supportive layer, the porosity of the pores is calculated from the following equation (Carniglia, 1986)

$$\varepsilon = \frac{\pi^4}{8} \cdot \frac{d^2}{4l^2} \cdot \left(1 - 1.32 \cdot \frac{d}{2l}\right) \quad (14)$$

where *1.32* = coefficient of volume loss; l = the average length of all pores, m, which is assumed not to change during the filtration process, and is determined at the initial condition (ε_0 = 60% and d_0 = 1 μm). Porosities were calculated from the foulants volume data from Imaris, based on its physical definition

$$\varepsilon = 1 - \frac{V_{fi} + V_m}{\frac{V_m}{1 - \varepsilon_0}} = 1 - (1 + \frac{V_{fi}}{V_m})(1 - \varepsilon_0) \quad (15)$$

where V_{fi} = the volume of foulants adsorbed onto the HFM supportive layer at different sampling events from Imaris, μm^3, and V_m = the volume of membrane samples (without foulants inside or outside) from Imaris, μm^3.

4.3 Results and Discussions

4.3.1 Evolution of Foulants Volumes

Table 4.1 lists the specific volumes of the three HFM foulants at different sampling times, and Fig. 4.1 displays the time course of specific volume for each foulant inside and outside the membrane. The physical meaning of specific volume is the volume of foulant constituents deposited on a unit area of membrane. Protein and polysaccharides were found to be the dominant fouling species (Fig. 4.1). Protein accounted for 20-54% of the foulants internally, 22-44% externally, and 21-47% totally; while polysaccharides accounted for 37-73% internally, 40-72% externally, and 39-73% totally (Fig. 4.2). Ng

and Ng (2010) observed that, under sub-critical flux conditions, protein was the most dominant fouling fraction in the initial fouling stage, and it also promoted the adherence of other foulants (polysaccharide, bacteria, and lipid). Despite the hydrophilic polyolefin membrane they used, they attributed the initial adherence of protein to the hydrophobic-hydrophobic or steric interactions between the protein molecules and the membrane material (Huisman et al., 2000). The hydrophobicity of the PVDF membrane may also explain the protein accumulation in this study. Using the same membranes, Yamamura et al. (2008) applied atomic force microscopy (AFM) and functionally modified microspheres to investigate the affinity of carbohydrate-like substances to PVDF and polyethylene membranes. A higher affinity of the hydroxyl group to the PVDF membrane was found possibly because of the high electronegative nature of the PVDF polymer. Although it was intended to partially explain the dominance of hydrophilic natural organic matter (NOM) in foulants of membranes for water treatment, it should also be applicable in wastewater treatment. Rosenberger et al. (2006) reported complete removal of polysaccharides in a MBR even though 30% of the original polysaccharide peak could penetrate the membrane in a membrane filtration system. When membrane fouling reached Stage 3 (36 d), the specific volume of each foulant increased enormously. Little difference existed in the specific volume between the protein and polysaccharides fractions, both of which were substantially greater than that of the biomass (Table 4.1).

Table 4.1. Specific volumes of foulants inside and outside the membrane and total specific volumes at sampling times (n = 8).

Sampling time	Inside the membrane			Outside the membrane			Total		
	Protein	Biomass	Polysaccharides	Protein	Biomass	Polysaccharides	Protein	Biomass	Polysaccharides
8 min	0.32 ± 0.50	0.04 ± 0.05	0.28 ± 0.27	0.30 ± 0.18	0.02 ± 0.04	0.36 ± 0.35	0.62 ± 0.53	0.06 ± 0.08	0.63 ± 0.57
18 min	0.15 ± 0.14	0.02 ± 0.03	0.10 ± 0.12	0.20 ± 0.16	0.11 ± 0.18	0.21 ±0 .26	0.35 ± 0.27	0.13 ± 0.21	0.31 ± 0.38
28 min	0.17 ± 0.15	0.07 ± 0.04	0.33 ± 0.18	0.37 ± 0.32	0.09 ± 0.06	0.52 ± 0.44	0.54 ± 0.39	0.15 ± 0.10	0.85 ± 0.58
6 hr	0.48 ± 0.11	0.15 ± 0.07	1.73 ± 0.85	0.79 ± 0.42	0.21 ± 0.09	2.59 ± 1.61	1.27 ± 0.45	0.36 ± 0.10	4.31 ± 1.71
36 d	7.32 ± 3.07	4.06 ± 1.53	8.14 ± 2.72	7.02 ± 3.59	1.57 ± 1.33	7.57 ± 3.47	14.34 ± 6.28	5.45 ± 1.76	15.71 ± 5.86

Note: There were 8 samples at each sampling time. The entire length of a sample (approx. 2 cm) was imaged 120 times for foulants at different depths, and analyzed for different fouling components at different locations. A group of 8 clean membrane samples was used as control. No foulants were detected, so data were not shown here.

Compared with the protein and polysaccharides, the biomass specific volume both internally and externally seemed negligible at the initial stage (Fig. 4.1). The small amount of biomass was likely a result of the attachment (both inside the pores and on the membrane surface) of the lysed DNA in the bulk solution or that of binding due to suction. The suction force might also lead to the collapse of microorganisms, and the lysed DNA either stayed on the surface or adsorbed onto the pore walls of the membrane channels. Because of the hydrophobicity and the electro-negativity of the membrane discussed above, proteins and polysaccharides adhered readily onto/into the membrane upon submersion of the membrane modules. This is consistent with the observation of rapid irreversible fouling and passive adsorption of colloids and organics (Ognier et al., 2002a). It was established that proteins had a stronger affinity to sludge flocs than polysaccharides in relation to hydrophobicity and surface charge (Masse et al., 2006). Thus the attached proteins, which would bind with bacteria more easily, may form a conditioning layer (Ng and Ng, 2010; Choi et al., 2005; Ognier et al., 2002b), and enhance the adherence of bacteria in later stages.

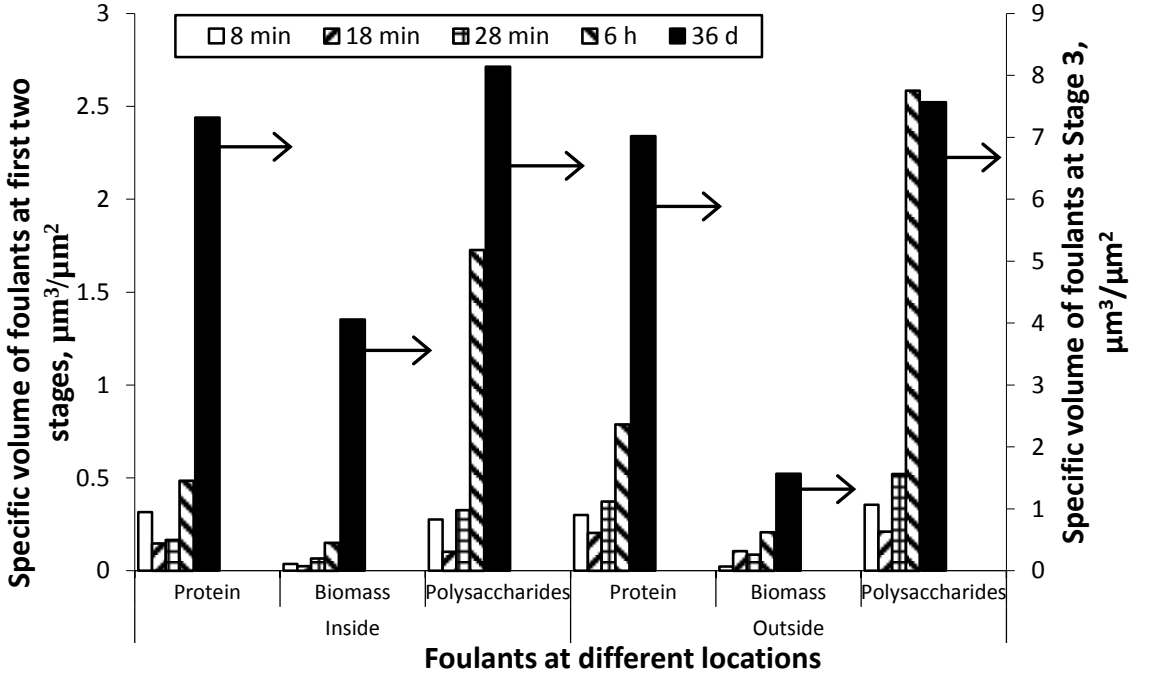

Figure 4.1. Time courses of specific volumes of membrane foulants inside and outside the membrane (refer to Table 4.1 for standard deviations).

Each constituent profile showed a trend similar to that from the TMP profile (Fig. 4.1). The specific volumes for various foulants at the first three sampling times were at the same level, until they slightly increased at the 4th sampling time (6 h, in the second stage of membrane fouling). At Day 36 when the experiment was terminated due to the sharp TMP jump, the specific volumes of all three constituents jumped sharply. A point of greater interest, therefore, is to identify the contributions to membrane fouling from accumulations of foulants inside and outside the membrane, respectively.

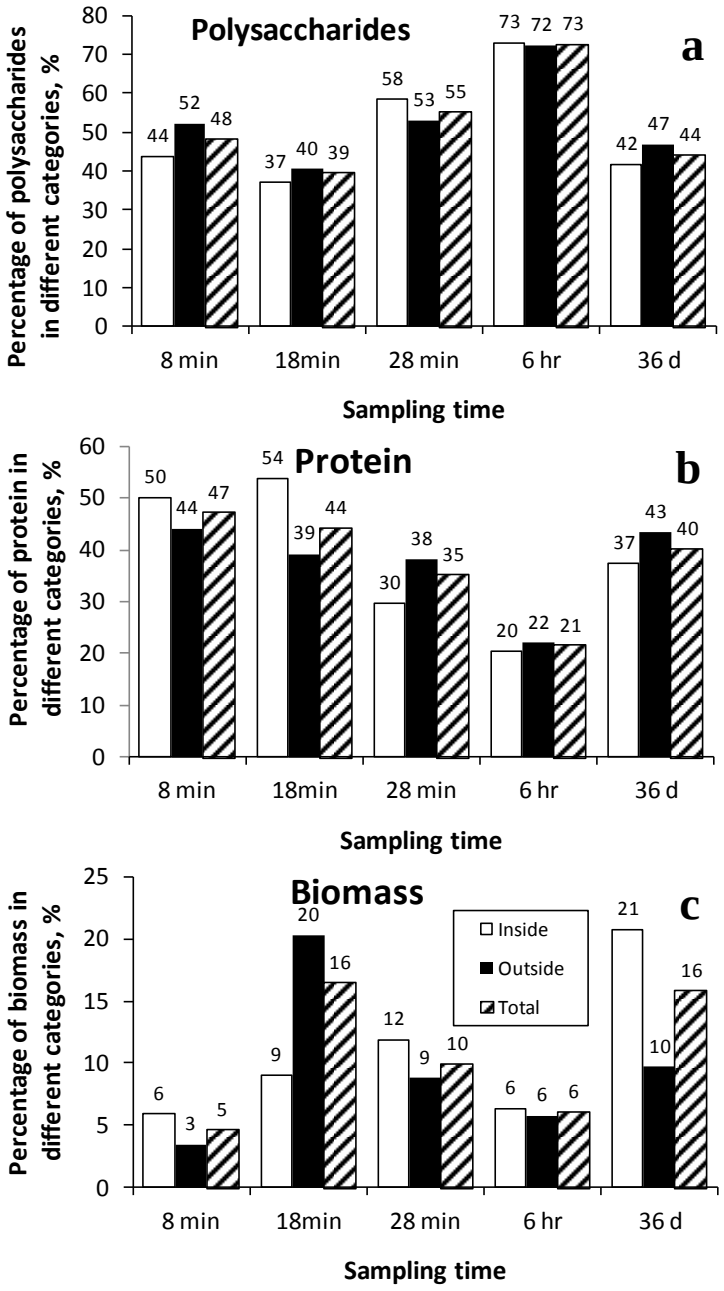

Figure 4.2. Evolution of specific volume for various membrane foulants inside and outside the membrane, and their total specific volume.

4.3.2 Internal and External Fouling

In the classical fouling mechanisms, pore constriction represents internal fouling, whereas pore blockage (complete and intermediate) and cake formation represent external fouling (Duclos-Orsello et al., 2006). Pore constriction is caused by the deposition of foulants inside the membrane structure (i.e., pore channels), and pore blockage and cake formation by that on the membrane surface. The resistance due to the mechanisms is proportional to the bulk concentration and the volume of filtrate (Crittenden et al., 2005). In other words, the volume of foulants inside and outside the membrane reveals the roles of different fouling mechanisms in MBRs.

Fig. 4.3 summarizes the ratio of the specific volume inside the HFM to that of the total HFM for different foulants. It provides a special insight to determine fouling mechanisms. In general, the ratios decreased and then increased until the end of the experiment. Adsorption may play an important role during the early stage of filtration with a clean membrane, and the adsorption capacity is quickly exhausted (Crittenden et al., 2005). Upon the submersion of the membrane module, both membrane pores and membrane surface showed adsorption sites for proteins and polysaccharides, which led to the attachment of microbes. Due to a larger surface area provided by the tortuous internal structure of the membrane, more fouling constituents were absorbed inside in the initial stage, narrowing the pore channels inside the membrane. This caused a significant increase of TMP, and so pore constriction was more significant in this stage. As the adsorption capacity (both internal and external) was exhausted, foulants tended to deposit on the membrane surface (intermediate pore blockage and/or cake formation). Some particles might also be trapped inside the pore channels (complete pore blockage) of the

HFM, although the amount was far less than that accumulated on the membrane surface. Therefore, external fouling (pore blockage and cake formation) dominated during Stage 2. These findings were consistent with those of Tracey and Davis (1994), who concluded the fouling mechanism to be pore constriction or pore blockage in the beginning, followed by cake formation later. The adsorption led to the continuous pore narrowing of the membrane channels, while the deposition on the membrane surface resulted in cake formations on the surface. Due to the accumulation of membrane foulants both inside and outside the membrane, TMP continued to increase gradually until it encountered a sharp jump at Stage 3. The jump was accompanied by a noticeable increase in the ratio of the specific volume inside the membrane to that outside for the three fractions. It is likely that the amount of foulants inside the membrane reached a critical value, above which TMP increased tremendously in order to maintain the flux. Again, pore constriction was decisive in Stage 3.

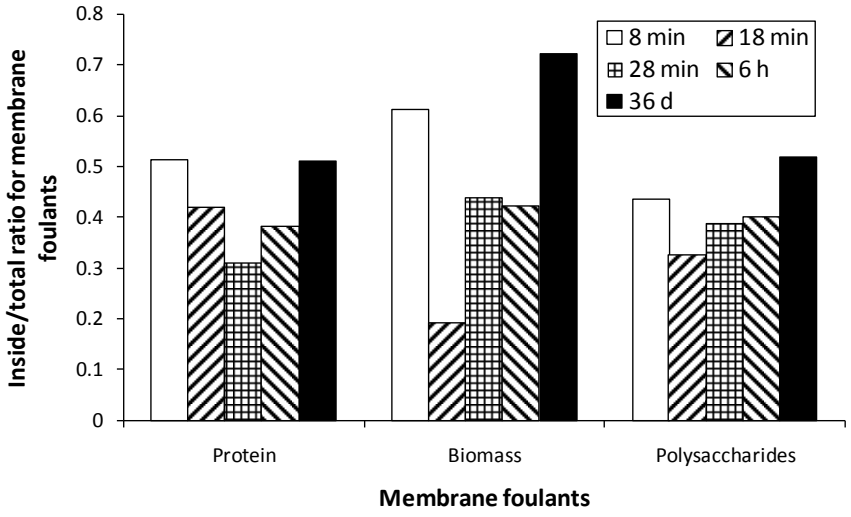

Figure 4.3. Ratios of inside volume to total volume of each membrane foulant.

The fouling mechanisms discussed above can be verified in the changes of porosities of membrane and cake layer (Fig. 4.4). Both profiles are similar to each other. During the first stage, both porosities decreased slightly due to adsorption of proteins and polysaccharides. Yet if one should compare the effect of the decrease of a porous medium and that of a newly formed cake layer on filtration performance, it is not difficult to tell that the former would be more significant, since pores were constricting within the membranes whereas cake layers were forming in the latter case. Moreover, it is possible that some joints of the pore passages were blocked so that the actual membrane porosity might be lower than Fig. 4.4 suggests. The cake layer started to expand on the membrane as filtration continued. Because of the cake layer (or the conditioning layer), most of the macromolecules and small particles, which would otherwise be absorbed to the pores, were instead bound on the membrane surface. The rate of pore clogging within the membrane was thus slowed down, and the cake layer played a greater role in fouling. The impact of pore narrowing was lessened until the membrane porosity (about 28%) was finally too low to maintain flux under the previous pressure. At such a low porosity, pore constriction, or even pore blockage would be more important in filtration.

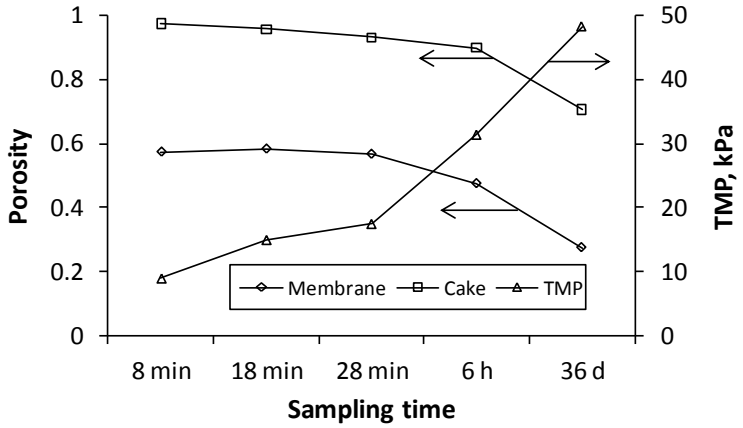

Figure 4.4. Porosities of membrane and cake layer, and TMP at different sampling times.

4.3.3 Modeling of Membrane Fouling

Most previous models link observational indicators (e.g., flux, bulk sludge concentration, etc.) with fouling resistance, which is represented by TMP. Those models provide valuable implications on the operations of MBRs. To elucidate fouling mechanisms, other researchers linked the membrane fouling with observation of porosity changes of either cake layer or inside the membrane (Ng and Ng, 2010; Wang et al., 2008). However, to our knowledge, no attempts have been made to model the porosities of both the membrane and the cake layer in the correlation to fouling resistance, which is desirable to explain the phenomenon fundamentally.

While all the parameters in the internal fouling model (Eq. (13)) were obtainable, d_p in the external fouling model was not. Nor have there been other studies reporting the evolution of the particle size clogging the cake layer. ImageJ was used in this study for the particle size analysis. Due to the resolution of the software, however, the distribution of d_p (reflected by the area of the particles in ImageJ) was of a one-side bell-shape. The mode value always stayed the same at the minimum readable scale (1.4 μm if converted from area to diameter). Conducting a focused beam reflectance measurement, Wang et al. (2008) found a similar one-side bell-shaped size distribution for the particles of the membrane foulants at the end of a filtration cycle. The majority (88%) of the membrane foulants distributed in a size range of 0–2.0 μm, with the mode also orienting towards the minimum scale, which was 0.5 μm. Both studies provided important information about the possible particle size of the predominant foulants, yet the data in neither study could be used in the modeling. It is easily understandable that the mode of particle size during

filtration would increase due to either the adsorption of fine particles onto one another or the attachment of larger particles on the membrane, or both. Therefore, unless a more sensitive instrument is introduced for the purpose of monitoring d_p, the only solution to this dilemma, to our best knowledge, would be to back-calculate d_p by assuming the model is valid. If, and only if, the back-calculated *dp*'s are within a reasonable range and showing an increasing trend at the same time, the model may be proved valid.

A summary listing the results of porosities, d_p, modeled TMP_{in} and TMP_{ex}, and experimental TMP is shown in Table 4.2. d_p was about 0.09 to 0.14 μm at the 1st stage, increased to about 0.23 in the 2nd stage, and was about 0.68 μm at the end of the experiment. We believe that these d_p values are reasonable because d_p represents the foulants that comprised the cake layer; lager particulates, such as bacteria (d = 1–3 μm), may be retained at the surface of the cake layer, yet their percentage may be much smaller due to less amount of attachment or collapse upon suction pressure. In general, the d_p values are small in the 1st and 2nd stages but are consistent with the range (0.5–2.0 μm) reported by Wang et al. (2008) at the 3rd stage. The exact reason why and how d_p increases with time is under investigation.

Table 4.2. Summary of porosities and modeling results based on experimental TMP.

Sampling time	Experimental TMP, kPa	Porosity, %		Model				
				Internal		External		Total TMP, kPa
		Membrane	Cake layer	d, µm	TMP, kPa	d, µm	TMP, kPa	
8 min	9	0.57	0.97	1.1	6.57	0.14	2.43	9
18 min	15	0.58	0.96	1.11	6.61	0.09	8.39	15
28 min	17.5	0.57	0.93	1.09	6.55	0.14	10.95	17.5
6 h	31.4	0.48	0.9	0.97	6.75	0.23	24.65	31.4
36 h	48.3	0.28	0.71	0.69	11.91	0.68	36.39	48.3

According to the model, the contributions of the internal and external fouling could be quantified (Fig. 4.5). The results of the quantification verified the experimental findings. It is interesting to notice that at the 1st stage, internal resistance played a major role (73% contribution) for initial build-up of TMP, but the quick formation of the cake layer made increasing contributions to the TMP build-up (from the initial 27% at 8 min to 62.6% at 28 min). It was the external fouling that contributed mostly (78.5%) to the TMP during the long-term filtration process (stage 2). It is interesting to notice that the contribution of external resistance by the cake layer is more or less stable at the 2nd and 3rd stages (75.3 to 78.5%). This is surprising since it has been generally accepted that the impact of a cake layer on TMP rise would become more significant as the cake layer builds up (Zhang et al., 2006; Chang et al., 2002; Song, 1998). Zhang et al. (2006) reported that fouling due to cake layer was expected to worsen over time although it is possible that cake layer might not affect fouling too adversely. An increase in the foulants volume or the thickness of a cake layer may not necessarily increase the TMP remarkably because the open channels for fluid passage in the newly formed cake layer may be much larger than that of the existing cake layer or that inside the membrane.

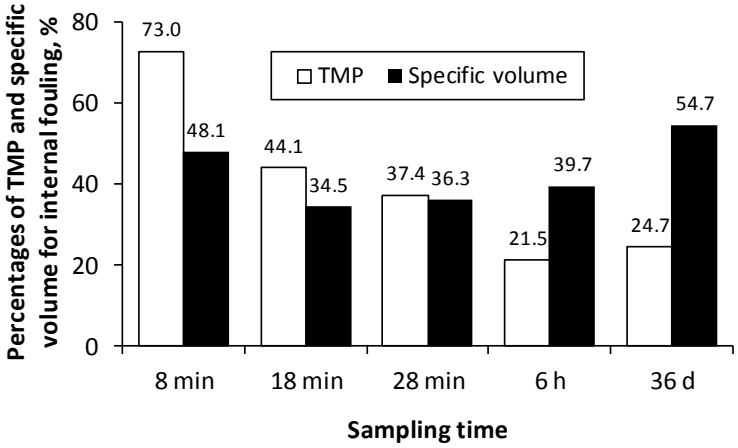

Figure 4.5. Contributions of internal fouling to TMP based on the model, and to total foulants volume.

It is also interesting to notice that the percentage of TMP caused by internal fouling changes at different stages. At the beginning of the 1st stage, internal fouling (pore constriction) played a substantially greater role (73%) upon the commencement of the MBR. In the 2nd stage, internal fouling (pore constriction) only contributed about 21% of the TMP. Afterwards, the percentage of TMP_{in} increased at Stage 3 (from 21.5% to 24.7%), and the total TMP jumped. While a change of TMP_{in} from 21.5% to 24.7% seems not significant, analysis of membrane porosity indicates that the membrane porosity decreased from 47.6% to 27.6%. With this huge porosity decrease, it is highly possible that the membrane pores were dramatically narrowed and a certain amount of them were completely blocked. Therefore, the results of this study imply that, despite its smaller percentages, internal fouling could be the major reason to have caused the TMP jump at the end of filtration while external fouling dominated the most part of the process.

4.4 Conclusions

Membrane fouling in MBRs was characterized in terms of three foulant components, namely proteins, polysaccharides and bacteria (nucleic acid) with the aid of CLSM and Imaris. Proteins and polysaccharides were found to be the predominant foulants, and the specific volume (foulant volume/membrane area) of both was about three times that of microbes. Contributions of the foulants to membrane fouling was also investigated, internally (inside the membrane) and externally (outside the membrane, cake layer). It was found that the ratio of the specific volume inside the membrane to that outside the membrane decreased in the first two stages and increased at Stage 3. It indicated that external fouling might have dominated the long-term Stage 2, whereas internal fouling might lead to the total TMP jump in the 3-stage fouling map.

A mathematical model was proposed to help understand the fouling process better. The model dynamically linked TMP to the changes of membrane and cake layer porosities, membrane pore size, and the size of particles attached onto the membrane outside. The interpretations support the conclusions of the experiment quantitatively.

4.5 Reference

Carmen, P.C. (1937). “Fluid flow through granular beds.” *Tran.Instn. Chem. Engrs.*, 15, S21–S48.

Carmen, P.C. (1938). “Fundamental principles of industrial filtration.” *Chem. Eng. Res. Des.*, 16, 168–188.

Carniglia, S.C. (1986). “Construction of the tortuosity factor from porosimetry.” *J. Catalysis*, 102, 401–418.

Chang, IS., Le-Clech, P., Jefferson, B., and Judd, S. (2002). "Membrane Fouling in Membrane Bioreactors for Wastewater Treatment." *J. Environ. Eng.*, 128, 1018–1029.

Crittenden, J.C., Trussell, R.R., Hand, D.W., Howe, K.J., and Tchobanoglous, G. (2005). *Water Treatment: Principles and Design*, John Wiley & Sons, Inc., Hoboken, New Jersey.

Cho, B.D. and Fane, A.G. (2002). "Fouling transients in nominally sub-critical flux operation of a membrane bioreactor." *J. Membr. Sci.*, 209, 391–403.

Cho, J., Song, K.G., Yun, H., Ahn, K.H., Kim, J.Y., and Chung, T.H. (2005). "Quantitative analysis of biological effect on membrane fouling in submerged membrane bioreactor." *Water Sci. Technol.*, 51, 9–18.

Choi, H., Zhang, K., Dionysiou, D.D., Oerther, D.B., and Sorial, G.A. (2005). "Effect of permeate flux and tangential flow on membrane fouling for wastewater treatment." *Sep. Purif. Technol.*, 45, 68–75.

Duclos-Orsello, C., Li, W., and Ho, C.C. (2006). "A three mechanism model to describe fouling of microfiltration membranes." *J. Membr. Sci.*, 280, 856–866.

Eckenfelder, W.M. (1966). *Industrial water pollution control*, McGraw-Hill, New York.

Fan, X., Urbain, V., Qian, Y., and Manem, J. (2000). "Ultrafiltration of activated sludge with ceramic membranes in a cross-flow process." *Water Sci. Technol.*, 41, 243–250.

Fane, A.G. and Fane, S.A. (2005). "The role of membrane technology in sustainable decentralized wastewater systems." *Wat. Sci. Tech.*, 51 (10), 317–325.

Ferrando, M., Rozek, A., Zator, M., Lopez, F., and Guell, C. (2005). "An approach to membrane fouling characterization by confocal scanning laser microscopy." *J. Membr. Sci.*, 250, 283–293.

Han, S.S., Bae, T.H., Jang, G.G., and Tak, T.M. (2005). "Influence of sludge retention time on membrane fouling and bioactivities in membrane bioreactor system." *Process Biochem.*, 40, 2393–2400.

Huisman, I.H., Pradanos, P., and Hernandez, A. (2000). "The effect of protein-protein and protein-membrane interactions on membrane fouling in ultrafiltration." *J. Membr. Sci.*, 179, 79–90.

Hermanowicz, S.W. (2004). "Membrane Filtration of Biological Solids: A Unified Framework and its Applications to Membrane Bioreactors." *Proceedings, Water Environment Membrane Technology 2004 Conference*, June 9, 2004, Seoul, South Korea.

Juang, Y., Adav, S.S., Lee, D., and Lai, J. (2010). "Influence of internal biofilm growth on residual permeability loss in aerobic granular membrane bioreactors." *Environ. Sci. Technol.*, 44, 1267–1273.

Kallioinen, M., and Nyström, M. (2008). Membrane surface characterization. In *Advanced Membrane Technology and Applications*, Li, N.N., Fane, A.G., Ho, W.S.W., and Matsuura, T. (eds.), Ch. 32, pp. 841–877. John Wiley & Sons, Inc., Hoboken, New Jersey, 2008.

Kimura, K., Naruse, T., and Watanabe, Y. (2009). "Changes in characteristics of soluble microbial products in membrane bioreactors associated with different solid retention times: Relation to membrane fouling." *Wat. Res.*, 43, 1033–1039.

Le-Clech, P., Chen, V., and Fane, T.A.G. (2006). "Fouling in membrane bioreactors used in wastewater treatment." *J. Membr. Sci.*, 284, 17–53.

Masse, A., Sperandio, M., and Cabassud, C. (2006). "Comparison of sludge characteristics and performance of a submerged membrane bioreactor and an activated sludge process at high solids retention time." *Wat. Res.*, 40, 2405–2415.

Meng, F., Chae, S., Drews, A., Kraume, M., Shin, H., and Yang, F. (2009). "Recent advances in membrane bioreactors (MBRs): Membrane fouling and membrane material." *Wat. Res.*, 43, 1489–1512.

Ng, T.C.A. and Ng, H.Y. (2010). "Characterisation of initial fouling in aerobic submerged membrane bioreactors in relation to physic-chemical characteristics under different flux conditions." *Wat. Res.*, 44, 2336–2348.

Ognier, S., Wisniewski, C., and Grasmick, A. (2002a). "Characterisation and modelling of fouling in membrane bioreactors." *Desalination*, 146, 141–147.

Ognier, S., Wisniewski, C., and Grasmick, A. (2002b). "Membrane fouling during constant flux filtration in membrane bioreactors." *Membr. Technol.*, 2002, 6–10.

Rosenberger, S. and Kraume, M. (2003). "Filterability of activated sludge in membrane bioreactors." *Desalination*, 151, 195–200.

Rosenberger, S., Laabs, C., Lesjean, B., Gnirss, R., Amy, G., Jekel, M., and Schrotter, J.C. (2006). "Impact of colloidal and soluble organic matter on membrane performance in membrane bioreactors for municipal wastewater treatment." *Wat. Res.*, 40, 710–720.

Song, L. (1998). "Flux decline in crossflow microfiltration and ultrafiltration: mechanisms and modeling of membrane fouling." *J. Membr. Sci.*, 139, 183–200.

Svarosky, L. (1977). *Solid-Liquid Separation*, Butterworth & Co Ltd, London.

Tracey, E.M., and Davis, R.H. (1994). "BSA fouling of track-etched polycarbonate microfiltration membranes." *J. Coll. Interf. Sci.*, 167, 104–116.

Visvanathan, C., Ben Aim, R., Parameshwaran, K. (2000). "Membrane separation bioreactors for wastewater treatment." *Critical Reviews in Environmental Science and Technology*, 30, 1–48.

Wang, Z., Wu, Z., Yin, X., and Tian, L. (2008). "Membrane fouling in a submerged membrane bioreactor (MBR) under sub-critical flux operation: Membrane foulant and gel layer characterization." *J. Membr. Sci.*, 325, 238–244.

Yamammoto, K., Hiasa, H., Mahmood, T., and Matsuo, T. (1989). "Direct solid liquid separation using hollow fiber membrane in an activated sludge aeration tank." *Water Sci. Technol.*, 21, 43–54.

Yamamura, H., Kimura, K., Okajima, T., Tokumoto, H., and Watanabe, Y. (2008). "Affinity of functional groups for membrane surfaces: Implications for physically irreversible fouling." *Environ. Sci. Technol.*, 42, 5310–5315.

Zhang, J., Chuan, H.C., Zhou, J., and Fane, A.G. (2006a). "Factors affecting the Membrane Performance in Submerged Membrane Bioreactors." *J. Membr. Sci.*, 284, 54–66.

Zhang, T.C. and Bishop, P.L. (1994). "Evaluation of tortuosity factors and effective diffusivities in biofilms." *Wat. Res.*, 28, 2279–2287.

CHAPTER 5

CONCLUSIONS

5.1 Fulfillment of Research Objectives

The ultimate goal of the project was to incorporate innovative renewable energy/energy saving technologies (water/wastewater, construction, and so forth) into green building and community design and construction. Under this mission, this work was aimed to propose an efficient technology to reclaim greywater (GW) in that the reuse of treated GW decreases the fresh water requirement, and the efficiency of the technology saves energy. Accordingly, a technological combination of shredded tire biofilter (STB) and membrane bioreactor (MBR) was evaluated to treat GW. The combination was proven to be effective in GW reclamation as the final effluent met the wastewater reuse guidelines (urban reuse) suggested by the U.S. Environmental Protection Agency (EPA). MBRs ensured the high-quality reusable water, whereas the degradation of organic contents of GW in STBs decreased the energy consumption that would be otherwise required of MBRs in the forms of areation and pumping. Moreover, the use of shredded tires in STBs shed light on their applications in bio-retention basins and constructed wetland treating stormwater, which may enlarge disposal alternatives for scrap tires. Membrane fouling was investigated to unveil the fundamental mechansims, and a model was also proposed to aid the understanding. Both of the experimental results and the modeling may provide insights on fouling alleviation and thus energy saving. Specifically, the following objectives of the study were achieved through this research:

1. To assess whether STBs could effectively treat GW (or whether shredded tires can be used as a packing material in biological filters) by investigating the performance of treating GW at various hydraulic retention times (HRTs);
2. To study the impact of tire shred size on the treatment performance of STBs, the treatment performance at different depths along STBs, and properties of biofilms in STBs if they were proved to be effective;
3. To investigate the performance of MBRs in reclaiming GW by comparing the effluent water quality with the water reuse guidelines suggested by the U.S. EPA (USEPA, 2004); and
4. To fundamentally understand the mechanisms behind the membrane fouling phenomenon in MBRs.

5.2 Summary of Conclusions

The combination of STBs and MBRs was proven effective in GW reclamation. GW was pre-treated in STBs, and the following conclusions on STBs can be reached:

1. STBs degraded certain organic contents and decreased turbidity in GW, and can be used as a pre-treatment process for GW reclamation;
2. The degradation of BOD mainly occurred in the upper layers in STBs, and the STB performance was subject to the fluctuations of influent quality;
3. As HRT increased, STBs showed better treatment performance, and decrease in shredded tire size enhanced the performance; and

4. The biofilm properties showed that bacteria could attach on shredded tires and grow, and proved that shredded tires can be used as a packing material in biological filters.

MBRs were used to further treat GW that had been treated in STBs, and the following conclusions are drawn:

1. Water quality of MBR effluent met the water reuse guidelines suggested by USEPA; and
2. Although controversial reports on the effects of SRT and MLSS on membrane fouling exist, this study indicated that longer SRT and higher MLSS concentration decreased fouling propensity.

Membrane fouling in MBRs was characterized in terms of three foulant components, namely proteins, polysaccharides and bacteria (nucleic acid) with the aid of confocal laser scanning microscope (CLSM) and Imaris. Proteins and polysaccharides were found to be the predominant foulants, and the specific volume (foulant volume/membrane area) of both was about three times that of bacteria. Contributions of the foulants to membrane fouling was also investigated, internally (inside the membrane) and externally (outside the membrane, cake layer). It was found that the ratio of the specific volume inside the membrane to that outside the membrane decreased in the first two stages but increased at Stage 3. It indicated that external fouling might have dominated the long-term Stage 2, whereas internal fouling might lead to the two TMP jumps in the 3-stage fouling map.

A mathematical model was proposed to help understand the fouling process better. The model dynamically linked TMP to the changes of membrane and cake layer porosities, membrane pore size, and the size of particles attached onto the membrane outside. The interpretations support the conclusions in the experiment quantitatively.

5.3 Implications for Future Research

Synthetic GW was used in the evaluation of STBs and MBRs. The recipe (Jefferson et al., 2001) is well representative of real GW, yet the combination should be tested with real GW as the compositions are more complicated. As GW is defined as wastewater excluding that from kitchen and toilet, it is expected that hair, dead skin, cloth fiber, etc. may clog STBs. This issue is under investigation.

Surfactants are possible contamination of the environment by the widespread use of detergent and soap (Scott and Jones, 2000), and so are heavy metals a threat to the environment (Fu and Wang, 2011). Lin and Juang (2002) reported heavy metal (Cu^{2+} and Zn^{2+}) removal from water by sorption using surfactant-modified montmorillonite. It is hypothesized that surfactants may be first absorbed to shredded tires in STBs, which may be able to remove heavy metals after adsorption and meanwhile solve the metal leaching problem of shredded tires. Because of the limited time, this is not initiated. Yet if this hypothesis is confirmed, the technology may be promising in treating stormwater and protecting waterbodies.

Findings regarding the membrane fouling mechanisms should aim at the establishment of efficient fouling control strategies or the development of anti-fouling membrane materials. For example, flocculants can be added to MBRs onto which the

major foulants of protein and polysaccharides can absorb instead of onto the membrane (Lee et al., 2007). Membrane surface can also be modified according to the adsorption of protein and polysaccharides.

5.4 References

Fu, F. and Wang, Q. (2011). "Removal of heavy metal ions from wastewaters: A review." *J. Environ. Manag.*, 92, 407–418.

Lee, WN., Chang, IS., Huang, BK., Park, PK., Lee, CH., and Huang, X. (2007). "Changes in biofilm architecture with addition of membrane fouling reducer in a membrane bioreactor." *Proc. Biochem.*, 42, 655–661.

Lin, SH. and Juang, RH. (2002). "Heavy metal removal from water by sorption using surfactant-modified montmorillonite." *J. Haz. Mater.*, B92, 315–326.

Jefferson, B., Burgess, J.E., Pichon, A., Harkness, J., and Judd, S.J. (2001). "Nutrient addition to enhance biological treatment of greywater." *Wat. Res.*, 35, 2702–2710.

Scott, M.J. and Jones, M.N. (2000). "The biodegradation of surfactants in the environment." *Biochimica et Biophysica Acta*, 1508, 235–251.

APPENDIX A

DETERMINATION OF MEAN DENSITIES, POROSITY AND THICKNESS OF BIOFILMS ATTACHED ON IRREGULAR-SHAPED MEDIA

A-1 Abstract

Biofilm density, porosity, and thickness are biofilm architecture properties that are important but often difficult to measure. In this study, wet and dry biofilm densities and biofilm porosity in shredded tire biofilters were determined using conventional methods but using a new porosity equation. Methods for determining the surface area and mean biofilm thickness covering tire chips were developed on the basis of box and ellipsoid shape models using the length, width, and thickness data for the tire chips making up the filter medium, as measured with a digital caliper, and the tire chip volume calculated from their measured weight (V_{MW}). The methods were evaluated and compared, via linear regression analysis, with the results from accurate X-ray computed tomography scanning. Results indicate that an ellipsoid shape model, combined with a modified form of the length-width-thickness data, derived from digital caliper measurements, and the value of V_{MW}, is the best combined model to compute the surface area and biofilm thickness. The combined method may be applicable for biofilm thickness measurement in attached growth systems packed with other irregular shaped media.

A-2 Introduction

Biofilm density, porosity, and thickness are biofilm architecture properties related to mass transfer and microbial distribution, and thus are important in both theoretical modeling and practical application (Bakke and Olsson, 1986). Estimation of biofilm thickness, however, is a difficult task. Measurement techniques for biofilm thickness reported in the literature can be classified as non-destructive and destructive methods. Non-destructive methods often depend on different instruments or tools to provide high-resolution results without destruction to the biofilm itself. Bakke and Olsson (1986)

established an optical method to measure biofilm thickness, in which the thickness is proportional to the measured vertical displacement by light microscopy. A number of studies adopted this approach to quantify biofilm thickness (Peyton, 1995; Milferstedt et al., 2006; Bouletreau et al., 2011). Freita dos Santos and Livingston (1995) developed an in- situ and noninvasive projection technique for this purpose. Other instruments also were used to measure biofilm thickness, such as glass pipettes with a tip diameter of approximately 3 μm (Zhang et al., 1995), confocal laser scanning microscopy (Stoodley et al., 1999), and laser triangulation sensors (Okkerse et al., 2000). A summary of these methods can be found in Paramonova et al. (2007). Destructive methods (e.g., scanning electron microscopy, microtome) often involve sample preparation steps that may change the biofilm thickness and properties, leading to less-representative results.

All the aforementioned techniques require delicate equipment and laborious work. Based on the assumption that biofilms possess planar structures with relatively constant and/or regular thickness (Wimpenny et al., 2000), biofilm thickness can be calculated by dividing the volume of the biofilm by the surface area the biofilm covers. This method may not provide in-depth insight into the microscopic heterogeneity in biofilm structure, but its merit lies in the macro- and practical applications like biofilm growth and decay monitoring. Horn and Hempel (1997) calculated the mean thickness of the biofilm in a tube reactor, in which the surface area was known. The volume of the biofilm was obtained by dividing the weight difference between the reactor with and without biofilms by the wet biofilm density (assuming 1 g/cm^3). This method is easy and straightforward because the volume of the biofilm, V_{MW}, can be estimated by weighing. To estimate biofilm thickness, other researchers used the method developed by Horn and Hempel or

modified the methods by assuming irregular-shaped medium particles to be simple spheres (Schreyer and Coughlin, 1999; Shin et al., 1999; Horn et al., 2002; Manz et al., 2003; Rabah, 2003). In all these methods, the challenge is to obtain the value of the surface area of the medium if it is unknown. This usually is the case with biofilm in trickling filters. It may be estimated by assuming a specific shape for the particles making up the medium; however, the error resulting from this assumption may make it impossible to validate the assumption itself. For instance, Shin et al. (1999) assumed that the tire chips had a spherical shape after volume measurements and so calculated the specific surface area to be 403 m^2/m^3. However, the specific surface area measured by our X-ray computed tomography (CT) scan of our shredded tires with a similar size range (passing a #3–#4 mesh) was 1449 m^2/m^3. This large difference makes their conclusion about the specific surface area (and thus the biofilm thickness) less convincing.

In light of the above analysis, measurement of the thickness of the biofilms attached to irregular-shaped media is still a formidable challenge. In addition, while measurement of biofilm density and porosity is well established (Zhang and Bishop, 1994), some improvement in porosity measurement is still needed. It is imperative to develop simple/straightforward methods for the measurement of the biofilm thickness and porosity, which is the major objective of this study. Specifically, this paper focuses on the development of methods for determining the surface area and the mean biofilm thickness with mathematical models and with data consisting of the three longest lines of each filter medium particle, defined as the length, width, and thickness, measured with a digital caliper in combination with the value of V_{MW}.

A-3 Materials and Methods

Measurements of filter medium. The key to calculating biofilm thickness is obtaining the surface area of the filter medium (shredded tires in this case) that is as accurate and readily obtainable as possible. We propose to measure the length (L), width (W) and thickness (T) of the filter medium with a digital caliper and then use existing models to calculate the surface area of the medium. L is the largest surface-to-surface distance, W is the largest surface-to-surface distance that is perpendicular to the direction in which L was measured, and T is the largest surface-to-surface distance that is perpendicular to both L and W, so that $L \geq W \geq T$ (Taylor et al., 2006).

In this study, two types of shredded tire (also referred to as tire chips) were used. Type A tire chips are in the size range of a #30 mesh sieve (0.6 mm) with a measured packed porosity of 0.49 (BAS Recycling, Inc., San Bernardino, CA, USA). Type B tire chips are in the size range of a #3–#4 mesh (4.8-6.7 mm) with a measured packed porosity of 0.53 (Bruckman Rubber Co., Hastings, NE, USA). The density of both types of tire chips was measured to be 1.15 g/cm^3. The L, W, and T of two sets of Type B (each set with 10 tire chips) and one set of type A (10 tire chips) were measured using a digital caliper with an estimated uncertainty of ± 0.5 mm. The accuracy of reading the digital caliper is actually ± 0.02 mm, but the uncertainty in estimating the perpendicularity condition for W and T dominates the measurement. Actually, the uncertainty in L is probably less, more like ± 0.1 mm. In addition, each tire particle was also weighed with an analytical scale (Mettler AE 100, Alfie Packers, Inc., Omaha, NE) to obtain an extra set of volume data (V_{MW})

that was used to calculate the volume for each tire chip using the estimated density. The uncertainty of the scale was ± 0.1 mg.

X-ray computed tomography. Thirty tire chips were imaged using X-ray computed tomography (X-ray CT), 20 of type B (larger chips) and 10 of type A (smaller chips). The particles were immobilized in a container, which was then scanned at a voxel size ranging from 15 μm/voxel to 25 μm/voxel. The 2-D slices obtained from X-ray CT scanning were packed together into 3-D images, and each particle was analyzed using spherical harmonic functions from which the values of volume, surface area, L, W, and T were computed (Taylor et al., 2006). Because of the demonstrated accuracy of this method for particle shape and size measurement, the X-ray CT results were used as "ground truth" against which to compare results from other measurement methods and model calculations. The estimated uncertainty for the volume and surface area computations are about 2 % to 3 %, while that for the L, W, and T computations are about 3 % to 5 %.

Models for calculation of surface area and volume of media. Two three-parameter shape models, box and ellipsoid, were investigated as equivalent shape models for irregular rocks by Taylor et al. (2006), and were adopted in this study:

$$V_{box} = 8abc \tag{1}$$

$$V_{ell} = \frac{4\pi}{3} abc \tag{2}$$

where, a, b, and c are half of the measured L, W, and T, respectively. The surface areas of both models are (Taylor et al., 2006):

$$SA_{box} = 8(ab + ac + bc) \tag{3}$$

$$SA_{ell} = 4\pi\left[\frac{(a^p b^p + a^p c^p + b^p c^p)}{\left[3 - k(1 - 27abc(a+b+c)^{-3})\right]}\right]^{1/p} \tag{4}$$

where $p = \ln(2)/\ln(\pi/2) \approx 1.5349$ and $k = 0.0942$ (Thomsen, 2004).

We used three data sets for computing the volumes and surface areas of the media: the L, W, and T from a) the X-ray computed tomography (CT) analysis (designated with "-CT"); b) digital caliper measurements (designated with "-MEAS"), and c) the ratio data created based on "-MEAS" (designated with "-RA."). The ratio data was computed by using the length data from the digital caliper measurements as the length L in this data set. The width W was computed from the length data by using the quotient of the length divided by the mean length to width ratio that was computed from the digital caliper measurements (i.e., $W_i = L_i/(L/W)_{Mean}$, where i = 1, 2, …20 for each individual tire chips) The thickness T was computed similarly from the length L by using the quotient of L divided by the mean length to thickness ratio, as also computed from the digital caliper measurements (i.e., $T_i = L_i/(L/T)_{Mean}$ for every particle). The RA data set was generated to try and see if a simpler procedure could be used for estimation of the specific surface area of the tire chips. It should also be noted that the ellipsoid shape model, using the RA data, yielded better results than that with the other two data sets (more below), which was also why the RA data set was created.

Volumes and surface areas calculated from the two models using Eqs. (1)–(4), using the three sets of data, were plotted against the particle volumes and surface areas as

obtained by CT analysis, respectively. Because of its known accuracy (Taylor et al., 2006), the CT data was thought of as the "correct": data, and the goodness of the various model/data combinations tried were judged based on how close to the CT data the results were. Linear correlations were evaluated by comparing the slopes, y-intercept and R^2 coefficients of different models, which were used as the criteria with which to select corresponding models. Once the best model were chosen, the volume and surface area can be then calculated with the models, which allows the calculation of the average specific surface area (SSA) of the medium (e.g., tire chips). In addition, if necessary the specific surface areas, SSA, of each tire chip can be obtained by dividing the surface area calculated by the selected model by the volume of each tire particle measured with V_{MW}.

Biofilter setup. Four parallel shredded tire biofilters (STBs) were used to culture biofilm by treating synthesized greywater (GW) under anaerobic conditions. Two STBs (Fig. A-1) were filled with Type A tire chips and two with Type B. The biofilters were inoculated with activated sludge sampled from a local wastewater treatment plant for biofilm accumulation for 5 days, and then were fed continuously with artificial GW (Table A-1) for evaluation of their performance. The flow pattern of the STBs was gravity flow, and the outlets of the STBs were kept higher than the top media so that the entire media in each STB was kept in a saturated condition. Aluminum foil was used to wrap the column to avoid algae growth inside the reactors. Influent pumps were controlled to run STBs at hydraulic retention times (HRTs) of 2.5 and 10 hours. The performance of STBs and why shredded tires were selected as the filter media are described in Hu et al. (2011).

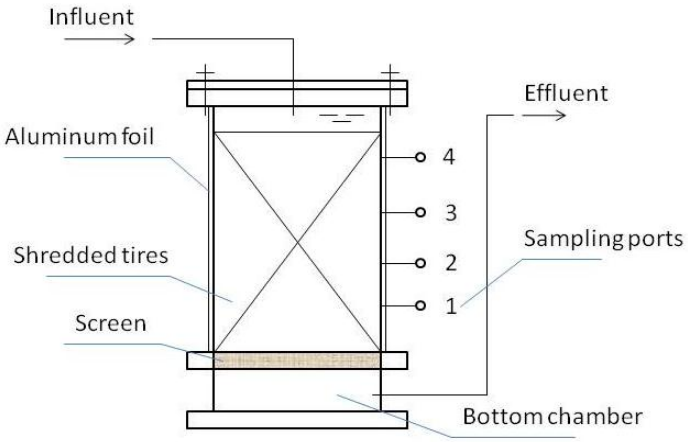

Figure A-1. Schematic diagram of a shredded tire biofilter (STB). The STB is constructed from a 6.35 cm inner diameter acrylic pipe with a total height of 49 cm and medium height of 36 cm (excluding the bottom chamber).

Table A-1. Synthetic greywater recipe (Jefferson et al., 2001).

Item	Quantity (made up with 10 L tap water)
Synthetic soap	0.64 g
Hair shampoo	8.0 mL
Sunflower oil	0.1 mL
Tertiary effluent	24.0 mL

Biofilm sampling and testing. For each biofilm analysis, ten shredded tire chips coated with biofilms were randomly collected from each of the three layers (i.e., top = 25 cm to 36 cm, middle = 13 cm to 25 cm, and bottom = 0 cm to 13 cm from the screen, respectively) in each STB. It was achieved by first pouring out tire chips in different layers consecutively, and then randomly selecting from those whose coatings were not compromised (e.g., tire chips with biofilm not touching the bench). The sampled tire chips were analyzed by the following steps: a) drained on an aluminum rack for 20 min; b)

weighed in both air and water to determine the volume of the shredded tires before the removal of biofilms (Archimedes' method, assuming 1 g/mL for the density of water) (Taylor et al., 2006); c) vortexed in 20 mL deionized (DI) water three times for 1 min each time, and removed from DI water; and d) washed with 5 mL DI water. The suspensions in step c) were collected together with the wash water and were used to measure total solids (TS) and total volatile solids (TVS) as per the *Standard Methods* (APHA et al., 2005); e) after biofilm removal, the tire chips were drained on the aluminum rack for 20 min and weighed in both air and water to determine the total volume (V_T) of the 10 STB tire chips after biofilm removal. The same analytic scale was used for weighing; and f) the total volume of biofilms (V_B) attached on the 10 tire chips was calculated with the difference between the volumes determined before (Step b) and after biofilm removal (Step e).

Calculation of biofilm properties. Biofilm dry density can be calculated using the following equation (Tchobanoglous and Burton, 1991):

$$\frac{M_s}{D_d} = \frac{M_f}{D_f} + \frac{M_v}{D_v} \tag{5}$$

where D_d is dry density of biofilm (mg/cm^3 dry biomass); M_s is dry mass of solids in biofilm (mg); D_f is density of fixed mineral solids in biofilm (assuming 2.5 mg/cm^3); M_f is dry mass of fixed mineral solids in biofilm (mg); D_v is density of volatile solids in biofilm (assuming 1.0 mg/cm^3); and M_v is dry mass of volatile solids in biofilm (mg). Wet density is obtained from equation (6) (Tchobanoglous and Burton, 1991):

$$\frac{1}{D_w} = \frac{W_{ds}}{D_d} + \frac{W_{tw}}{\rho_w} \tag{6}$$

where D_w is wet density of biofilm (g/cm^3 total biofilm); W_{ds} is dry solids content of biofilm (%); W_{tw} is water content of biofilm (including water both inside and outside of cells, %); and ρ_w is density of water (1 mg/cm^3). The equation for porosity calculation is modified from Zhang and Bishop (1994):

$$\varepsilon = \left(1 - \frac{V_w}{V_b}\right) \cdot 100 = \left(1 - \frac{M_s}{D_d} \cdot \frac{1}{(1 - W_{wt}) \cdot V_b}\right) \cdot 100 \quad (7)$$

where ε is porosity of the biofilm (%); V_w is the volume of biofilm including water inside cells but excluding water outside of cells (cm^3); V_b is the measured total biofilm volume (cm^3) (= volume of biofilm with water inside cells + volume of water outside of cells); and W_{wi} is the water content inside the cells (assuming 80 %).

The biofilm thickness was calculated by dividing the total biofilm volume (V_T) by the surface area (SA) covered by the biofilms. The surface area SA was the product of the volume of the sample of shredded tires and the value of SSA calculated either from a model or from the CT analysis. The biofilm thickness based on the model was compared to that based on CT analysis; the corresponding difference was regarded as the criterion whether the model can be accepted (e.g., a difference greater than 5 % to 10 % suggests that model modification may be needed). It should be noted that the difference between SSA values can also be used as a criterion, but the differences between biofilm thickness carries more practical meaning from the perspective of environmental engineering.

Model verification. In this study, data from Type B tire chips were used for model selection (and modification, see below), and data from Type A tire chips and rocks (Taylor et al., 2006) were used for model verification by comparing their results to that

obtained from CT analysis. Since the CT scan generated the most accurate data in terms of length, width and thickness, the CT data were used as the "standard" for model verification.

Table A-2. Spatial distributions of biofilm densities and porosities.

HRT[1], tire type, and location	Dry density, g/cm^3	Wet density, g/cm^3	Porosity, %
10 h, A, top layer	1.034	1.008	59.12
10 h, A, middle layer	1.124	1.013	32.57
10 h, A, bottom layer	1.058	1.008	65.75
2.5 h, A, top layer	1.099	1.006	71.65
2.5 h, A, middle layer	1.122	1.010	62.45
2.5 h, A, bottom layer	1.125	1.015	58.69
10 h, B, top layer	1.132	1.030	38.73
10 h, B, middle layer	1.130	1.078	68.44
10 h, B, bottom layer	1.179	1.012	69.18
2.5 h, B, top layer	1.113	1.036	45.82
2.5 h, B, middle layer	1.066	1.005	36.71
2.5 h, B, bottom layer	1.121	1.036	28.27

[1] HRT = Hydraulic retention time.

A-4 Results and Discussions

Biofilm wet density, dry density and porosity. Table A-2 lists the spatial distributions of biofilm densities and porosities, which were calculated using Eqs. (5)–(7). Knowing biofilm densities, porosities, and thicknesses is crucial to the identification of significant components of biofilm structure and the proper interpretation of experimental findings and understanding of reactions occurring in biofilms (Fruhen et al., 1991; Lawrence et al., 1991; Zhang and Bishop, 1994). As this study is focused only on the method to measure

biofilm thickness, however, the significance of these other properties is not discussed here.

Surface area and volume of tire chips measured by CT analysis and calculated from models. The L, W and T of the 20 Type B shredded tires from both the CT analysis and digital caliper measurements are listed in Table A-3. The results of linear regression analysis of the digital caliper LWT measurements (ordinate) plotted against the CT LWT measurements (abscissa) are given in Table A-4 (slopes, y-intercept and R^2 coefficients). In column 5, the % difference is the difference between the average dimension as measured by CT compared to the average dimension as measured by the digital caliper, using the numbers listed on the last line of Table A-3 ("Average"). In column 6 of Table A-4, the y-intercept is expressed as a percentage of the maximum abscissa value. According to Taylor et al. (2006), the slope is a factor to indicate how useful and physical the linear correlation is, with a slope closer to unity being more useful and physical. Another factor is the y-intercept as a percentage of the maximum abscissa, which is used as a check on how "realistic" the correlation is (Taylor et al., 2006). Since both ways of measuring L, W, and T should give zero for a zero size particle, the graphs analyzed should ideally go through the origin and the y-intercept should be zero. Therefore, the smaller the percentage, the more realistic the correlation. In our case, the slopes range from 0.80–1.02, and the y-intercepts as a percentage of the maximum abscissa range from 2.9 % to 9.2 %, which indicate that these correlation are acceptable. The greatest discrepancy between the average CT and digital caliper measurement data lies in the width, with a 9.6 % difference (column 5 of Table A-4). In fact, t-test analysis indicate

that the two data sets are statistically the same ($\alpha = 0.05$; $p = 0.672$ for length, $p = 0.228$ for width, and $p = 0.828$ for thickness), indicating the digital caliper measurements are as valid as the CT measurements, in a statistical sense.

Table A-3. Dimensions of Type B tires chips from X-ray CT scanning data and digital caliper measurements.

Shredded Tire #	CT			Digital Caliper Measurement		
	Length, mm	Width, mm	Thickness, mm	Length, mm	Width, mm	Thickness, mm
1	19.93	13.00	10.77	20.07	11.28	9.56
2	11.56	7.33	5.83	12.50	5.32	5.26
3	13.80	11.18	6.07	13.61	10.01	5.58
4	10.76	9.37	4.24	8.94	7.29	4.34
5	12.72	6.97	4.08	12.07	6.58	5.10
6	11.97	5.79	3.97	11.65	5.92	4.76
7	9.27	6.29	2.96	8.30	6.13	2.97
8	9.69	6.41	4.53	7.82	4.90	4.88
9	7.62	4.94	3.25	7.85	4.90	4.24
10	9.80	5.75	3.20	9.72	5.24	3.77
11	13.06	8.46	7.24	12.70	7.65	6.91
12	10.36	8.51	5.78	8.61	7.49	5.69
13	9.79	7.18	3.75	9.60	6.25	3.53
14	8.31	7.11	6.81	7.95	7.24	6.27
15	11.07	8.96	7.42	10.69	9.27	9.20
16	8.60	8.24	3.45	8.13	7.32	3.20
17	7.44	7.22	4.92	7.57	5.97	4.12
18	9.94	5.85	4.82	9.65	5.66	5.54
19	8.17	5.40	3.87	8.46	5.54	4.19
20	9.90	6.72	3.52	10.11	6.33	3.91
Average	10.69	7.53	5.02	10.30	6.81	5.15

Table A-4. Results of linear regression of digital caliper measurements of Type B chips vs. X-ray CT scan data.

Dimension	Slope	y-Intercept	R^2	[%] difference	[%] of maximum abscissa
Length	1.02	0.59	0.939	3.6	2.9
Width	0.80	0.79	0.868	9.6	7.0
Thickness	0.85	0.88	0.860	-2.5	9.2

Calculated from the digital caliper measurements listed in Table A-3, the mean length to thickness ratio, $(L/T)_{Mean}$ ($= \Sigma(L_i/T_i)/20$, L_i and T_i = length and thickness of i^{th} individual chip, i = 1, 2, …, 20) is 2.092, and the mean length to width, $(L/W)_{Mean}$ ratio is 1.537. The equivalent values for the CT measurements were 2.269 and 1.445, only a 6 % to 8 % difference, respectively. Based on the digital caliper measurement ratios, the ratio data was then generated. Although little difference would have been made if the average CT measurement ratios were used, it was thought better to use the digital caliper measurements since this is a faster and far less expensive measurement technique, and very accessible to all engineers and scientists. The three L-W-T data sets (i.e., CT analysis, digital caliper measurements, and ratio data set) were used as input in Eqs. (1)–(4), and the model results for particle volume and surface area were plotted against the CT scanned volume and surface area (used as the "true values") for regression analysis and are displayed in both parts of Fig. A-2. Table A-5 summarizes the linear correlation results between each model calculated with each data set and the CT scanned values. Since there four models (two volumes and two surface areas) and three LWT datasets, there are 4 x 3 = 12 entries in Table A-5.

Using a similar analysis as that used for the LWT correlations, the slopes and the y-intercepts as a percentage of the maximum abscissa value were the criteria used to compare the models against each other to decide which was the best for the purpose. Considering the volume correlations (Fig. A-2b and top half of Table A-5), the ellipsoid model using the measured data (ELL-MEAS-V) had a slope (1.25) closest to unity, but the y-intercept as a percentage of the maximum abscissa (15.9 %) was too high to make it a "realistic" model. The slope of the ellipsoid model using the ratio data (ELL-RA-V,

1.43) was second closest to unity, and its y-intercept as a percentage of the maximum abscissa (0.8 %) was the lowest of all six correlations. Therefore, the "Ell-RA" model was determined to be the best model to use to calculate the volume of the shredded tires based on the RA LWT measurements. In exactly the same way, the "Ell-RA" model is the optimal model among the evaluated models to compute the surface area of the shredded tires based on the RA LWT measurements.

Table A-5. Summary of linear correlations between X-ray CT scanning data and results from six models.

Models	Slope	y-Intercept	R^2	[%] of maximum abscissa value
Box-CT-V	3.13	17.66	0.993	2.0
Ell-CT-V	1.64	9.25	0.993	1.0
Box-MEAS-V	2.41	62.12	0.957	6.9
Ell-MEAS-V	1.25	142.85	0.711	15.9
Box-RA-V	2.74	14.08	0.936	1.6
Ell-RA-V	1.43	7.37	0.936	0.8
Box-CT-SA	2.00	11.56	0.989	1.9
Ell-CT-SA	1.06	14.83	0.984	2.4
Box-MEAS-SA	1.57	65.45	0.933	10.5
Ell-MEAS-SA	0.90	26.44	0.929	4.2
Box-RA-SA	1.81	8.55	0.888	1.4
Ell-RA-SA	0.97	4.59	0.888	0.7

Box-CT-V (or -SA) = box shape model with CT data used to calculate volume (or surface area); Ell-CT-V (or -SA) = ellipsoid shape model with CT data used to calculate volume (or surface area); Box-MEAS-V (or -SA) = box shape model with measured data to calculate volume (or surface area); Ell-MEAS-V (or -SA) = ellipsoid shape model with measured data used to calculate volume (or surface area); Box-RA-V (or -SA) = box shape model with ratio data to calculate volume (or surface area); Ell-RA-V (or -SA) = ellipsoid shape model with ratio data used to calculate volume (or surface area).

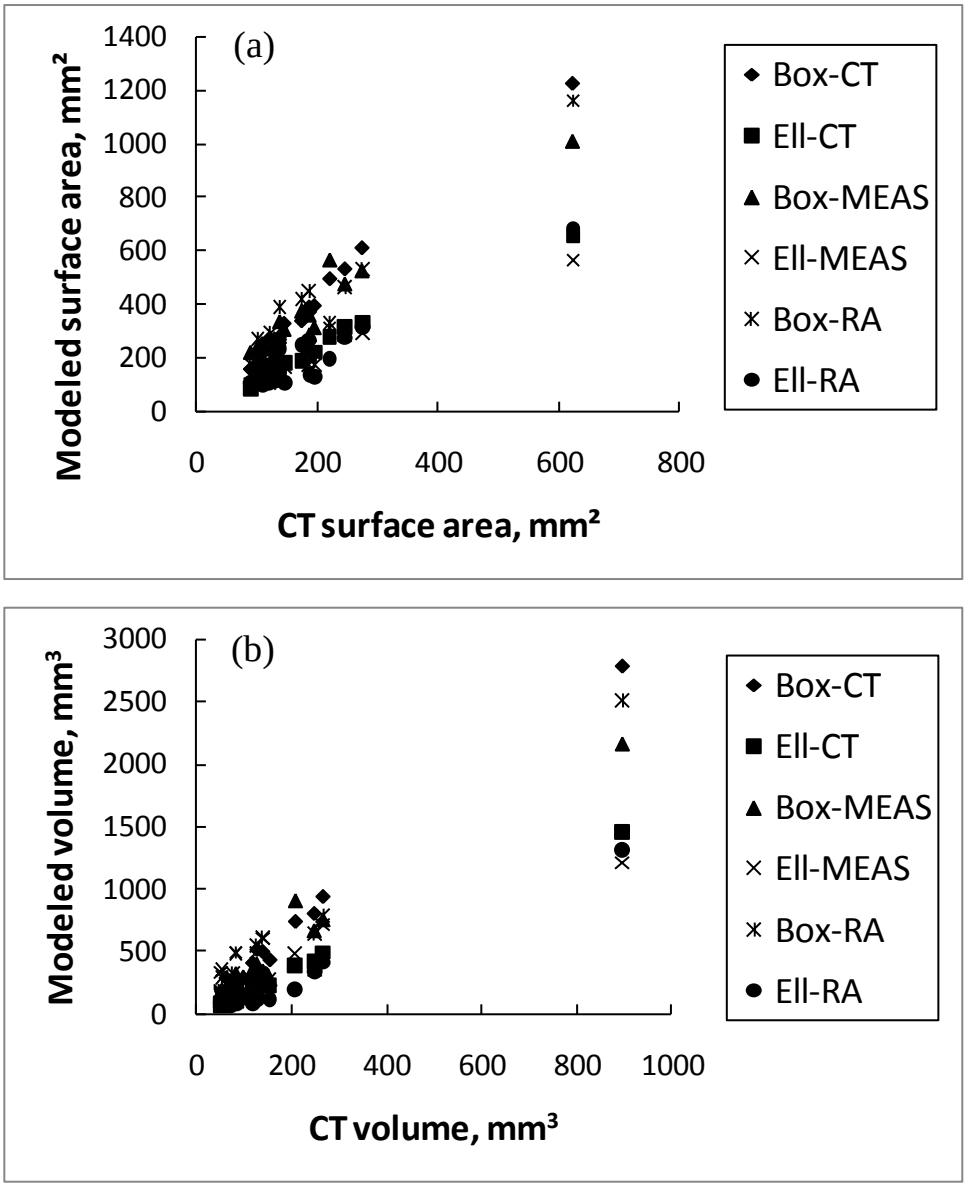

Figure A-2. Relationships between (a) surface area modeled by Eqs. (2) and (4) and that from X-ray CT scanning and (b) volume modeled by Eqs. (1) and (3) and that measured by X-ray CT. Box-CT = box shape model with CT scanning data; Ell-CT = ellipsoid shape model with CT scanning data; Box-MEAS = box shape model with measured data; Ell-MEAS = ellipsoid shape model with measured data; Box-RA = box shape model with ratio data; Ell-RA = ellipsoid shape model with ratio data.

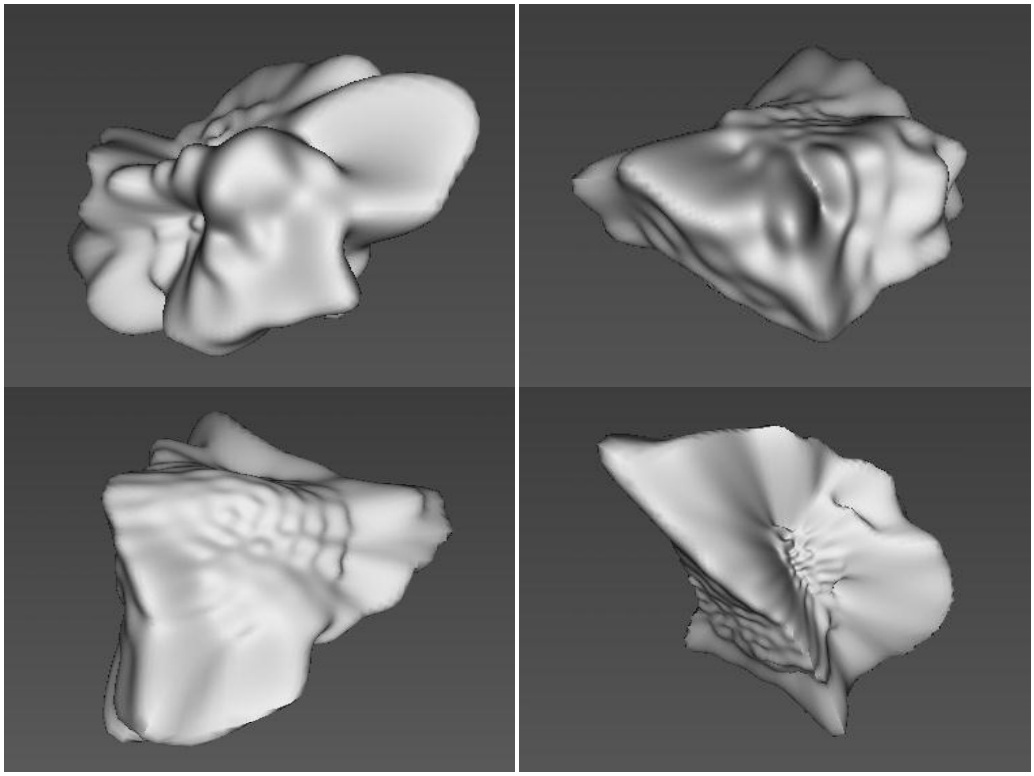

Figure A-3. VRML images of four typical shredded tires, type B.

It seems perhaps coincidental that the same model and the same set of measurements were identified as the "best" model to calculate both volume and surface area. Yet a closer look at the tire chips in Fig. A-3 would favor the ellipsoid model over the box model. These pictures were generated from the X-ray CT scans of actual particles from Table 3 using a spherical harmonic reconstruction (Taylor et al. (2006)). Taylor et al. (2006) also found that the ellipsoid shape model showed a better linear correlation, in terms of slopes closer to unity and y-intercepts a lower percentage of the maximum abscissa value, with the X-ray CT data than did the box shape model using X-ray CT LWT measurement data for rocks of various sizes. It is interesting to note that in this present study, it is the ratio data that provides the best fits in both volume and surface

area. Again, this is probably due to the shape of the tire chips (see Fig. A-3). Using the mean values of the L/W and L/T ratios, instead of all the actual digital caliper measurements, makes the ellipsoid model using the ratio data a better model fit to the X-ray CT results.

Biofilm thickness. Now that the surface area is known, the next step is to compute the biofilm thickness. We used four different methods to do so: the CT scan data, the RA data, data assuming the tire chips were spheres, and a combined model defined in the following, as shown in Table A-6 for the type B tire chips (bottom half of Table A-6).

Table A-6. Mean biofilm thicknesses from X-ray CT scan data and the three models.

HRT, tire type, location	Mean biofilm thickness, mm			
	CT scan	Ell-RA model	Combined model	Sphere
(1)	(2)	(3)	(4)	(5)
10 h, A, top layer	0.121	0.159	0.126	0.164
10 h, A, middle layer	0.043	0.056	0.044	0.058
10 h, A, bottom layer	0.063	0.082	0.065	0.085
2.5 h, A, top layer	0.310	0.409	0.322	0.421
2.5 h, A, middle layer	0.130	0.172	0.135	0.176
2.5 h, A, bottom layer	0.091	0.120	0.095	0.124
10 h, B, top layer	0.082	0.122	0.080	0.116
10 h, B, middle layer	0.101	0.150	0.098	0.142
10 h, B, bottom layer	0.109	0.162	0.105	0.153
2.5 h, B, top layer	0.132	0.195	0.128	0.186
2.5 h, B, middle layer	0.063	0.093	0.061	0.088
2.5 h, B, bottom layer	0.044	0.066	0.043	0.063

For the first method (column 3 in Table A-6), we used the LWT RA data to calculate the volume using eq. (2), the surface area using eq. (4), and specific surface area for each of the 20 B tire chips (= $(\text{Ell-RA-SA})_i/(\text{Ell-RA-V})_I$, i = 1, 2, …20). We then calculated the average specific surface area (SSA_{Avg}) of the tire chips. Using this average value, we computed the total surface area (SA_T) of the biofilm based on the total volume of the tire chips sampled from the STBs (V_T) on which biofilms attached, using $SA_T = SSA_{Avg} \cdot V_T$. Finally, the mean biofilm thickness (T_B) was calculated by dividing the volume of the attached biofilm (V_B determined as before) by the average surface area of the tire chips, $T_B = V_B / SA_T$. The results of this first method are shown in column 3 in Table A-6. An exactly analogous calculation was performed in the same way using the X-ray CT data and the results are displayed in column 2 of Table A-6. The values of biofilm thickness derived from the Ell-RA model were always greater than those from the X-ray CT scan data. This is not surprising as for the same tire particle the ELL-RA model yielded a smaller specific surface area value (0.976 mm^2/mm^3, Table A-7) than the CT value (1.449 mm^2/mm^3, Table A-7) for the type B tire chips. Although the trend of the spatial distribution of biofilm thickness in different layers as seen in the CT data in Table 6 was followed by the ELL-RA model, the average difference between the results of columns 3 and 2 was about 48 % and that is unacceptably large.

An inspection reveals that the most of the difference between columns 3 and 2 comes from the volume estimate from the Ell-RA-V model, which gives a volume that is about 40 % too large (correlation slope = 1.43 in Table A-5) for the tire chips. The slope for the surface area was 0.97 or close to unity, which then yields a specific surface area that is smaller by about 40 % compared to the X-ray CT results. Hence, we needed to

find another model or method for computing the tire chip volume that is more accurate. Besides using a mathematical model based on LWT data to compute the volume, another method of obtaining the volume (V_{MW}) of an individual tire chip is via direct measurements of the weight of tire chips and using the estimated tire chip density, that is, V_{MW} = mass/density. A linear correlation between V_{MW} and the volume from X-ray CT analysis of the 20 tire chips gave a slope of 0.93, a y-intercept of 8.54 that is equal to only 0.7 % of the maximum abscissa value, and an $R^2 = 0.996$. Compared with a slope of 1.43, this is an obvious improvement on the accuracy of the volume values.

Table A-7. Comparison of results from three different models with X-ray CT scan data.

Media	Parameter	CT scan	Sphere	Ell-RA model	Combined model
Type A tire chips	Specific surface area, mm^2/mm^3	2.282	1.680	1.732	2.195
	Absolute difference, %	-	26.4	24.1	3.8
Type B tire chips	Specific surface area, mm^2/mm^3	1.449	1.028	0.976	1.495
	Absolute difference, %	-	29.0	32.6	3.2
Rocks[1]	Specific surface area, mm^2/mm^3	0.501	0.404	0.400	0.532
	Absolute difference, %	-	19.3	20.1	6.1

[1] Data from Taylor et al. (2006).

Therefore, for the second method ("Combined model" in column 4 of Table A-6), we calculated the volume of each tire chip from its measured weight for all the 20 type B tire chips (V_{MW}). Then the specific surface area was computed using this volume value and the Ell-RA value of surface area ($SSA_i = (\text{Ell-RA-SA})_i/V_{MW}$) for each tire chip. We then calculated the average specific surface area [$SSA_{Avg} = \Sigma SSA_i /20$] and the total

surface area (SA) of the biofilm ($SA_T = SSA_{Avg} \bullet V_{MW}$), and finally the mean biofilm thickness ($T_B = V_B/SA_T$). The results of the second method, termed "the combined model", are shown in column 4 of Table A-6. The average difference between the CT analysis and the combined model decreased to -3.1 %, which is an acceptable difference. Therefore, the combined model should be applicable to determine the specific surface area, and hence the mean biofilm thickness.

The mean biofilm thickness based on assuming that tire chips were spherical and using the volume measurements derived from the weight and estimated density (V_{MW}) was also calculated and listed in column 5 in Table A-7. The volume of each tire chip was set equal to the volume of a sphere and the sphere diameter determined. The specific surface area was then calculated using the formula for the surface area of a sphere. The average error is 35.8 % for the Type A tire chips, and 40.9 % for the type B tire chips, compared to the X-ray CT data. These errors are close to those from the Ell-RA model, and are also unacceptably large.

Model verification. Both the combined model (with the Ell-RA model for surface area and the weight measurements for volume) and the Ell-RA model (for both surface area and volume) were applied to Type A shredded tires, with the results shown in the top half of Table A-6. The difference of the mean biofilm thickness between the results from the combined model and from the CT data was about 4.0 %, which is much smaller than the 31.8 % difference between the results from the Ell-RA model alone (for both surface area and volume) and the CT data. The sphere data for type A was similar to the Ell-RA data and had the same kind of large differences from the CT data.

The specific surface areas were also compared to each other for the type A and type B tire chips and for the rocks studied in Taylor et al. (2006), using the X-ray CT data, the spherical particle model, the Ell-RA model, and the combined model. The comparison is meaningful since obtaining specific surface area is the key to calculating the mean biofilm thickness as discussed above. The results are listed in Table 7. The differences between the specific surface area from CT analysis and the combined model are 3.8 % for Type A tire chips, 3.2 % for Type B tire chips, and 6.1 % for rocks, which are by far the smallest among the three models. The results in Tables 6 and 7 prove the applicability of the combined model to accurately calculate the specific surface area, and, more importantly, the mean thickness of the biofilm covering irregular-shaped media.

Implementation, limitation, and implications. The measurements of biofilm densities and porosities require both the weight and volume of biofilms to be known. This can be achieved by: 1) removing biofilms from filter media; 2) weighing biofilms after drying and ignition; 3) determining biofilm volumes using weighing and Archimedes' method; and 4) calculating biofilm densities and porosities with Eqs. (5)–(7). The calculation of biofilm thickness also requires the surface area of the filter media to be known. For filter media with irregular shapes, the surface area can be calculated by multiplying the specific surface area and the volume of the media on which the biofilms are attached. In order to obtain the specific surface area, one can measure the length, width, and thickness of the medium directly with a digital caliper (or other tools). The data are then used to generate the ratio data (RA), and the ratio data are input into the ellipsoid shape model for surface area calculations (Ell-RA-SA). Either Archimedes' method or the weight measurement

can be employed for particle volume determination. With the surface area and the volume, one can compute the specific surface area of the media, and the surface area covered by the biofilms. The biofilm thickness is then just the biofilm volume divided by the particle surface area, which assumes that the biofilm thickness is small compared to the average particle size. In all the data shown in Table 6, this was indeed the case.

This method is not necessary for biofilm reactors where the surface area for biofilm growth is known (Bakke and Olsson, 1986; Horn et al., 2003); nor is it necessary in filters whose packing media are of regular shape or of known specific surface area. The combined method developed in this study has been demonstrated for rocks and shredded tire chips, and may be applicable to attached processes filled with other kinds irregular shaped media (e.g., gravel, sand, rock, woodchips, shredded tires), since the surface area for these types of media is difficult to measure or model accurately, especially without the aid of instruments like CT. The method(s) discussed here, however, may offer an easier solution to obtain the surface area and thus the biofilm thickness, together with information on biofilm density and porosity.

A-5 Conclusion

A simple, straight-forward method was proposed to better estimate biofilm thickness properties, using only simple mass measurement and digital caliper measurements. The box and ellipsoid shape models with three sets of length-width-thickness data (six models in total) were evaluated against X-ray computed tomography data, which was taken to be the accurate standard. The ellipsoid shape model, using length (L), width (W), and thickness (T) data as modified with the ratio data calculated from the digital caliper

measurements data, was determined to calculate the biofilm thickness. This procedure proved to be more accurate than the other models, as compared to the accurate X-ray CT measurements. It was found necessary, however, to directly measure the volume of the filter media using weighing and an estimated density in order to obtain accurate values of specific surface area for the tire chips. Combining the two, the results for biofilm thicknesses were found to agree well, to within a few percent, with the X-ray CT data. The results of this paper should find application in biofilm thickness calculation with other filter media for a faster, easier, but nonetheless accurate, approach.

A-6 References

APHA, AWWA, and WEF (2005). *Standard Methods for the Examination of Water and Wastewater*, 21st Ed., American Public Health Association, Washington, D.C.

Bake, R. and Olsson, P.Q. (1986). "Biofilm thickness measurements by light microscopy." *J. Microb. Meth.*, 5, 93–98.

Bouletreau, S., Charcosset, J.-Y., Gamby, J., Lyautey, E., Mastrorillo, S., Azemar, F., Moulin, F., Tribollet, B., and Garabetian, F. (2011). "Rotating disk electrodes to assess river biofilm thickness and elasticity." *Wat. Res.*, 45, 1347–1357.

Freitas dos Santos, L.M. and Livingston, A.G. (1995). "Membrane-attached biofilms for VOC wastewater treatment I: novel in situ biofilm thickness measurement technique." *Biotechnol. Bioeng.*, 47, 82–89.

Fruhen, M., Christan, E., Gujer, W., and Wanner, O. (1991). "Significance of spatial distribution of microbial species in mixed culture biofilms." *Wat. Sci. Tech.*, 23, 1365–1374.

Horn, H. and Hempel, D.C. (1997). "Growth and decay in an auto-/heterotrophic biofilm." *Wat. Res.*, 31, 2243–2252.

Horn, H., Reiff, H., and Morgenroth, E. (2003). "Simulation of growth and detachment in biofilm systems under defined hydrodynamic conditions." *Biotechnol Bioeng.*, 81, 607–617.

Hu, M., Zhang, T.C., Stansbury, J., Dahab, M., Shi, J., Neal, J., Alahmad, M., Berryman, C., Li, H., Schwer, A., and Shen, Z. (2010). "Combination of shredded-tire biofilter

and membrane bioreactor for greywater reclamation." *Proceedings of the 6th International Conference on Sustainable Water Environment: Water Infrastructure in Time of Climate Change*. July 29–31, 2010, Newark, DE, pp. 361–365.

Jefferson, B., Burgess, J.E., Pichon, A., Harkness, J., and Judd, S.J. (2001). "Nutrient addition to enhance biological treatment of greywater." *Wat. Res.*, 35, 2702–2710.

Lawrence, J.R., Korber, D.R., Hoyle, B.D., Costerton, J.W., and Caldwell, D.E. (1991). "Optical sectioning of microbial biofilms." *J. Bacteriol.*, 173, 6558–6567.

Manz, B., Volke, F., Goll, D., and Horn, H. (2003). "Measuring local flow velocities and biofilm structure in biofilm systems with magnetic resonance imaging (MRI)." *Biotechnol. Bioeng.*, 84, 424–432.

Milferstedt, K., Pons, M.N., and Morgenroth, E. (2006). "Optical method for long-term and large-scale monitoring of spatial biofilm development." *Biotechnol. Bioeng.*, 94, 773–782.

Okkerse, W.J.H., Ottengraf, S.P.P., and Osinga-Kuipers, B. (2000). "Biofilm thickness variability investigated with a laser triangulation sensor." *Biotechnol. Bioeng.*, 70, 619–629.

Paramonova, E., de Jong, E.D., Krom, B.P., van der Mei, H.C., Busscher, H.J., and Sharma, P.K. (2007). "Low-load compression testing: a novel way of measuring biofilm thickness." *App. Environ. Microb.*, 73, 7023–7028.

Peyton, B.M. (1996). "Effects of shear stress and substrate loading rate on *Pseudomonas Aeruginosa* biofilm thickness and density." *Wat. Res.*, 30, 29–36.

Rabah, F.K.J. (2003). *Denitrification of high-strength nitrate wastewater after using fluidized-bed biofilm reactors*. Ph.D. dissertation, University of Nebraska-Lincoln.

Schreyer, H.B. and Coughlin, R.W. (1999). "Effects of stratification in a fluidized bed bioreactor during treatment of metal working wastewater." *Biotechnol. Bioeng.*, 63, 129–140.

Shin, H., Yoo, K., and Park, J. (1999). "Removal of polychlorinated phenols in sequential anaerobic-aerobic biofilm reactors packed with tire chips." *Wat. Environ. Res.*, 71, 363–367.

Stoodley, P., Boyle, J.D., DeBeer, D., and Lappin-Scott, H.M. (1999). "Evolving perspectives of biofilm structure." *Biofouling*, 14, 75–90.

Taylor, M.A., Garboczi, E.J., Erdogan, S.T., and Fowler, D.W. (2006). "Some properties of irregular 3-D particles." *Powder Technol.*, 162, 1–15.

Tchobanoglous, G. and Burton, F.L. (1991). *Wastewater Engineering Treatment, Disposal, and Reuse* 3rd Ed. Metcalf & Eddy, McGraw-Hill, New York.

Thomsen, K. (2004). at http://home.att.net/~numericana/answer/ellipsoid.htm#ellipsoid. See also M.S. Klamkin (1971), "Elementary approximations to the area of n-dimensional ellipsoids", Amer. Math. Mon. 78, PP.280-283; "Corrections to Elementary approximations to the area of n-dimensional ellipsoids", ibid., 83 (1976) 478.

Zhang, T.C. and Bishop, P. (1994). "Density, porosity, and pore structure of biofilms." *Wat. Res.*, 28, 2267–2277.

Zhang, T.C., Fu, Y.C., and Bishop, P.L. (1995). "Competition for substrate and space in biofilms." *Water Environment Research*, 67, 992–1003.

APPENDIX B

IMAGE ANALYSIS IN ImageJ AND Imaris

B-1 ImageJ

ImageJ is a public domain, Java-based image processing program developed at the National Institutes of Health (NIH). The porosity of the cake layer and particle size were obtained from ImageJ in the form of areal fraction in the software via the following procedures:

1. Import images to ImageJ. If a merged image (one showing all Red, Green and Blue channels) is imported, one should go to: Image→Stackes→Image to Stack so that all channels can be analyzed separately.
2. Using the Polygon Selection tool in the tool bar, select the area of interest (see figure below), the membrane in this case, and go to: Image→Crop.

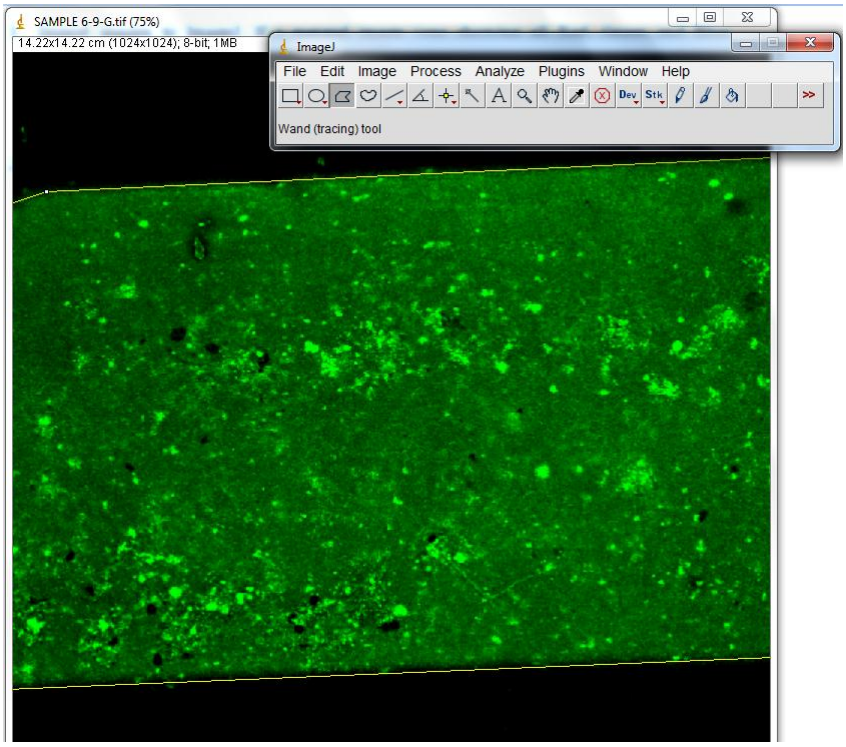

3. Go to: Image→Adjust→Threshold, and adjust the threshold values to select the objects of interest, foulants in this case (brighter spots), like the figure showing

below (foulants are selected in red, image is zoomed out here for illustration purpose, one can zoom in to better select by going to: Image→Zoom→Zoom In).

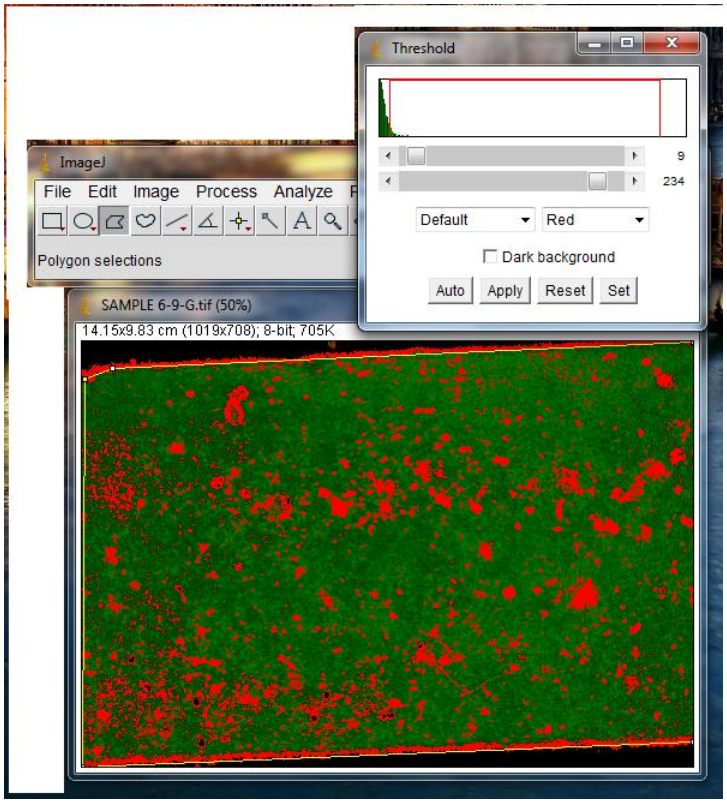

4. Go to: Analyze→Set Measurements, and select parameters of interest, e.g., Area and Area fraction for cake layer porosity in this case.
5. Go to: Analyze→Measure, and export the data for cake layer porosity.
6. Go to: Analyze→Analyze Particles, and export the data for the area of particles, which can be converted to the particle size by assuming sphere shape.

At least 8 different images were analyzed this way at each sampling time to minimize errors. The version used was ImageJ 1.43u (National Institute of Health, MD).

B-2 Imaris

Imaris is commercial software that provides leading functionality for the visualization, segmentation and interpretation of 3D and 4D microscopy datasets. Volumes of various foulants inside and outside the membrane were analyzed in Imaris, which was used to interpret membrane fouling mechanisms. The steps are:

1. Import the experimental files [1] from CLSM to Imaris, which automatically recognizes three channels: *Red*, *Green* and *Blue*, such as in the image below.

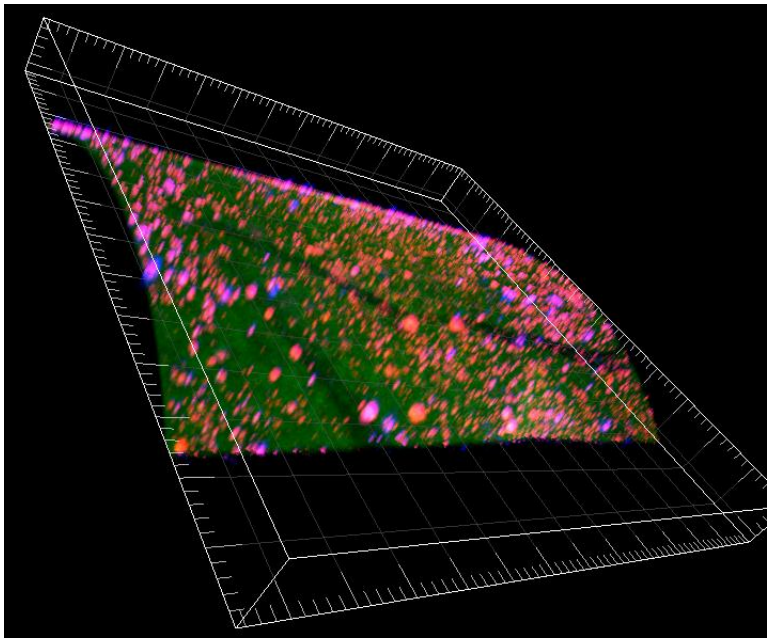

2. Using the *Add new Surfaces* tool in the tool bar, create a surface using the *Green Channel* (Green is chosen because of the green auto fluorescence of the membrane).

[1] Each experimental file is a stack of 120 images taken of different depths at the fouled membranes, and should be distinguished from the images processed in ImageJ.

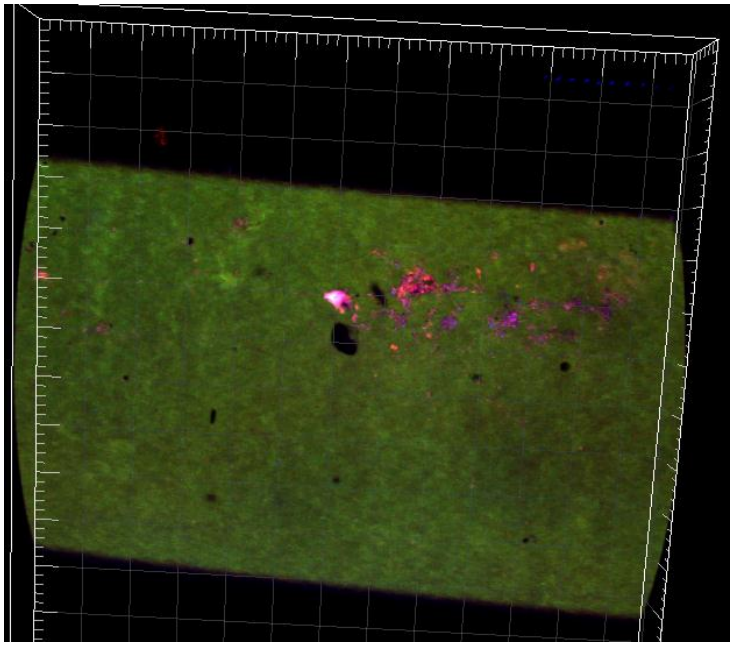

3. Adjust threshold value so that all the green color is selected (see figure below), and the volume data can be exported from the Statistics tab as the volume of the membranes.

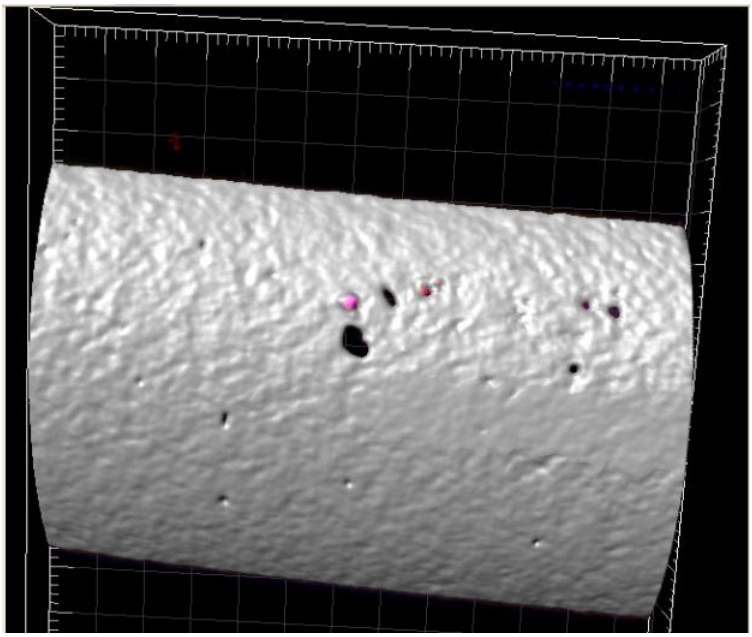

4. Go to: Edit→Mask All, and choose the *Red Channel* with voxels inside surface set to 0 (i.e., foulants represented by Red inside the membrane are not considered), and a new masked channel will be created.

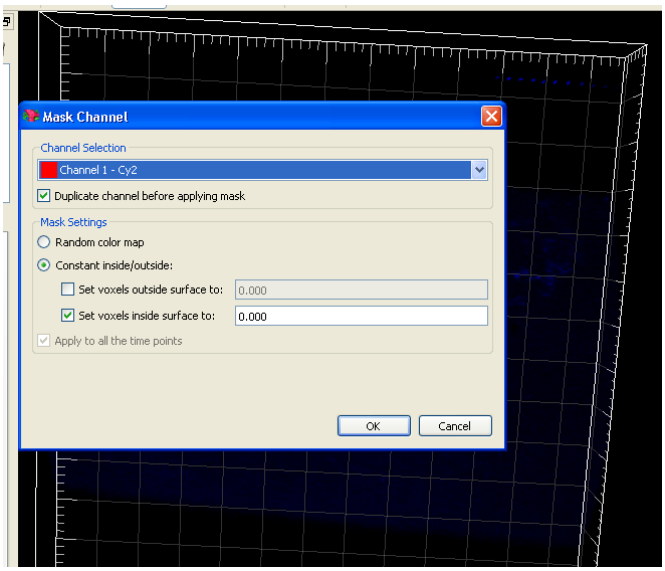

5. Selecting the newly masked channel, create another new channel, and adjust the threshold so that the brighter red color outside the membrane is selected, like the figure showing below.

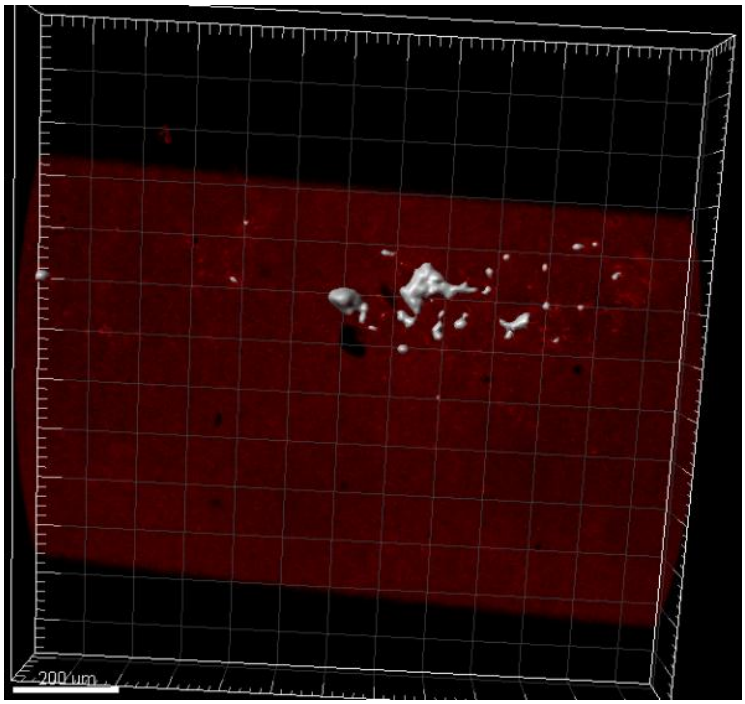

6. Go to the Statistics tab, and export the data as the outside volume of foulant represented by *Red*.

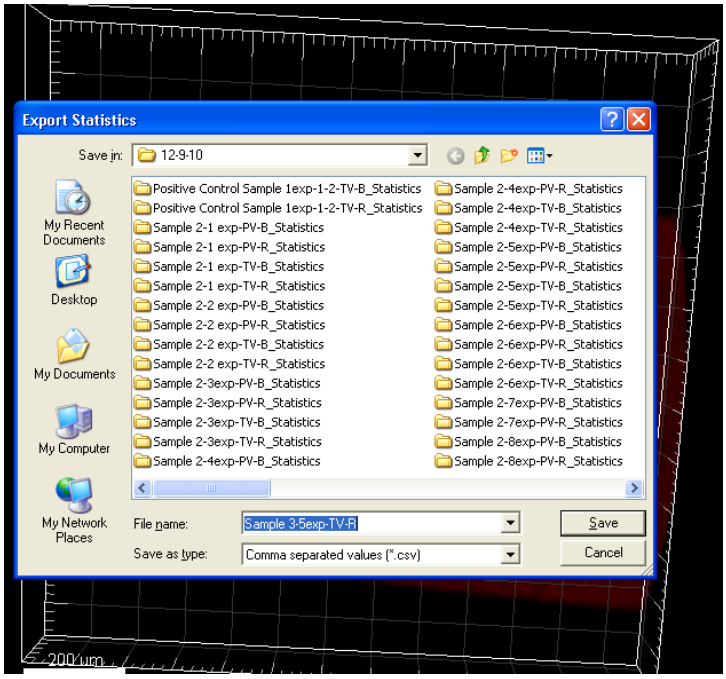

7. Repeat Steps 4-6 with voxels outside surface set to 0 (i.e., foulants represented by *Red* selected outside the membrane are not considered), and export data as the inside volume of foulant represented by *Red*.

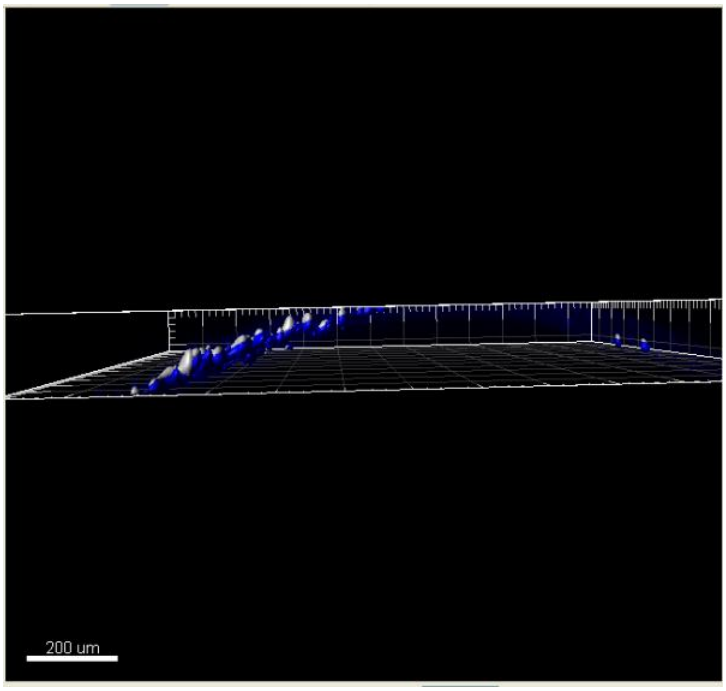

8. Repeat Steps 4-7 for *Blue Channel*, and export data.
9. Similar to Step 2, create another surface using the *Red* (or *Blue*) *Channel*, and repeat Steps 3-7 for the *Green Channel*, and export data.
10. The total volume for each foulant is the sum of the volumes inside and outside the membrane.

At least 8 different images were analyzed this way at each sampling time to minimize errors. The version used was Imaris v7.1.1 (Bitplane AG).

APPENDIX C

DATA COMPILATION

C-1 STB performance data in Phase 1.

Date	Raw			STB-8 (HRT = 2.5h)			STB-4 (HRT = 5h)			STB-2 (HRT = 10h)		
	BOD_5	Turbidity	pH	BOD_5	Turbidity	pH	BOD_5	Turbidity	pH	BOD_5	Turbidity	pH
	mg/L	NTU	-	mg/L	NTU	-	mg/L	NTU	-	mg/L	NTU	-
4/2/2010	92.1			48.2	19.28	6.86	36.9	10.30	6.77	18.5	8.41	6.95
4/9/2010	80.4			61.2	46.40	6.98	37.1	12.90	6.76	17.8	8.74	7.17
4/16/2010	100			67.5	44.70	6.94	34.4	13.90	6.88	24.6	6.32	6.95
4/23/2010	78.6			56.1	55.60	6.89	37.5	18.25	6.94	17.7	11.46	7.05
4/30/2010	82.5			68.4	62.80	7.04	42.8	35.70	6.93	21.5	27.10	6.92
5/7/2010	104			86.4	66.50	7.17	39.5	54.10	7.12	26.4	43.20	7.55
5/14/2010	116	100	6.9	87.5	200	6.7	58.6	34.6	6.9	24.9	43.3	6.8
5/21/2010	114	77.6	6.7	87.6	104	7.1	68.3	62.8	6.6	25.4	27.5	6.7
5/28/2010	118	44.4	6.8	88.2	89.7	6.8	75.6	60.3	6.8	26.3	50.1	6.8
6/4/2010	113	124	6.6	88.4	68.8	6.8	68.2	66	6.8	19.9	31	6.7
6/11/2010	112	84.6	6.8	91.1	70.6	7	70.3	46	6.8	19.4	38.3	6.8
6/18/2010	122	75.3	6.8	86.7	122	7.2	66.2	102	7.1	20.4	69.7	7
6/25/2010	125	75.3	6.9	88.7	104	7.1	56.6	82.6	7.2	24.1	28.2	7.1
7/2/2010	108	148	6.9	71.1	102	7.2	69.3	149	7.5	75.6	31.7	7.3
7/9/2010	-	85.5	6.8	70.2	93.3	6.9	71.1	65.2	6.9	69.3	42.6	6.8
7/16/2010	119	73.6	6.7	64.8	48.4	7.1	52.2	46	7.1	67.5	34.5	7.4
7/23/2010	110	83	6.9	55.8	142	7	40.5	202	7	72.9	108	7
7/30/2010	-	118	6.8	-	92.3	6.9	-	67.7	7.9	-	28.7	7.7
8/6/2010	109	68	6.7	59.4	164	7.4	69.3	148	7.3	76.5	70.8	7.1
8/13/2010	109	31.8	8	62.1	103	7.4	73.8	130	7.4	64.8	119	7.6
8/20/2010	172	85.6	6.4	99.6	13.4	6.5	45.6	8.24	6.5	32.7	3.65	7.3
8/27/2010	138	120	6.5	52.2	9.07	6.5	44.1	6.77	6.9	13.8	3.76	6.9
9/3/2010	109	57.1	7.3	71.4	12.4	6.5	48.3	10.9	7	20.7	5.92	7.1
9/10/2010	121	22.3	6.7	69.6	51.1	7.2	30.6	25.4	6.7	19.8	21.3	7
9/17/2010	103	111	6.6	91.2	60.8	6.7	56.4	47.1	6.9	33.3	47.1	7.8
9/24/2010	201	183	6.7	85.2	111	6.9	41.7	12.5	7.3	15.6	4.57	7.2
10/1/2010	106	25.9	7.4	90.6	19.1	7.1	45	17.1	8	28.8	10.7	7.9
10/8/2010				90	8.48	6.9	26.1	10.7	7.2	19.2	10.3	7.4
10/15/2010				104	18.5	6.7	41.1	18.6	7.1	33	6.29	7.5

Note: These data are for Fig. 3.3.

C-2 STB performance data in Phase 2.

Date	STB-8-B			STB-2-B			STB-8-S			STB-2-S		
	BOD_5	Turbidity	pH	BOD_5	Turbidity	pH	BOD_5	Turbidity	pH	BOD_5	Turbidity	pH
	mg/L	NTU	-	mg/L	NTU	-	mg/L	NTU	-	mg/L	NTU	-
1/14/2011	110	61.9	7.2	47.88	71.7	6.8	110.6	67.4	7.1	46.44	80.2	7
1/17/2011	120.9	122	6.9	46.5	72.6	6.7	125	123	7.1	47.1	88.3	7
1/19/2011	83.7	30.2	6.8	51.36	46.3	7.9	99.9	44.7	7.1	51.06	39.4	8
1/21/2011	53.7	67.6	6.9	47.04	25.7	6.8	64.95	141	7	48.18	113	7
1/24/2011	124.2	76.8	7.7	48.78	79.1	7.2	122.3	82.4	7	50.46	54.3	7.2
1/28/2011	120.3	545	6.8	80.4	76.6	7.2	119.7	154	6.8	15.9	30	7.2
1/31/2011	121.2	43.6	6.9	103.5	57.3	6.7	71.25	80.7	6.9	64.8	50	6.9
2/2/2011	119.6	70.3	7	102.9	61.4	6.9	108.2	100	7	64.5	48.9	7.1
2/7/2011	120.2	225	6.7	121.8	177	6.9	117.6	107	6.8	56.85	125	6.8
2/11/2011	120.3	62.8	7	122.3	72.2	6.8	121.1	42.9	7.1	58.35	89.9	6.8
2/16/2011	115.4	28.2	7	117.3	53.8	7.2	116.3	35.8	7.1	74.85	212	6.9
2/21/2011	228.1	109	7.1	235.4	64.1	7.7	226.1	65.6	7	183.9	38.1	6.9
2/25/2011	224.40	35.70	7.16	210.10	47.10	7.11	223.30	72.20	7.19	216.70	90.10	6.9
2/27/2011	187.50	23.30	7.28	178.90	25.90	7.54	199.60	24.10	7.33	177.20	19.00	7.5
2/28/2011	106.5	24.1	7	85.05	24.9	7.4	119.1	24.1	7.2	42.9	20.7	7.7
3/4/2011	112.5	20.2	7.2	77.25	19.1	7.4	99.15	17	7.3	77.55	26.4	7.4

Note: These data are for Fig. 3.4.

C-3 STB performance at different heights.

STBs	Sampling ports	DO, mg/L		BOD_5, mg/L		Turbidity, NTU		
		3/4/11	3/8/11	2/27/11	3/4/11	2/27/11	3/4/11	3/8/11
STB-2-S	4	2.82	3.14	65.1	79.5	74.2	16.3	29.4
	3	2.14	3.24	66.9	57	45.5	59.4	39.2
	2	2.41	3.44	69.9	64.35	38.3	21.4	48.7
	1	1.23	2.57	74.4	103.65	57.7	51.5	87.7
	0	2.59	0.04	42.9	77.55	19	26.4	36
STB-8-S	4	2.83	3.77	135.3	97.2	66.4	19.2	30.4
	3	1.9	2.93	166.05	124.95	55.1	18.9	44.5
	2	2.06	2.37	186.6	115.5	68.3	16.6	80
	1	1.94	1.48	106.65	93.3	109	34.3	152
	0	1.16	0.41	119.1	99.15	24.1	17	38.5
STB-2-B	4	3.15	2.81	54.3	61.2	25.5	17.3	43.9
	3	2.28	2.77	60	109.8	37.1	29.6	51.2
	2	2.48	2.5	108.6	94.8	54.2	20.3	59.3
	1	2.2	2.27	94.35	41.55	64.7	113	52.8
	0	2.34	0.33	85.05	77.25	25.9	19.1	33.2
STB-8-B	4	2.44	2.69	111.45	87.45	59.6	20.9	34.4
	3	2.24	2.7	106.35	64.5	33.3	22.9	38.4
	2	2.25	2.22	80.1	74.55	40.1	26.8	39.4
	1	2.5	2.38	68.25	115.8	39.2	54.7	39.5
	0	0.27	0.3	106.5	112.5	23.3	20.2	32

Note: These data are for Fig. 3.5.

C-4 Biofilm property data.

Date	STBs	Sampling ports	Tire+biofilm		Tire		D_d (g/mL)	D_w (g/mL)	Porosity (%)	Thickness (mm)
			M (g)	V (mL)	M (g)	V (mL)				
3/6/2011	STB-2-S	1	0.1978	0.1966	0.1818	0.1808	1.115	1.019	17.72	0.082
		2	0.4053	0.45	0.3990	0.3973	1.171	1.105	66.79	0.008
		3	0.3957	0.3929	0.3510	0.3270	1.266	1.009	88.02	0.006
		4	0.3103	0.3079	0.2753	0.2562	1.064	1.003	81.81	0.011
	STB-8-S	1	0.3233	0.32	0.2868	0.2663	1.250	1.029	62.02	0.023
		2	0.3681	0.3604	0.3265	0.2999	1.162	1.015	69.42	0.008
		3	0.3661	0.3623	0.3248	0.3015	1.210	1.016	74.18	0.013
		4	0.355	0.3511	0.3149	0.2922	1.266	1.011	86.59	0.006
	STB-2-B	1	1.1753	1.1497	1.0426	0.9567	1.187	1.017	70.10	0.013
		2	1.6565	1.6164	1.4694	1.3451	1.218	1.023	64.43	0.016
		3	1.3067	1.2974	1.1591	1.0796	1.195	1.014	75.98	0.010
		4	1.6472	1.6394	1.4612	1.3642	1.175	1.010	80.67	0.009
	STB-8-S	1	1.1535	1.149	1.0232	0.9561	1.181	1.024	56.08	0.037
		2	1.4391	1.4321	1.2766	1.1917	1.201	1.026	57.73	0.022
		3	1.7211	1.7162	1.5267	1.4281	1.168	1.015	70.87	0.012
		4	1.4918	1.4889	1.3233	1.2390	1.186	1.015	73.51	0.012
3/22/2011	STB-2-S	1	1.257	1.1468	0.8109	0.6448	1.045	1.002	80.18	0.733
		2	1.4749	1.4587	1.1882	1.0872	1.027	1.001	14.86	0.079
		3	1.834	1.6148	1.6859	1.4828	1.057	1.006	39.77	0.084
		4	2.2982	2.0023	2.1615	1.8695	1.029	1.003	45.11	0.067
	STB-8-S	1	2.0049	1.8381	1.3891	1.1083	1.217	1.013	74.45	0.620
		2	1.8542	1.6267	1.4146	1.2121	1.039	1.002	77.71	0.322
		3	2.2651	1.9796	1.8676	1.5771	1.022	1.001	76.42	0.240
		4	1.4914	1.1711	1.3208	1.1048	1.016	1.001	42.84	0.057
	STB-2-B	1	3.924	3.4927	3.178	2.8377	1.091	1.004	74.89	0.217
		2	1.8064	1.6426	1.6884	1.3345	1.123	1.020	69.94	0.217
		3	1.452	1.328	1.4104	1.1067	1.041	1.010	76.77	0.188
		4	1.4121	1.2245	1.4095	1.0985	1.159	1.585	76.03	0.108
	STB-8-S	1	2.648	2.4013	2.1144	2.0828	1.157	1.011	41.63	0.144
		2	3.6855	3.432	3.2196	2.7746	1.163	1.017	63.39	0.223
		3	3.003	2.6372	2.7118	2.3841	1.136	1.012	49.59	0.100
		4	2.499	2.3296	2.3347	2.1712	1.101	1.010	49.24	0.069

Note: These data are for Fig. 3.6.

C-5 MBR performance data.

Date	pH	Turbidity, NTU	BOD_5, mg/L
3/5/2010	7.36	0.623	5.64
3/12/2010	7.88	0.562	3.12
3/19/2010	7.97	1.28	2.6
3/26/2010	8	0.165	2.4
4/2/2010	7.64	0.313	3.09
4/9/2010	7.85	0.475	1.77
4/16/2010	8.18	0.224	2.04
4/23/2010	6.47	0.538	2.98
4/30/2010	7.56	0.289	1.5
5/7/2010	8.27	0.932	1.65
7/16/2010	7.53	1.81	5.29
7/23/2010	7.81	4.06	6.55
7/30/2010	7.68	2.2	8.58
8/6/2010	7.85	1.4	7.99
8/13/2010	7.72	1.38	17.53
8/20/2010	7.41	0.532	1.392
8/27/2010	7.4	0.404	1.092
9/3/2010	7.87	0.363	0.252
9/10/2010	7.63	0.294	1.392
9/17/2010	7.38	2.14	0.372
9/24/2010	7.58	0.335	1.632
10/1/2010	7.57	0.463	1.092
10/15/2010	7.3	0.453	1.872

Note: These data are for Fig. 3.7.

C-6 MBR TMP data.

Operating time, d	TMP, mbar			
	SRT = 100 d	SRT = 30 d	SRT = 20 d	SRT = 10 d
1	35	477	37	54
2	128	544	135	797
3	330	600	425	710
4	470	635	480	720
5	499	657	480	723
6	541	695	490	811
7	640	664	545	710
8	642	684	550	775
9	660	724	592	705
10	651	695	744	722
11	665	680	722	700
12	650	719	730	780
13	590	650	750	685
14	610	670	798	800
15	680	670		
16	630	707		
17	635	666		
18	582	611		
19	656	600		
20	615	665		
21	670	700		
22	700	689		
23	790	496		
24	680	603		
25	700	600		
26	810	608		
27	840			
28	893			

Note: These data are for Fig. 3.8.

C-7 MBR MLSS data.

Operating time, d	MLSS, mg/L			
	SRT = 100 d	SRT = 30 d	SRT = 20 d	SRT = 10 d
5	844	365	263	160
12	689	351	235	192
26	612	335	208	177
40	569	349	216	186
55	544	336	224	172
60	550	324	219	166
133	612	364	232	168
140	852	348	268	184
154	696	332	208	164
168	592	270	348	314
175	506	440	311	370
182	674	496	416	260
189	430	400	346	268
203	478	360	292	244
210	455	361	423	300

Note: These data are for Fig. 3.9.

C-8 Raw data from Imaris.

Sampling time	Outside foulants, μm^3			Inside foulants , μm^3			Membrane	
	Polysaccharides	Biomass	Protein	Polysaccharides	Biomass	Protein	Volume, μm^3	Area, μm^2
8 min	400913.71	26281.74	337024.80	309060.55	41911.13	352549.22	22639890.00	2234501.81
18min	232093.94	115680.92	227790.44	112204.21	27202.41	162292.46	21433229.29	2216466.34
28 min	586633.83	95147.07	423698.97	366710.70	73874.71	185717.53	20985454.39	2234783.42
6 hr	2829730.18	230738.79	862664.15	1914170.82	164735.36	533124.66	20820903.85	2202848.37
36 d	8182522.07	1491411.12	7647380.56	8828614.09	4422585.05	7970306.14	20495553.43	2183543.61

C-9 Data from ImageJ (n = 8).

Sampling time	Area fraction, %						
	Protein		Biomass		Polysaccharides		Total
	Average	Standard deviation	Average	Standard deviation	Average	Standard deviation	
8 min	0.74	0.88	1.10	0.45	0.77	0.71	2.61
18 min	1.07	0.85	1.07	0.54	2.11	1.81	4.26
28 min	1.24	0.68	2.07	1.12	3.52	1.71	6.83
6 hr	1.79	0.76	2.62	0.82	5.79	1.38	10.20
36 d	6.03	3.90	10.82	2.14	12.45	2.90	29.30

C-10 Data derived from C-8.

C-10A. Specific volumes of different foulants inside and outside the membrane.

Specific volume, $\mu m^3/\mu m^2$		8 min	18 min	28 min	6 h	36 d	36 d
Inside	Protein	0.315648	0.146632	0.165623	0.483995	1.829475	7.317899
	Biomass	0.037371	0.02466	0.066573	0.150929	1.014173	4.056693
	Polysaccharides	0.275587	0.10154	0.326832	1.72703	2.03515	8.140601
Outside	Protein	0.300077	0.203536	0.373064	0.788244	1.755515	7.022059
	Biomass	0.02358	0.105118	0.086018	0.207882	0.391382	1.565527
	Polysaccharides	0.355838	0.209988	0.520224	2.58532	1.892376	7.569502

C-10B. Ratio of internal foulant volume to total foulant volume.

Sampling time	Volume ratio for internal foulants		
	Protein	Biomass	Polysaccharides
8 min	0.51	0.61	0.44
18 min	0.42	0.19	0.33
28 min	0.31	0.44	0.39
6 h	0.38	0.42	0.40
36 d	0.51	0.72	0.52

C-10C. Membrane and cake porosities and TMP.

Sampling time	Porosity		TMP, kPa
	Membrane	Cake[1]	
8 min	0.573907	0.973874	9
18 min	0.58329	0.957437	15
28 min	0.567014	0.931729	17.5
6 h	0.475521	0.897996	31.4
36 d	0.275978	0.70698	48.3

[1] Cake porosity data from ImageJ

C-10D. Volume percentage of each foulant in the total foulant volume at different locations.

Sampling time	Percentages, %								
	Inside			Outside			Total		
	Protein	Biomass	Polysaccharides	Protein	Biomass	Polysaccharides	Protein	Biomass	Polysaccharides
8 min	50	6	44	44	3	52	47	5	48
18min	54	9	37	39	20	40	44	16	39
28 min	30	12	58	38	9	53	35	10	55
6 hr	20	6	73	22	6	72	21	6	73
36 d	37	21	42	43	10	47	40	16	44

C-10E. Contributions of internal and external fouling to TMP and foulants volume, respectively.

Sampling time	Percentage, %			
	TMP		Volume	
	Internal	External	Internal	External
8 min	73.0	27.0	48.1	51.9
18 min	44.1	55.9	34.5	65.5
28 min	37.4	62.6	36.3	63.7
6 h	21.5	78.5	39.7	60.3
36 d	24.7	75.3	54.7	45.3